AD NUMBER

AD886470

LIMITATION CHANGES

TO:

Approved for public release; distribution is unlimited.

FROM:

**Distribution authorized to U.S. Gov't. agencies and their contractors;
Administrative/Operational Use; JUL 1971. Other requests shall be referred to Air Force Avionics lab., Wright-Patterson AFB, OH 45433.**

AUTHORITY

AFAL ltr 5 Dec 1973

AFAL-TR-71-155
PART I

INTRA-VEHICLE ELECTROMAGNETIC COMPATIBILITY ANALYSIS

Dr. J.L. Bogdanor, M.D. Siegel, G.L. Weinstock

~~MCDONNELL~~ AIRCRAFT COMPANY
MCDONNELL DOUGLAS CORPORATION

TECHNICAL REPORT AFAL-TR-71-155, PART I
JULY 1971

AIR FORCE AVIONICS LABORATORY
AIR FORCE SYSTEMS COMMAND
WRIGHT-PATTERSON AIR FORCE BASE, OHIO

BLANK PAGE

NOTICE

When Government drawings, specifications, or other data are used for any purpose other than in connection with a definitely related Government procurement operation, the United States Government thereby incurs no responsibility nor any obligation whatsoever; and the fact that the government may have formulated, furnished, or in any way supplied the said drawings, specifications, or other data, is not to be regarded by implication or otherwise as in any manner licensing the holder or any other person or corporation, or conveying any rights or permission to manufacture, use, or sell any patented invention that may in any way be related thereto.

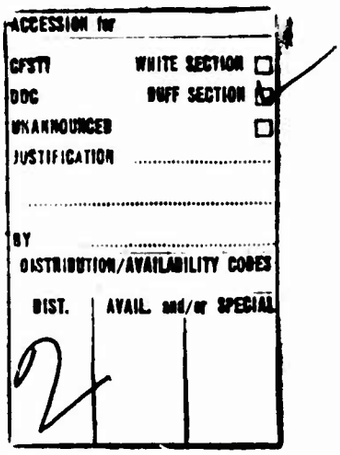

Copies of this report should not be returned unless return is required by security considerations, contractual obligations, or notice on a specific document.

AFAL-TR-71-155
PART I

INTRA-VEHICLE ELECTROMAGNETIC COMPATIBILITY ANALYSIS

Dr. J.L. Bogdanor, M.D. Siegel, G.L. Weinstock

MCDONNELL AIRCRAFT COMPANY
MCDONNELL DOUGLAS CORPORATION

TECHNICAL REPORT AFAL-TR-71-155, PART I
JULY 1971

FOREWORD

This report was prepared by the McDonnell Douglas Corporation, McDonnell Aircraft Company, Avionics Systems Technology Department under USAF Contract F33615-70-C-1333. The program was administered by the Air Force Avionics Laboratory (AFSC) Systems Avionics Division, Wright-Patterson Air Force Base, Ohio. The Air Force project engineer directing the technical aspects of the study was Herbert Bartman, AFAL/AAA.

This document is Technical Report AFAL-TR-71-155, Part I, and covers work accomplished from January 1970 to April 1971. Part II will describe verification methods and results, and Part III will be a users' manual.

This technical report has been reviewed and is approved.

W. A. Studebaker

WILLIAM A. STUDABAKER
Lt Colonel, USAF
Chief
System Avionics Division

ABSTRACT

A computer program was developed to predict and analyze electromagnetic interference between avionics systems on aerospace vehicles. It is an analytic tool to aid the user in establishing intra-vehicle electromagnetic compatibility. The program is used to derive information which is otherwise impractical or difficult to obtain. This part covers the investigation, research, and development phases of this program. A study of physical principles, previous work, and practical experience identified four predominant interference coupling paths:

- Antenna-to-antenna
- Wire-to-wire
- Electromagnetic field (antenna)-to-wire
- Box-to-box

Basic equations and analysis techniques were formulated for each coupling path. These were then assembled into four practical computer analysis programs using FORTRAN IV language. The programs are modular and thus can be run separately or combined into one integral program. This report contains a complete description of each program including the mathematical models, basic equations, and analysis procedures used. Examples of the application of the programs together with sample computer outputs are presented. The programs were developed for the CDC 6600 computer, but they are readily adaptable to other machines.

BLANK PAGE

TABLE OF CONTENTS

TABLE OF CONTENTS (Continued)

LIST OF FIGURES

LIST OF FIGURES (Continued)

LIST OF TABLES

LIST OF ABBREVIATIONS

AC	-	Alternating Current
ATACAP	-	Antenna-to-Antenna Compatibility Analysis Program
BL	-	Butt-line
BTBCAP	-	Box-to-Box Compatibility Analysis Program
dB	-	Decibel
dB μV/MHz	-	Decibel above on micro-volt per megahertz bandwidth
ECM	-	Electronic Countermeasures
EMC	-	Electromagnetic Compatibility
EMI	-	Electromagnetic Interference
EMP	-	Electromagnetic Pulse
FS	-	Fuselage Station
FSCP	-	Feasibility Study Change Proposal
FTWCAP	-	Field-to-Wire Compatibility Analysis Program
IEEE	-	Institute of Electrical and Electronics Engineers
IVEMC	-	Intra-vehicle Electromagnetic Compatibility
Hz	-	Hertz (cycles/second)
MCAIR	-	McDonnell Aircraft Company
MDC	-	McDonnell Douglas Corporation
μhy	-	Microhenry
RCVR	-	Receiver
RHAW	-	Radar Homing and Warning
RF	-	Radio Frequency
USAF	-	United States Air Force
WL	-	Water-line
WPAFB	-	Wright Patterson Air Force Base
WTWCAP	-	Wire-to-Wire Compatibility Analysis Program
XMTR	-	Transmitter

BLANK PAGE

SECTION 1

INTRODUCTION AND SUMMARY

Modern aerospace vehicles contain increasing numbers of complex and sophisticated avionics systems that must operate harmoniously to achieve mission objectives. Achieving electromagnetic compatibility (EMC) for such avionics is a complex and time consuming problem. To assist the engineer (whether DOD agency, prime contractor or sub-contractor) in establishing and maintaining intra-vehicle electromagnetic compatibility (IVEMC), the power and speed of modern computers can be utilized with significant time and cost savings. The engineer retains responsibility for the appropriate decisions as to what interference specifications and control measures are required, but with the tedious computations performed by the computing equipment, he can devote more of his time to the design decisions.

McDonnell Aircraft Company (MCAIR) under contract to the Air Force Avionics Laboratory, has developed analytical techniques for predicting electromagnetic interference (EMI) between avionic systems on aerospace vehicles. The techniques derived are specifically for analyzing coupling and interference propagation paths. The result is a series of interrelated computer programs to perform the operations indicated by the mathematical models developed for the solution of IVEMC situations. The development of the computer programs is divided into three phases: investigation, development, and verification. This part addresses the first two phases. The third phase will be described in part II.

Investigation Phase - During the investigation phase, the basic concepts and solution approaches were established. The IVEMC problem was examined, and the major EMI coupling paths were identified by reviewing the physical principles involved, previous investigation results, and McDonnell Douglas Corporation (MDC) and USAF experience with IVEMC problems. The basic equations and techniques for the mathematical models were then established and verified for a number of cases.

Development Phase - During the development phase, the basic equations and techniques were assembled into practical computer programs. The input data and the required outputs were determined, and the algorithms were formulated. The algorithms were coded for the CDC 6600 computer, and the programs debugged.

Verification Phase - A number of tests were performed to ensure the validity and accuracy of the prediction models. These included screenroom component tests, full scale mock-up tests in an anechoic chamber, and actual aircraft tests. Results from these and current tests will be included in part II which will be submitted in September 1971.

SECTION 2

APPROACH TO PROBLEM

2.1 ANALYTICAL APPROACH

To design for intra-vehicle electromagnetic compatibility, the engineer must have the ability to accurately predict levels of expected interference. The computer programs described herein are designed to assist him in making these predictions. The engineer, however, must assess application validity, since these programs are merely models of the actual physical situation. Of necessity, they contain many assumptions and approximations which the engineer must take into account.

These programs have a broad capability to analyze the actual case at hand; they can largely reduce reliance solely on past experience and "rules-of-thumb." The speed and accuracy of the computer can be utilized to obtain a picture of what interference will occur, how severe it will be, what the predominant coupling mode is, what the most offensive sources are, and what the most susceptible receptors are. Knowing this, the engineer can make decisions as to what can be done to reduce or eliminate the interference. The computer can then be used to verify the adequacy of these decisions. The adequacy of applicable EMI specifications can also be determined, and the specifications can be modified as needed.

These programs meet the needs in establishing IVEMC on multi-purpose air vehicles. Equipment on these vehicles must be interchangeable from one system to another, and often identical line-replaceable-units are used on widely different aircraft types. Further, these vehicles are subject to extensive modification, often to applications far different from that of the initial design. To apply over the broad range of air vehicle EMI analysis requirements, these programs are broad in scope and flexible. They will handle the large number of EMI situations encountered on these vehicles, and they can be easily modified for additional applications. The programs can be run as a group to provide total system EMI data, or they can be run independently for a particular coupling mode. Thus, if antenna-to-antenna coupling is of interest, only that program need be run.

These programs can also be used to develop special purpose specifications for limited production vehicles such as spacecraft. For a defined system configuration, the subsystem parameters can be fed into the computer, and the interference levels calculated. Specifications can then be written, or existing specifications can be modified as necessary for IVEMC.

2.2 PROBLEM DEFINITION

The first step in establishing these IVEMC analysis programs was to determine the predominant EMI coupling modes and paths. Once these were determined, mathematical models were devised for each mode. MCAIR had previously developed an antenna-to-antenna program (Ref 1), and a survey was initiated to determine other coupling modes for which useful prediction

programs could be devised within the scope of this contract. The range of USAF interference problems was examined. Also, an extensive literature search was conducted to review past approaches and limits of current practice. Future trends in avionics were surveyed. From these surveys, four coupling paths were determined most predominant:

- Antenna-to-antenna (transmitter-to-receiver) coupling
- Wire-to-wire coupling
- Electromagnetic field-to-wire coupling
- Box-to-box magnetic coupling

Antenna-to-Antenna Coupling - One of the most common interference problems on aerospace vehicles results from coupling from a transmitter antenna to a receiver antenna. Large numbers of radiating and receiving avionics are being carried on modern aircraft with a trend to higher powered transmitters and more sensitive receivers. One version of the F-4, for example, has transmitting/receiving subsystems which use more than 30 antennas. When a new subsystem, such as an ECM pod, is added to such a vehicle, determining the probable interference without the aid of a computer is a large, formidable task.

Wire-to-Wire Coupling - Coupling from one wire to another within a bundle has long been recognized as a serious source of EMI. With current trends toward higher density packaging, more compact bundles with smaller wires and thinner insulation, the problem is becoming more acute. MCAIR performed comprehensive investigations in this area and conducted an extensive literature search so as not to duplicate previous efforts.

Electromagnetic Field-to-Wire Coupling - Experience with avionics systems in aircraft, missiles, and spacecraft has shown coupling to wire bundles within the vehicle from external RF energy to be a major EMC concern. Usually, the energy was from an on-board radiating antenna and was coupled onto the wires via gaps or openings in the vehicle skin. Such apertures include radomes, canopies, landing gear doors, access doors, and engine intakes.

Box-to-Box Magnetic Coupling - Another common problem occurs when the 400 Hz magnetic field of an avionics box is coupled into sensitive circuits in other boxes. The usual source of these fields is from power transformers, but other high current devices such as solenoids, relays, and motors can also produce them. Common receptors for such interference include low level audio and video circuits as well as digital logic and servo circuits.

Other combinations of paths and coupling modes can and do cause interference, but the four listed above are the basic ones; and they meet the criterion of providing the engineer with practical, useful tools for establishing IVEMC. Further, since they are basic, the resulting mathematical models lend themselves to widespread applications in analyzing other coupling modes.

With the exception of the wire-to-wire program, only first-order effects were considered. (See Section 4.2.1.) In the past, many attempts have been made to analyze multi-order effects, such as intermodulation. While this is a potential source of EMI, experience has shown it to be rare when compared to direct, first-order interference. Multi-order EMI usually occurs only in special situations, as for example two transmitters tuned to a specific frequency differential simultaneously. This project was therefore directed to modeling only first-order effects.

2.3 UNDERLYING PRINCIPLES

For maximum usefulness, the analytic tools must be oriented toward the user - not the computer. That is, the computer should work for the user, not vice versa.

2.3.1 Data Format

These programs require and accept data which is normally available in several forms. The format and codes are easily learned so that extensive training and computer knowledge is not required of the user. Also, the data formats are common between the programs. The same data cards describing a wire bundle, for example, are accepted by both the field-to-wire and wire-to-wire analysis programs. This way, only one set of cards is needed for a given set of data. The cards are merely assembled in different ways for the different programs.

2.3.2 Default Features

Since these programs are intended for use early in the conceptual and design phases of vehicle development, they have to be usable before many of the basic equipment parameters are known. In this event, the programs have built-in default assumptions based on the applicable military specification or on mathematical expressions. Thus, an analysis can be performed with the default values so that the major EMI problem areas can be determined. Later, when the actual data and specifications become available, new analyses can be made to update the previous ones.

2.3.3 Program Outputs

After the data is read, each program prints a summary of this data including any default values that were inserted. Thus, a record of the data on which the analysis was based is provided. The default values are identified in the output summary.

The analysis results are provided as EMI margins in decibels (dB). (The EMI margin is defined as the ratio of the received signal at a given receptor from a given interference source to the susceptibility level of that receptor.) Thus, the degree of interference can be readily ascertained. Information on the cause of the interference and the analysis method utilized are also given in the output for each interference situation. In the antenna-to-antenna program, for example, the maximum EMI frequency and the maximum and minimum frequencies of coincidence between the transmitter and receiver

are given. Where applicable, outputs are provided that are directly relatable to military specifications. For example, the wire-to-wire program gives the received signal and susceptibility levels in dBμ V/MHz as used in the EMC specifications.

The programs also provide extensive diagnostic and error data. For example, if an input code is not recognized by the computer, it prints out the type of code as well as the bad data. This aids the user in locating a mispunched or cut of sequence data card.

The programs provide for the use of classified data. The classification is inputed for each subsystem, and the highest classification is printed on the top and bottom of each page of output.

2.3.4 Mathematical Model Formulation

The mathematical models were formulated to rapidly survey a large amount of data and give a reasonable indication of the interference that will occur. The models account for major effects on interference coupling (e.g., aircraft fuselage shading). The analysis results, however, are sufficiently accurate to provide for correct EMI engineering decisions. Thus, a balance is obtained between speed and accuracy.

The equations and computational methods that comprise the math model were formulated from basic electromagnetic relationships. These relationships include the basic definitions of capacitance and inductance, Maxwell's equations, and the wave equation. Where approximations were used, care was taken that the accuracy was retained. Further, the models were designed to give answers consistent with past experience and "real world" situations.

To ensure that all potential EMI is detected, worst-case assumptions are used for vague or undefinable parameters, such as wire separation within a bundle. In many cases statistical limits could be used, but in a vehicle development phase, where these programs are of most value, worst-case analysis is desired.

are given. Where applicable, outputs are provided that are directly relatable to military specifications. For example, the wire-to-wire program gives the received signal and susceptibility levels in dBμ V/MHz as used in the EMC specifications.

The programs also provide extensive diagnostic and error data. For example, if an input code is not recognized by the computer, it prints out the type of code as well as the bad data. This aids the user in locating a mispunched or out of sequence data card.

The programs provide for the use of classified data. The classification is inputed for each subsystem, and the highest classification is printed on the top and bottom of each page of output.

2.3.4 Mathematical Model Formulation

The mathematical models were formulated to rapidly survey a large amount of data and give a reasonable indication of the interference that will occur. The models account for major effects on interference coupling (e.g., aircraft fuselage shading). The analysis results, however, are sufficiently accurate to provide for correct EMI engineering decisions. Thus, a balance is obtained between speed and accuracy.

The equations and computational methods that comprise the math model were formulated from basic electromagnetic relationships. These relationships include the basic definitions of capacitance and inductance, Maxwell's equations, and the wave equation. Where approximations were used, care was taken that the accuracy was retained. Further, the models were designed to give answers consistent with past experience and "real world" situations.

To ensure that all potential EMI is detected, worst-case assumptions are used for vague or undefinable parameters, such as wire separation within a bundle. In many cases statistical limits could be used, but in a vehicle development phase, where these programs are of most value, worst-case analysis is desired.

The EM is computed by expanding Equation (3.1) into

$$EM = P + TFS + SF - CL_X - CL_R - SR \qquad (3.2)$$

where P = the transmitter power in dBm.
TFS = free space transmission factor in dB.
SF = shading factor in dB.
CL_x = transmitter cable loss.
CL_R = receiver cable loss.

The term "shading" refers to signal attenuation due to propagation around the aircraft exterior surfaces (fuselage and wings). Computation of the terms of Equation (3.2) is as follows.

3.2.2 Receiver Model

SR, the receiver threshold function, is represented by the curve shown in Figure 1. In the figure, F_{tr} and F_{cr} are the lower and upper frequencies of the receiver tuning range, and S_m is the minimum sensitivity level in dBm. The selectivity skirt levels are represented by SL_R (in dB) and skirt frequencies F_{ar} and F_{dr}, which are obtained with the receiver tuned to each end of its operating frequency range.

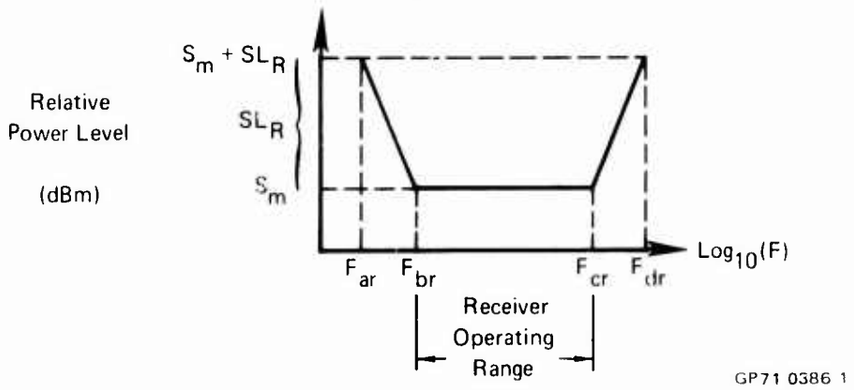

FIGURE 1 RECEIVER THRESHOLD LEVEL vs FREQUENCY

3.2.3 Transmitter Model

In a similar manner, the transmitter power spectrum, P, is represented as shown, in Figure 2. Only parameters for the fundamental curve shape are specified since those of the harmonics are assumed identical except for downward displacement attenuation. The limits of the operating frequency range are specified by F_{btf} and F_{ctf}. Skirts are represented by the skirt level, SL_X, and frequencies F_{atf} and F_{dtf}. P_m is the peak output power in dBm. The harmonic curves are displaced from the fundamental by a factor, HF, as shown.

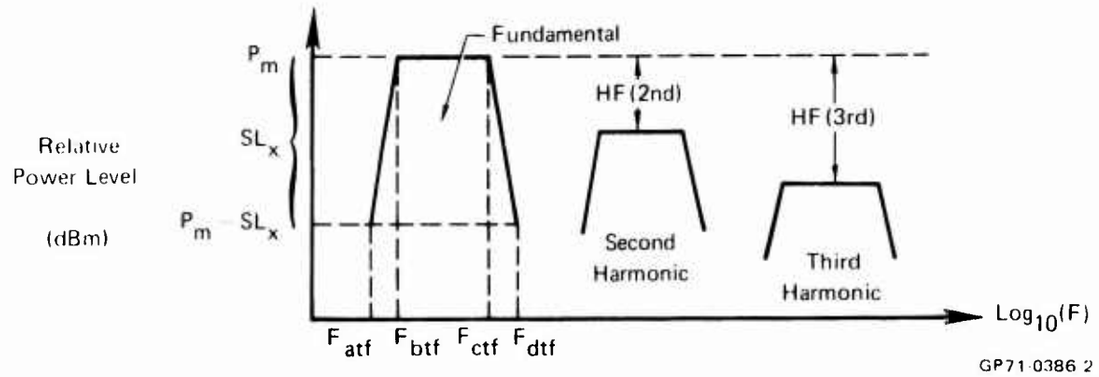

FIGURE 2 TRANSMITTER EMISSION POWER SPECTRUM

3.2.4 Propagation Model

The free space transmission factor, TFS, in Equation (3.2) is found by using the Friis transmission equation (Ref 2)

$$TFS = G_X + G_R + 20 \log_{10} \left[\frac{\lambda}{4 \pi D} \right] \quad (3.3)$$

where

G_X = gain of the transmitter antenna in dB

G_R = gain of the receiver antenna in dB

D = distance between the two antennas in meters

λ = the wavelength in meters

3.2.4.1 Antenna Gains

G_X and G_R are generally functions of direction and are determined by defining the angles Θ and Φ, as shown in Figure 3, in the spherical coordinate system commonly used for antennas. For an antenna at the origin, Θ and Φ to point P(X,Y,Z) are

$$\Theta = \tan^{-1} \sqrt{\frac{X^2 + Z^2}{Y}} \qquad (0 \leq \Theta \leq \pi \text{ radians}) \quad (3.4)$$

$$\Phi = \pi - \tan^{-1} \left(\frac{X}{Y} \right) \quad (0 \leq \Phi \leq 2 \pi \text{ radians}). \quad (3.5)$$

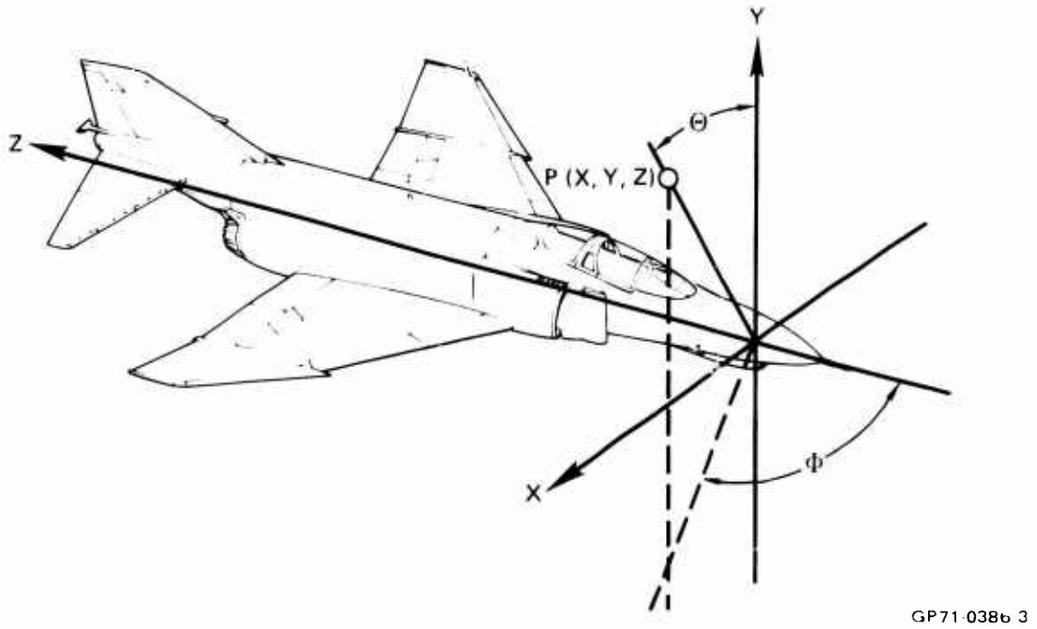

FIGURE 3 LOOK-ANGLE Θ AND Φ IN SPHERICAL COORDINATE SYSTEM FROM AN ANTENNA AT ORIGIN TO P (X, Y, Z)

The gain functions are approximated by a two-level model. The 3 dB limits of the antenna main beam are defined by the angles Θ_1, Θ_2, Φ_1, and Φ_2. The gain function is then

$$G(\Theta,\Phi) = \begin{cases} G_{MB} & \begin{pmatrix} \text{for } \Theta_1 \leq \Theta \leq \Theta_2 \\ \text{and } \Phi_1 \leq \Phi \leq \Phi_2 \end{pmatrix} \\ G_{MSL} & \text{otherwise} \end{cases} \tag{3.6}$$

In Equation (3.6) G_{MB} is the gain of the main-beam, and the G_{MSL} is the mean value of the side lobe gains. When G_{MB} and G_{MSL} are unknown they are computed as follows: (Ref 2)

$$G_{MB} = 10 \log_{10} \left[\frac{4\pi}{(\Theta_2 - \Theta_1)(\Phi_2 - \Phi_1)} \right] \tag{3.7}$$

and (Ref 3)

$$G_{MSL} = -8.3 + 0.5\, G_{MB} \tag{3.8}$$

A special situation exists for downward-pointing antennas in that Θ_1, Θ_2, Φ_1 and Φ_2 cannot be defined as above. In this case, new main-beam angles, Θ_1' and Θ_2', are defined in the Y-Z (pitch) plane and Φ_1', and Φ_2' in the X-Y (roll) plane as shown in Figure 4. New look angles are then computed using

$$\Theta' = \tan^{-1} [D_A \sin\Theta \sin \Phi/Y] \tag{3.9}$$

$$\Phi' = \tan^{-1} [D_A \sin\Theta \cos \Phi/Y] \tag{3.10}$$

where $D_A = \sqrt{X^2 + Y^2 + Z^2}$

The gains are determined using the new angles in Equations (3.6), (3.7), and (3.8).

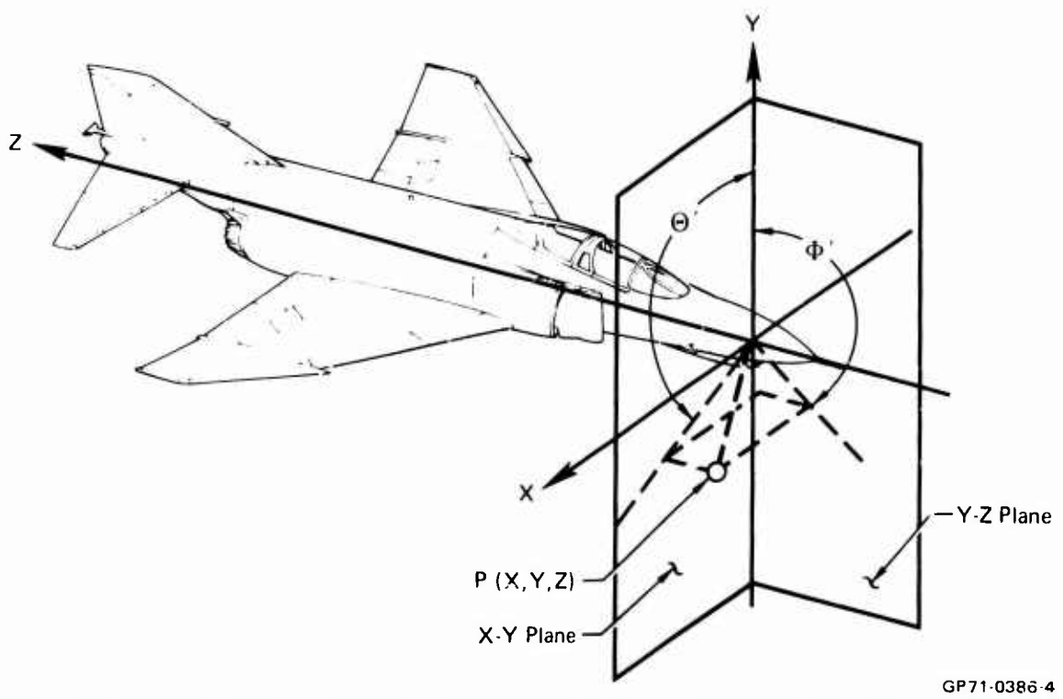

FIGURE 4 LOOK-ANGLE Θ' AND Φ' FOR THE SPECIAL CASES OF A DOWNWARD-POINTING ANTENNA. Φ' IS THE ANGLE IN THE X-Y (ROLL) PLANE, AND Θ' IS THE Z-Y (PITCH) PLANE

3.2.4.2 Distance Evaluation

The antenna separation, D in Equation (3.2), is determined using the aircraft model shown in Figure 5. **Antenna locations are specified in the** usual fuselage station (FS), waterline (WL) and butt-line (BL) system used for aircraft. For analysis, these locations are converted by the computer into cylindrical coordinates (ρ, θ, Z) (ρ and Z are in inches, θ is in radians). The Z-axis of the cylindrical coordinate system is the centroid of the aircraft and is displaced vertically from the WL = 0 line, a distance denoted as WLC. The base of the conical nose section is specified by FSN.

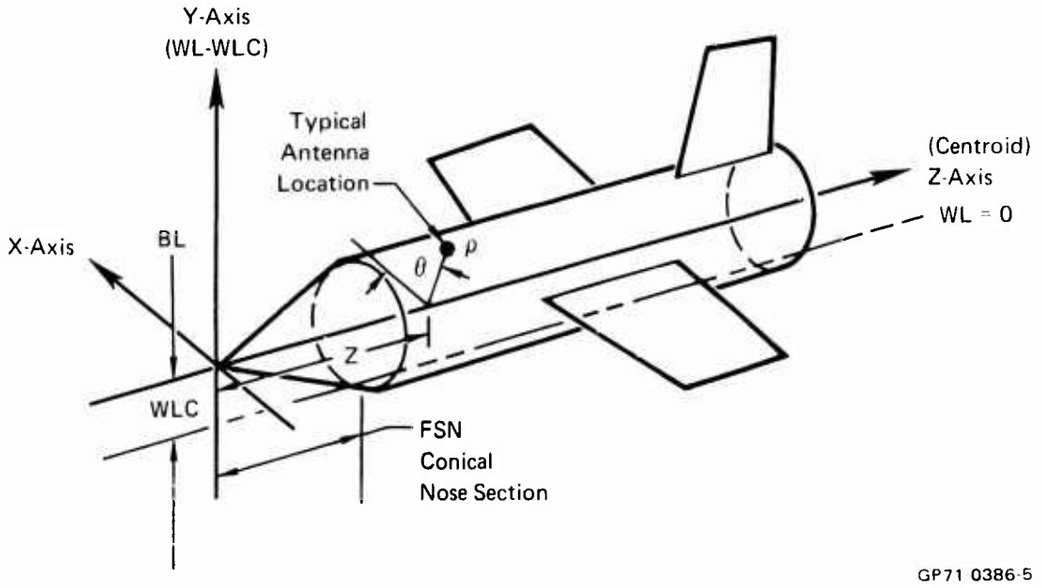

FIGURE 5 MODEL USED TO APPROXIMATE AIRCRAFT

D is determined by using the combination of straight lines, conical spirals, and/or cylindrical spirals that gives the shortest distance between the two antennas over the aircraft surface. The combination used depends on the relationship of the two antennas to the fuselage and wings. With both antennas on the fuselage, a conical spiral is used when one or both antennas are forward of FSN, and a cylindrical spiral is used when both are aft of FSN.

For the conical spiral, the distance between two points,

$P_1 (\rho_1, \theta_1, Z_1)$ and $P_2 (\rho_2, \theta_2, Z_2)$ is

$$D_{con} = \left| \frac{\theta_1 c - \theta_2 d}{2} + \frac{a^2 + b^2}{2a} \ln \left| \frac{a\theta_1 + c}{a\theta_2 + d} \right| \right|$$

where $a = \dfrac{\rho_2 - \rho_1}{\theta_2 - \theta_1}$ (3.11)

$$b = \frac{Z_2 - Z_1}{\theta_2 - \theta_1}$$

$$c = \sqrt{a^2 + b^2 + a^2\theta_1^2}$$

$$d = \sqrt{a^2 + b^2 + a^2\theta_2^2}$$

For the cylindrical spiral ($\rho_1 = \rho_2 = \rho_f$), the distance between two points is

$$D_{cyl} = \sqrt{\rho_f^2 (\theta_2 - \theta_1)^2 + (Z_2 - Z_1)^2} \quad (3.12)$$

Straight line distances are found using

$$D_{sl} = \sqrt{\rho_1^2 + \rho_2^2 - 2\rho_1\rho_2 \cos(\theta_2 - \theta_1) + (Z_2 - Z_1)^2} \quad (3.13)$$

When one antenna is off the fuselage but the other is on, as illustrated in Figure 6, D is a combination of straight line and cylindrical spiral segments.

The tangent point on the fuselage for which D is minimum has a coordinate (assuming ρ_2, θ_2, Z_2 is the point off the fuselage)

$$\theta_t = \theta_2 \pm \tan^{-1}\left[\frac{\sqrt{\rho_2^2 - \rho_1^2}}{\rho_1} \right] \quad (3.14)$$

(The appropriate sign is used that produces minimum D.) The Z coordinate of the tangent point is

$$Z_t = \frac{\rho_1 |\theta_1 - \theta_t| Z_2 + Z_1 \sqrt{\rho_2^2 - \rho_1^2}}{\rho_1 |\theta_1 - \theta_t| + \sqrt{\rho_2^2 - \rho_1^2}} \quad (3.15)$$

ρ_1 now becomes ρ_f in Equation 3.13 and (θ_1, Z_1) become (θ_t, Z_t) respectively when calculating the straight line segment.

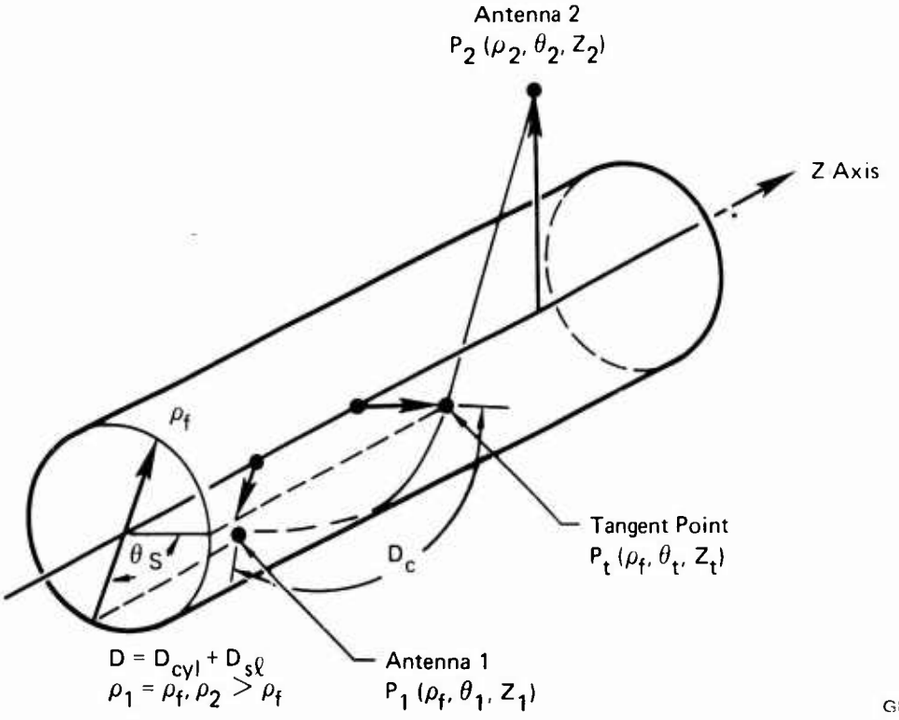

FIGURE 6 DISTANCE BETWEEN TWO ANTENNAS WHEN ONE IS LOCATED OFF FUSELAGE AND A PORTION OF THE PATH IS AROUND THE FUSELAGE

When both antennas are off the fuselage and the shortest path between them is around the fuselage, D consists of two straight line segments and one cylindrical spiral segment as shown in Figure 7. In this case, there are two tangent points. The θ coordinate for the tangent points, θ_{t1} and θ_{t2}, are computed using Equation (3.14) above, and the Z coordinates are

$$Z_{t1} = \frac{B\ (Z_1 + Z_2) + Z_2\ A_1}{B\ (B + A_1 + A_2)} \tag{3.16}$$

$$Z_{t2} = \frac{Z_1 B + Z_2\ A_1}{B + A_1}$$

where $A_1 = \sqrt{\rho_1^2 - \rho_f^2}$

$$A_2 = \sqrt{\rho_2^2 - \rho_f^2} \tag{3.17}$$

$B = \rho_f\ |\theta_{t1} - \theta_{t2}\ |$

ρ_f = radius of the fuselage.

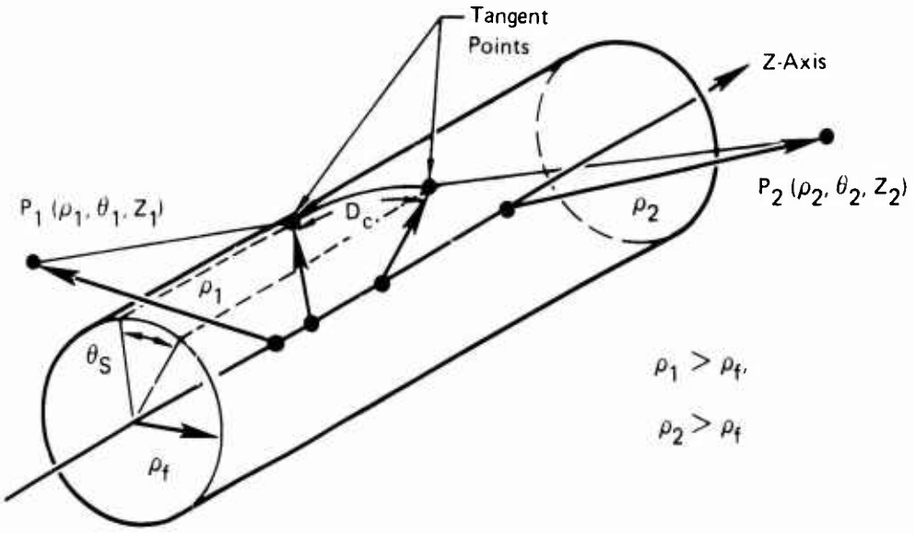

FIGURE 7 DISTANCE BETWEEN TWO ANTENNAS WHEN BOTH ARE OFF THE FUSELAGE AND THE PATH IS AROUND THE FUSELAGE

In the event that a wing intersects the propagation path, the wing must be included in the distance calculation as well as the shading calculation. The propagation path around the wing edge must be determined such that its total length, D, is a minimum. First, the forward or aft wing edge is selected, depending on which path will have the shortest total distance. This is determined by calculating the intersection of the wing and a straight line between the two antennas. Once the wing edge is determined, an iterative technique is used to find the point on that edge such that the propagation path is a minimum. A typical example, with both antennas off the fuselage is shown in Figure 8. For this, the distances are determined from the wing point to each antenna using the techniques described above. The result is the minimum distance D.

3.2.4.3 Fuselage Shading and Diffraction

Where a portion of the propagation path is around the fuselage, or any curved surface, allowance must be made for shading effects. An equation for the fuselage shading, as a portion of the shading factor SF in Equation (3.2), was derived from Hasserjian and Ishimaru (Ref 4). In their work, a function was given relating propagation around an infinite conducting cylinder to that over a flat plane. The function can be reasonably approximated by

$$SF_C = \frac{-A}{(\eta A + \xi)}$$

where $A = \rho_f \theta_s^2 \sqrt{\frac{2\pi}{\lambda D_c}}$

$$\eta = \begin{cases} 5.478 \times 10^{-3}, \text{ for } A < 26 \\ 3.340 \times 10^{-3}, \text{ for } A \geq 26 \end{cases}$$

$$\xi = \begin{cases} 0.5083, \text{ for } A < 26 \\ 0.5621, \text{ for } A \geq 26 \end{cases} \qquad (3.18)$$

and SF_C = fuselage (cylindrical) shading factor (dB)
ρ_f = radius of cylinder (meters)
θ_s = angle around cylinder of propagation path (radians)
λ = wavelength (meters)
D_C = distance of cylindrical segment of propagation path (meters)

The error for this approximation is less than 2 percent in the normal range of use ($A < 100$).

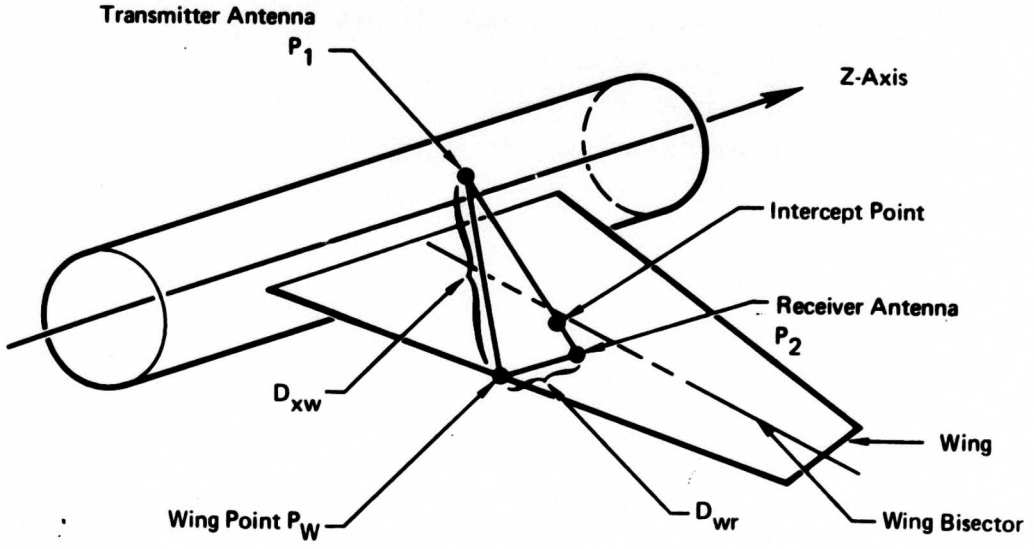

GP71-0386-8

FIGURE 8 TYPICAL PROPAGATION PATH WITH WING SHADING

3.2.4.4 Wing Shading and Diffraction

When a portion of the propagation path is around the wing, or any surface edge, allowance must be made for diffraction effects (Ref 5 and 6). An incident electric field can be related to a diffracted electric field using optic theory and lowering the frequency range to radio frequency (Ref 5). From Figure 9, the diffraction attenuation function for the wing can be calculated using

$$SF_W = 20 \log_{10} \left| \frac{\mathcal{E}_r}{\mathcal{E}_x} \right|$$

$$\text{where} \quad \left| \frac{\mathcal{E}_r}{\mathcal{E}_x} \right| = \frac{\sec \frac{1}{2} (\alpha_x - \alpha_r) \pm \csc \frac{1}{2} (\alpha_x + \alpha_r)}{2 \sin \beta \sqrt{2\pi k D_{wr}}}$$

and SF_W = Wing shading factor (dB)

$\mathcal{E}_x$ = Incident electric field from transmitter at wing point (3.19)

$\mathcal{E}_r$ = Received electric field at receiver antenna

α_x = Angle between Y' axis and incident wave propagation vector

α_r = Angle between Y' axis and receptor wave propagation vector

β = Azimuthal angle of incident wave propagation vector (in wing plane)

k = $2\pi f/c$ = Propagation constant

c = Velocity of Light (3×10^8 m/sec)

D_{wr} = Distance from wing point to receptor point (meters)

The total shading factor in Equation (3.2) is then the sum of the edge and cylindrical surface factors.

$$SF = SF_C + SF_W \tag{3.20}$$

3.3 ANALYTIC ASSUMPTIONS AND APPROXIMATIONS

The mathematical model includes assumptions and approximations. This is necessary when modeling complex or unknown functions, such as antenna patterns, for computer analysis. These can be divided into receiver, transmitter, antenna, and default categories.

3.3.1 Receivers

The following assumptions and approximations are included in the receiver sensitivity model:

- The receiver sensitivity is constant throughout its operating frequency range (minimum discernible signal).

- The selectivity skirts are log-linear.
- There are no receiver responses below F_{ar} and above F_{dr} (no spurious responses; significant image frequency responses are inputted as separate receiver responses).
- There is no signal discrimination; that is, any signal exceeding the threshold level will appear at the receiver output.

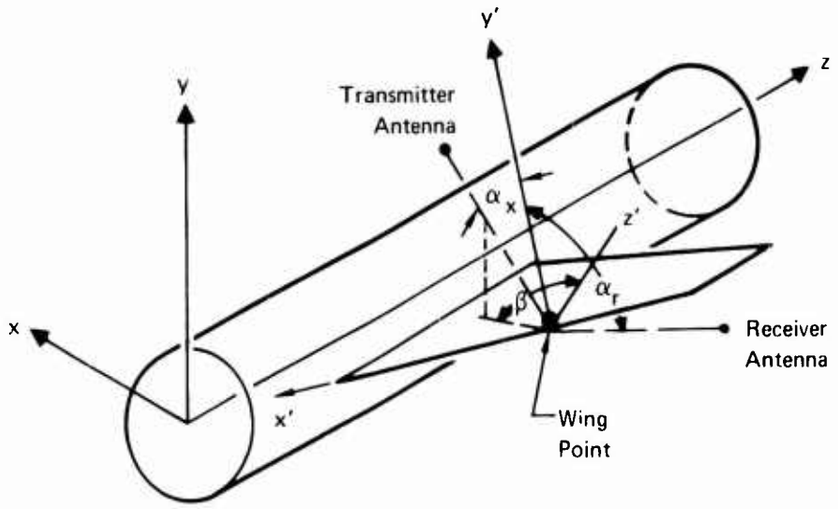

GP71-0386 9

FIGURE 9 DIFFRACTION COORDINATE SYSTEM WHEN THE PROPAGATION PATH IS AROUND THE WING EDGE. ATTENUATION FUNCTION IS CALCULATED USING ANGLES IN THIS COORDINATE SYSTEM

3.3.2 Transmitters

The following assumptions and approximations are included in the transmitter spectrum signature model:

- The power output is constant throughout the fundamental operating frequency range (i.e., transmitter rated peak power).
- The skirts are log-linear.
- The only spurious outputs are harmonics.
- The spectrum shape of each harmonic is the same as that of the fundamental.

3.3.3 Antennas

To approximate antenna patterns, the ECAC two level model was used. This model assumes:

- The gain in the main beam (G_{MB}) is constant for all angles within the 3 dB points.
- The gain outside of main beam is constant and equal to G_{MSL} (mean of sidelobe gain).
- The relationship of the approximation model to a typical radar antenna pattern is shown in Figure 10. Three-dimensional approximation patterns for typical radar and communication antennas are illustrated in Figures 11 and 12, respectively.
- The antennas are 100 percent efficient and there is a perfect impedance match to the load or source.

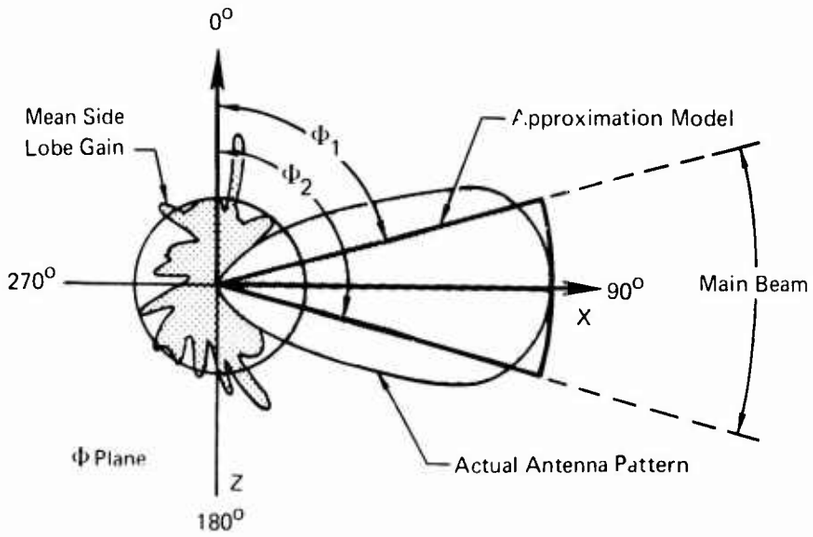

FIGURE 10 TWO-LEVEL APPROXIMATION MODEL FOR DIRECTIONAL ANTENNAS

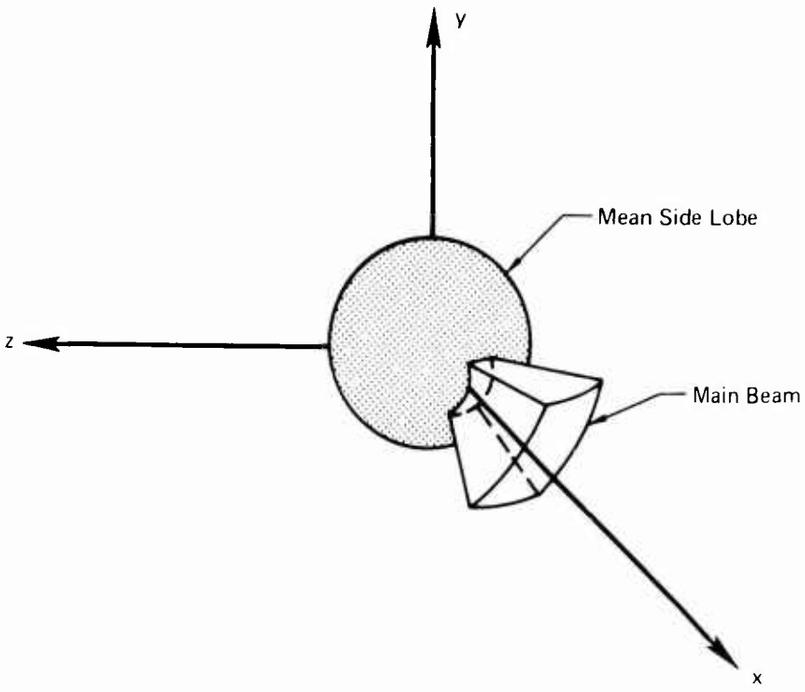

GP71 0386 11

FIGURE 11 ANTENNA MODEL APPLIED TO TYPICAL RADAR ANTENNA

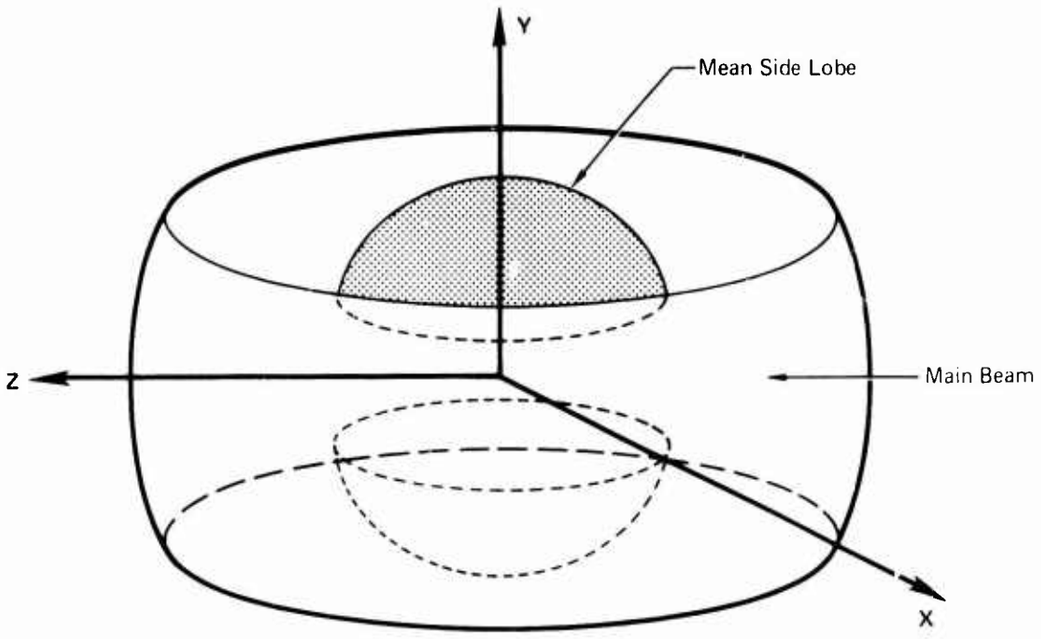

GP71 0386 12

FIGURE 12 ANTENNA MODEL APPLIED TO TYPICAL COMMUNICATIONS ANTENNA WITH DOUGHNUT PATTERN

3.3.4 Default Assumptions

The above assumptions and approximations apply to the basic mathematical model and are used in all calculations. Also included in the procedure are default assumptions for use only when certain equipment parameters are not known or not specified. These are as follows:

- Transmitter harmonics are 60 dB below the fundamental, and the highest significant harmonic is the third. (The program may accommodate to the sixth.)
- Receiver selectivity skirts conform with Figure 23, page 26, of MIL-I-6181D (to the -80 dB point).
- Transmitter spectrum skirts are as defined above.
- The antenna main beam gain is calculated using Equation (3.7).
- The antenna mean side lobe gain is calculated using Equation (3.8).

3.4 COMPUTER PROGRAM DESCRIPTION

3.4.1 Input Data Required

This is a brief summary of the input parameters required by ATACAP. The information is categorized into aircraft and subsystem data. Subsystem data is further divided into transmitter, receiver, and antenna data.

Aircraft Data. This data describes the physical dimensions of the aircraft and fits the cylindrical model to the actual vehicle shape. There is also an option for using a round or flat bottomed cylinder. All of the data is in inches and relative to butt-line (BL), water-line (WL), and fuselage station (FS) as commonly used on aircraft. The aircraft data required are summarized as follows (see Figure 5):

- Centroid WL
- Conical Nose Limit FS
- Bottom WL (for flat-bottomed cylinder)
- Location of Wing Corners (WL, BL, FS)

Subsystem Data. For the purpose of this analysis, a subsystem is defined as a group of single band transmitters and receivers using a series of common antennas. (Multiple bands and spurious responses are specified as separate receivers and transmitters.) The following data is used:

- Transmitter Data
  - Frequency range covered

- Skirt frequencies
- Output power
- Harmonics (up to sixth)
- Antennas used
- Emission bandwidth

- Receiver Data
  - Frequency range covered
  - Skirt frequencies
  - Sensitivity
  - Antennas used
  - Bandwidth

- Antenna Data
  - Antenna type
  - Location on aircraft (BL, WL, FS)
  - Main beam gain
  - Mean side lobe gain
  - Main beam limit angles

3.4.2 Analysis Procedure (Algorithm)

The procedure used in the program to implement the mathematical model is illustrated in the flowchart of Figure 13. The flowchart is more easily understood if the two analysis steps are kept in mind:

- Frequency coincidence
- EMI margin

The rest merely involves data routing and manipulation.

First, all the data for one aircraft is read from punched cards. The computer examines the data, decodes the alphanumeric codes, and inserts the default values where needed. Also, the highest security classification of the subsystems is determined so that it can be printed at the top and bottom of each page. A summary of the input and default data is then printed.

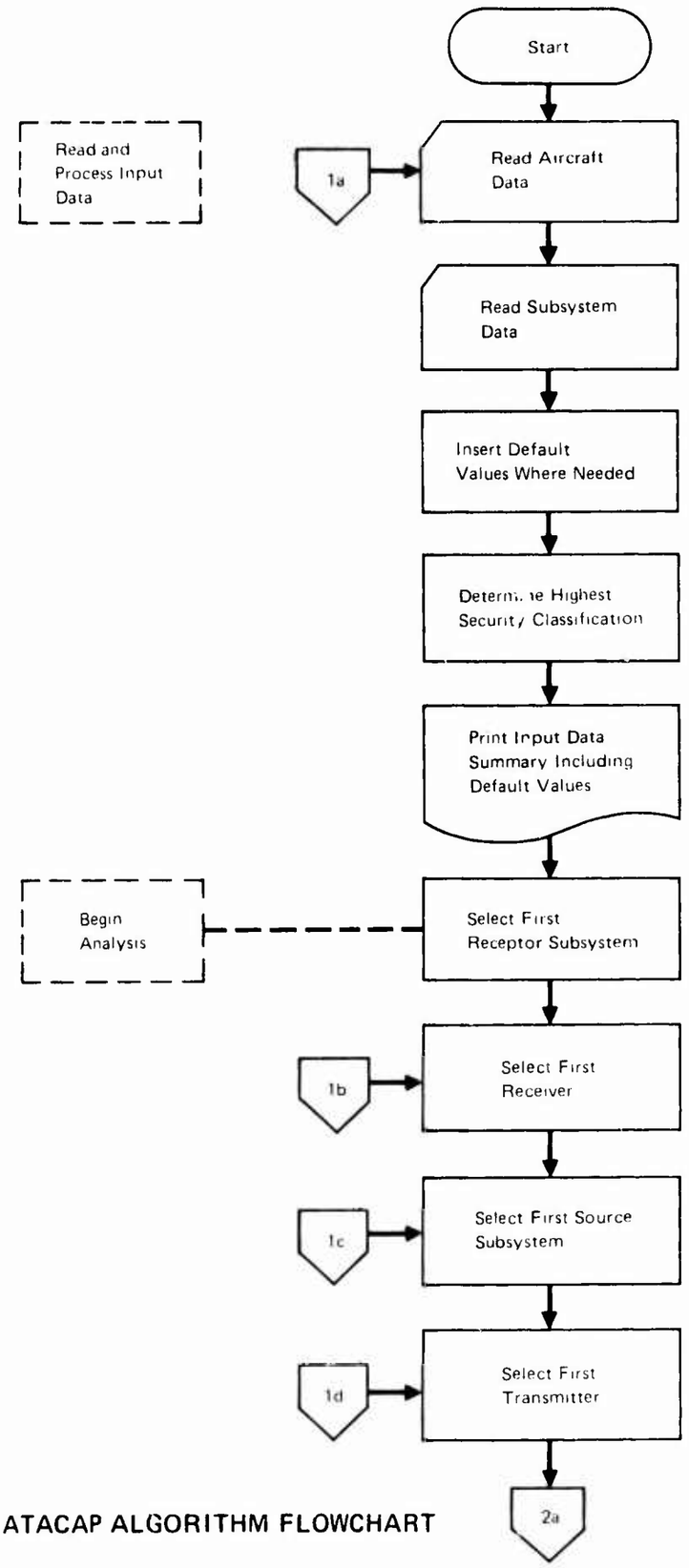

FIGURE 13 ATACAP ALGORITHM FLOWCHART

GP71 0386 13

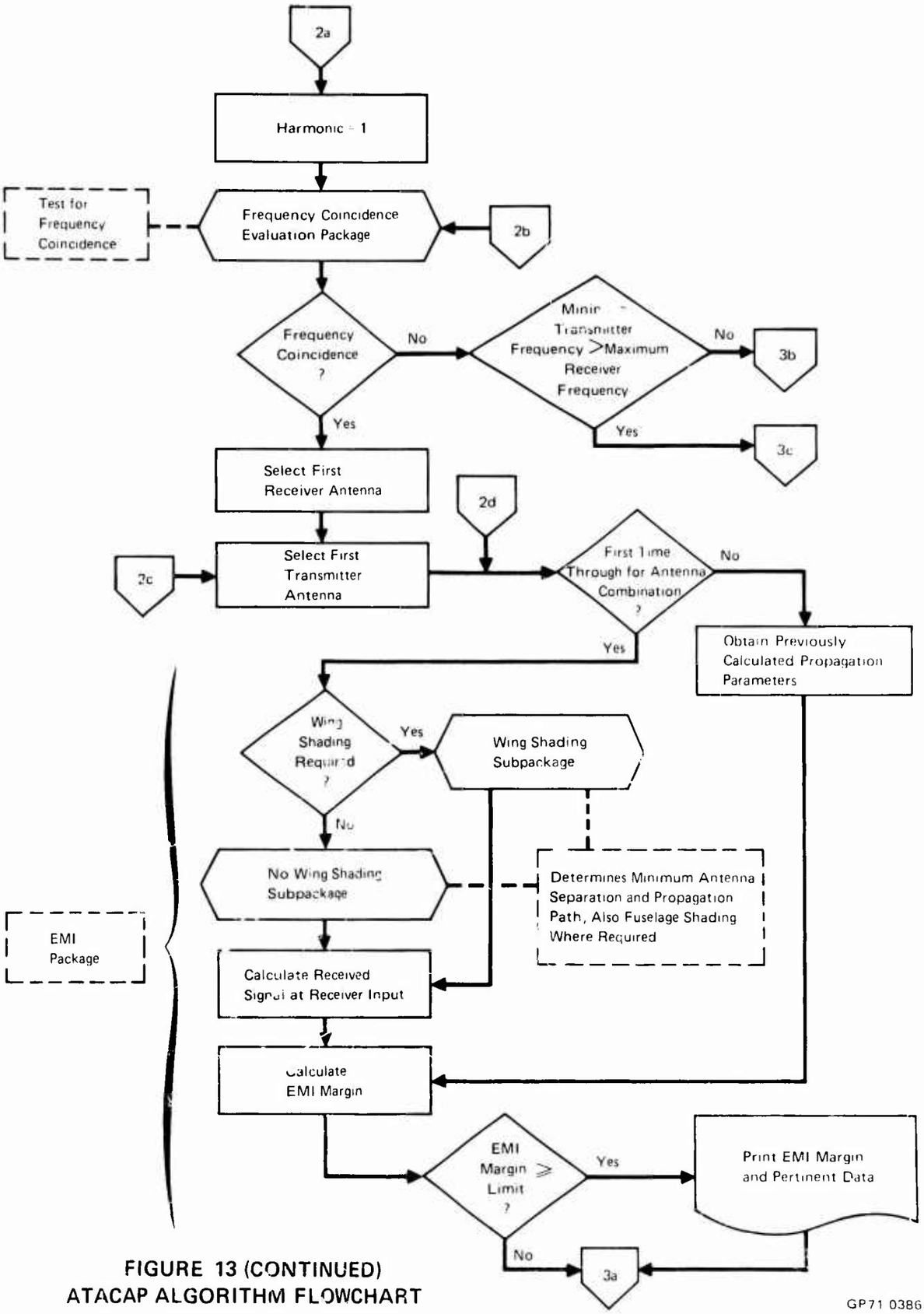

FIGURE 13 (CONTINUED)
ATACAP ALGORITHM FLOWCHART

GP71 0386 14

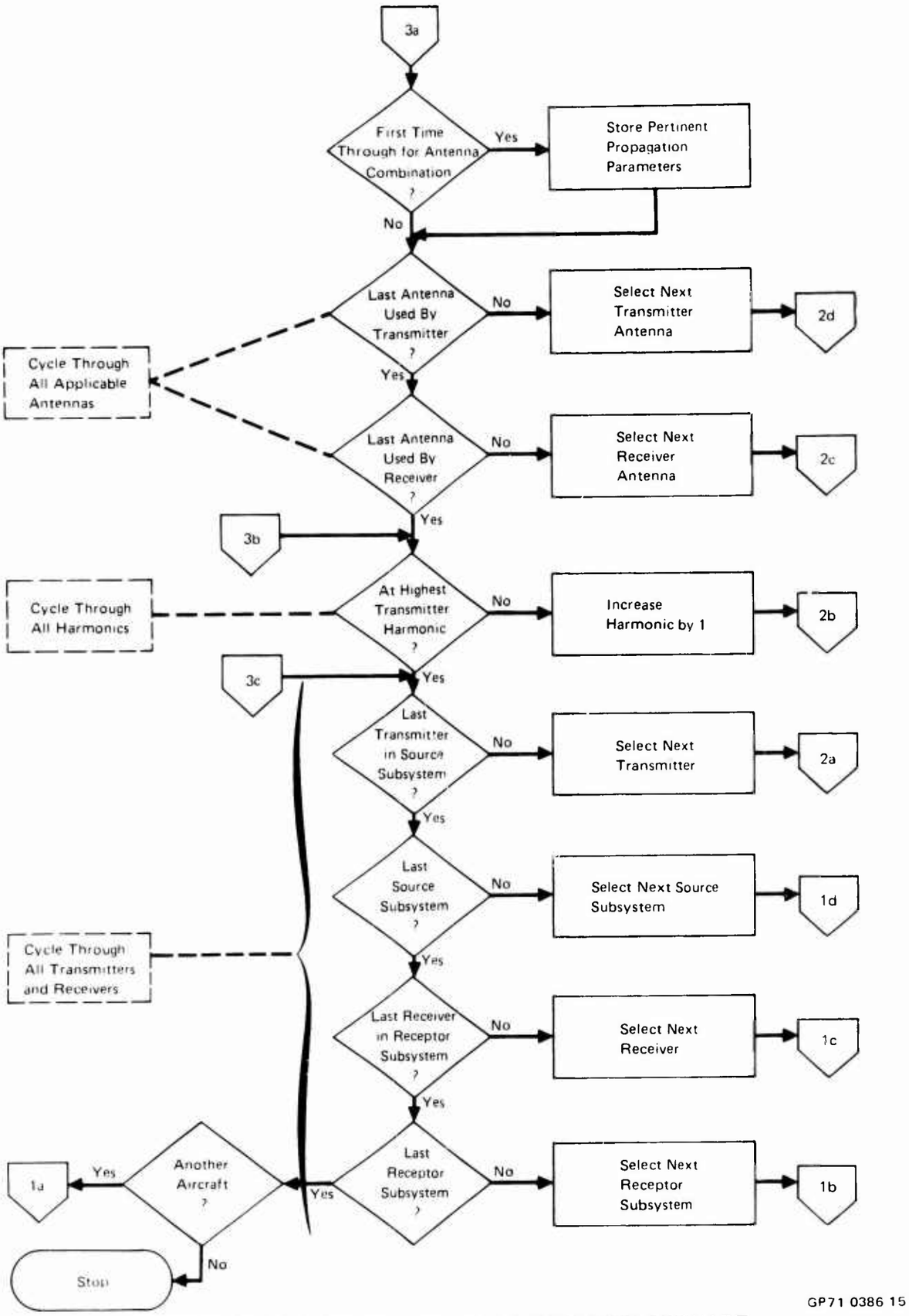

FIGURE 13 (CONCLUDED) ATACAP ALGORITHM FLOWCHART

The analysis involves selecting each receptor and determining what sources will interfere with it. A transmitter and receiver are selected from the data. Their frequency ranges, including the significant harmonics of the transmitter, are compared for coincidence. If no coincidence is found, compatibility is assumed, and they are not analyzed further. If there is coincidence, the EMI margin is determined by calculating the power received at the receiver front-end and comparing it to the receiver threshold. Worst-case EMI margins are calculated for all antenna combinations using the shortest path along the aircraft surface. All cases with margins exceeding the value specified in the input data are listed in the computer output. This procedure is repeated for all subsystem combinations on the vehicle. The EMI margin calculations include shading due to the aircraft surfaces, diffraction around wings, free space transmission losses, and coaxial cable losses.

The first time an antenna pair is encountered, the relevant propagation data such as distances, angles, antenna gains, etc., is stored. When the same antenna pair is again encountered at a different frequency (harmonic), only the frequency-dependent portions of the propagation equations are calculated. This saves much redundant calculation and speeds execution time considerably.

ATACAP contains a "new systems" feature which, for reasons of clarity, was omitted from the flowchart. This feature is used when a set of new subsystems is added to an existing vehicle. Since the existing avionics are assumed compatible with each other, they are not compared for EMI, but the new subsystems are compared with each other and with the old systems.

3.5 PRELIMINARY VERIFICATION

The ability of ATACAP to successfully predict EMI was checked by comparing early predictions with later tests on F-4 aircraft containing complex electronic subsystems and numerous antennas including ECM/RHAW equipment. Examination of Air Force, Navy, and MCAIR EMC test records showed 112 tests were conducted against which the ATACAP predictions could be compared. Of the interference cases found in the tests, only 2 percent of these cases were not predicted, and only 18 percent of the predicted interference cases did not appear.

The numerical accuracy of the model has also been checked by comparing the ATACAP predicted antenna coupling with 132 measurements on a KC-135 aircraft made by the Air Force Avionics Laboratory. The results are summarized in a histogram in Figure 14.

3.6 APPLICATION EXAMPLE AND SAMPLE OUTPUT

A typical use of ATACAP was a study performed for the USAF (FSCP 10R2 MOD2362). In this study, a number of transmitting and receiving subsystems were evaluated for compatibility on the F-4C, F-4D, and F-4E. A typical configuration is shown for the F-4D in Figure 15.

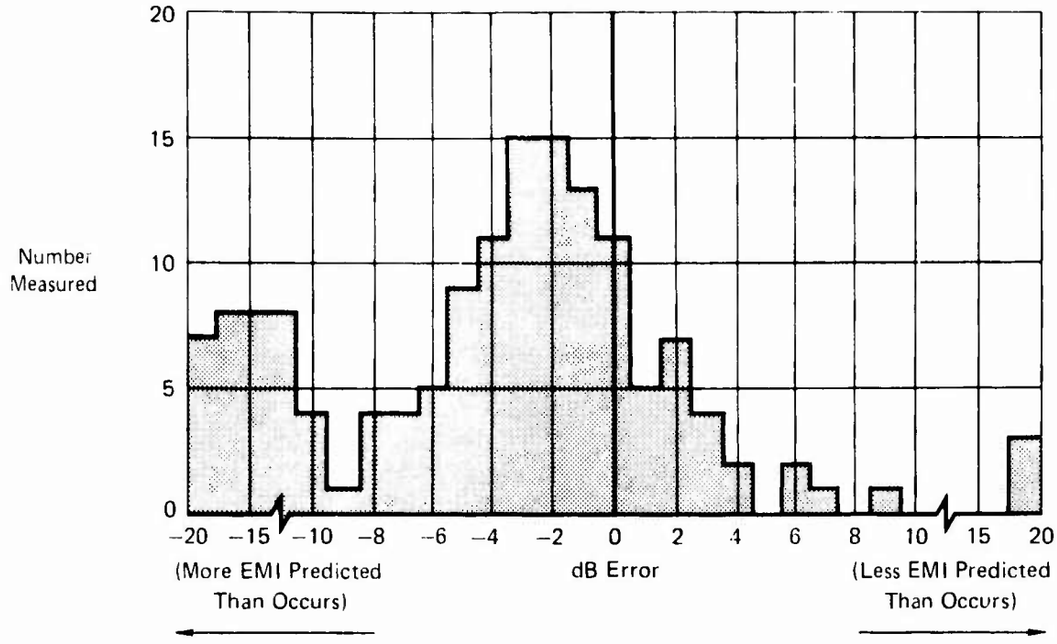

FIGURE 14 PRELIMINARY MODEL VERIFICATION

132 UHF ANTENNA COUPLING MEASUREMENTS ON KC-135

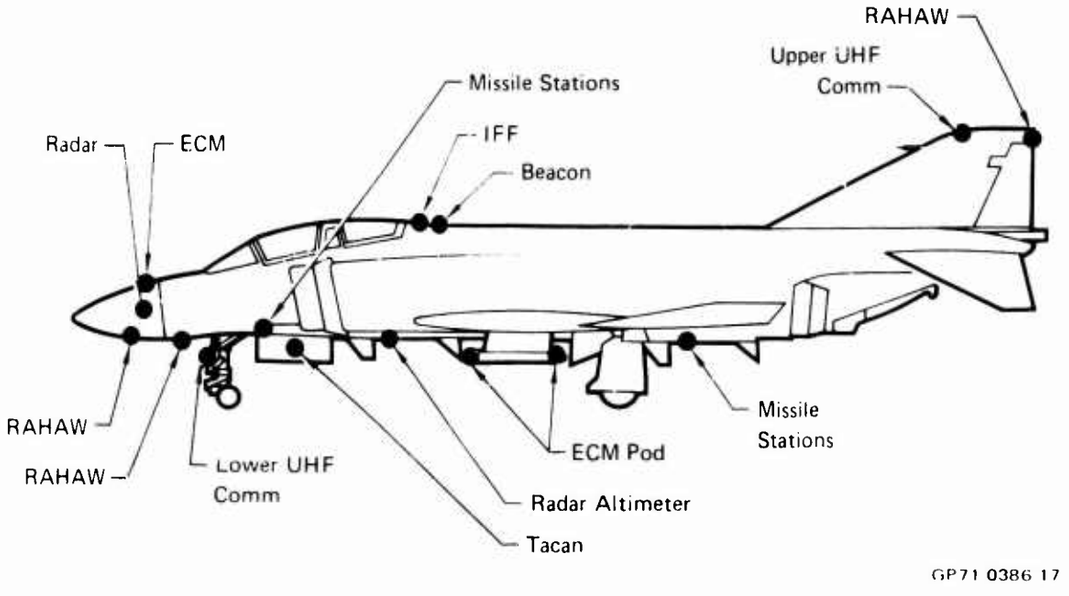

FIGURE 15 ANTENNA -TO-ANTENNA PROGRAM

F-4D ECM/RAHAW COMPATIBILITY STUDY (FSCP 10R2 MOD 2363)

The data for the subsystems of Figure 15 was fed into ATACAP, and a sample of the computer output is shown in Figure 16. The source and receptor subsystems are identified in the output for each predicted EMI situation. The EMI margin is shown, and other data is presented to aid the user in evaluating the interference and determining how to prevent it. The maximum EMI frequency is shown with the minimum and maximum coincidence frequencies. Also given are the free space propagation loss, the fuselage shading, and the wing shading, all in dB. Codes are given which show the type of frequency coincidence and the type of propagation path between the antennas. Finally, an output is provided for convenience to show whether or not both the receiver and transmitter have inter-subsystem blanking provisions. The results of this example analysis are summarized in Table I.

TABLE I ANALYSIS RESULTS

Susceptible Receivers	Radar	UHF Comm	Tacan	ECM	ECM POD	ECM POD	ECM POD	IFF	Radar Altimeter
RAHAW	39	17	ϕ	ϕ	63	−6	−17	ϕ	ϕ
RAHAW	ϕ	6	−4	ϕ	72	12	ϕ	6	ϕ
UHF Comm	ϕ	ϕ	ϕ	ϕ	26	32	− 3	ϕ	ϕ
Tacan	ϕ	7	ϕ	13	−3	ϕ	ϕ	ϕ	12
Radar	ϕ	ϕ	ϕ	ϕ	17	23	ϕ	ϕ	19
ECM	17	−10	18	ϕ	−4	16	ϕ	ϕ	ϕ
ECM POD	25	ϕ	ϕ	84	ϕ	ϕ	ϕ	−7	ϕ
IFF	ϕ	7	40	ϕ	ϕ	12	−6	ϕ	−3
Missile	−6	ϕ	ϕ	10	12	54	−1	11	ϕ

1 Numbers are EMI margin in dB (amount by which receiver threshold is exceeded)

GP71-0386-18

2 ϕ shows EMI margin less than −20 dB

F-4E

ATACAP COMPUTER PROGRAM TEST RUN

RECEPTOR -- SUBSYSTEM =IMAGPOD , RCVR =LO BND

SOURCE SUBSYSTEM	XMTR IDENT	HARM	MAX EMI FREQ- MHZ	MIN COINC FREQ- MHZ	MAX COINC FREQ- MHZ	COINCIDENCE XMTR	COINCIDENCE RCVR	BLKG
UHF COMM	COMXTR	3	1000.000	986.689	1362.271	MAIN	MAIN	NO

EMI MARG	RCVR ANTENNA IDENT	RCVR ANTENNA LOBE	XMTR ANTENNA IDENT	XMTR ANTENNA LOBE	*--PROPAGATION--* FR SP	FUSL	WING	PROP CODE P	W	XW	WR
-36.5	INPYOR	MAIN	NOSEOR	MAIN	-42.5	0.0	0.0	9	0	0	0
-34.3	INPYOR	MAIN	ADF	MAIN	-43.3	0.0	0.0	9	0	0	0
-39.5	OBPYOR	MAIN	NOSEOR	MAIN	-45.5	0.0	0.0	9	0	0	0
-37.1	OBPYOR	MAIN	ADF	MAIN	-46.1	0.0	0.0	9	0	0	0
-37.4	CENTOR	MAIN	NOSEOR	MAIN	-43.4	0.0	0.0	9	0	0	0
-35.2	CENTOR	MAIN	ADF	MAIN	-44.2	0.0	0.0	9	0	0	0

SOURCE SUBSYSTEM	XMTR IDENT	HARM	MAX EMI FREQ- MHZ	MIN COINC FREQ- MHZ	MAX COINC FREQ- MHZ	COINCIDENCE XMTR	COINCIDENCE RCVR	BLKG
TRANSPDR	TSPXTR	1	1090.000	942.294	1237.706	MAIN	MAIN	YES

EMI MARG	RCVR ANTENNA IDENT	RCVR ANTENNA LOBE	XMTR ANTENNA IDENT	XMTR ANTENNA LOBE	*--PROPAGATION--* FR SP	FUSL	WING	PROP CODE P	W	XW	WR
57.9	INPYOR	MAIN	TOPBCK	MAIN	-40.3	-7.6	-15.0	7	1	21	40
61.3	OBPYOR	MAIN	TOPBCK	MAIN	-43.8	-3.4	-12.3	7	1	21	40
52.1	CENTOR	MAIN	TOPBCK	MAIN	-46.4	-3.3	-18.9	7	1	21	21

SOURCE SUBSYSTEM	XMTR IDENT	HARM	MAX EMI FREQ- MHZ	MIN COINC FREQ- MHZ	MAX COINC FREQ- MHZ	COINCIDENCE XMTR	COINCIDENCE RCVR	BLKG
TACAN	TACXTR	1	1025.000	886.102	1283.126	MAIN	MAIN	YES

EMI MARG	RCVR ANTENNA IDENT	RCVR ANTENNA LOBE	XMTR ANTENNA IDENT	XMTR ANTENNA LOBE	*--PROPAGATION--* FR SP	FUSL	WING	PROP CODE P	W	XW	WR
56.0	INPYOR	MAIN	TACUPR	MAIN	-40.4	-6.5	-17.9	7	1	21	40
79.9	INPYOR	MAIN	TACLWR	MAIN	-40.9	0.0	0.0	9	0	0	0
57.4	OBPYOR	MAIN	TACUPR	MAIN	-41.5	-3.5	-18.4	7	1	21	40
76.2	OBPYOR	MAIN	TACLWR	MAIN	-44.6	0.0	0.0	9	0	0	0
50.9	CENTOR	MAIN	TACUPR	MAIN	-45.1	-2.8	-22.0	7	2	21	21
79.0	CENTOR	MAIN	TACLWR	MAIN	-41.8	0.0	0.0	9	0	0	0

IMAGPOD

GP71-0386-56

FIGURE 16 SAMPLE ATACAP COMPUTER OUTPUT FORMAT

SECTION 4

WIRE-TO-WIRE COMPATIBILITY ANALYSIS PROGRAM (WTWCAP)

4.1 BACKGROUND

Achieving wire-to-wire compatibility on modern, high-performance air vehicles is a formidable task. An F-4 aircraft, for example, contains over 16,000 wire segments. In advanced vehicles, more wires are needed, and higher density bundles with smaller wires and thinner insulation are being used. An analysis tool is needed that can rapidly and reliably indicate the EMI in such bundles.

The current state-of-the-art was determined by reading all of the available reports (Refs 7 - 14). Investigation was conducted into applicable electromagnetic field theory, circuit theory, transmission line theory, and numerical analysis methods. From this, mathematical models and analysis techniques were tested on the computer and compared to measured data.

4.2 DETAILED DESCRIPTION OF WTWCAP PREDICTION MODEL

4.2.1 Basic Model

Coupling between wires is a multi-wire transmission line problem because the coupling mechanisms are distributed along the wires. In general, RF magnetic and electric field effects are interrelated and cannot be separated. However, at frequencies where the wavelength is large compared to the bundle lengths, a lumped-parameter circuit quite accurately approximates the distributed parameter circuit. Such a lumped parameter pi circuit is illustrated in Figure 17 for two wires above a ground plane.

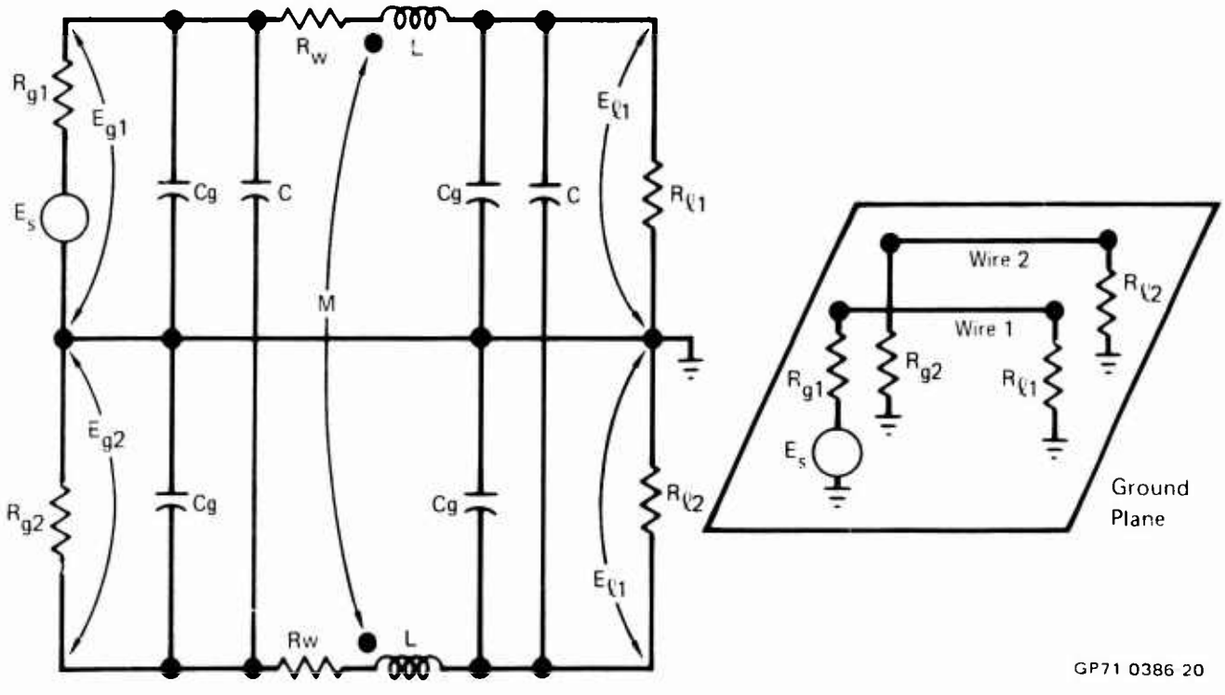

FIGURE 17 TWO-WIRE COUPLING WITH SINGLE PI LUMPED PARAMETER CIRCUIT MODEL

As the frequency is increased, accuracy is lost because the lumped parameters no longer represent the distributed parameters. However, if the number of circuit pi sections is increased, as shown in Figure 18, accuracy can be maintained to as high a frequency as desired. This can be seen in Figure 19 which shows the transfer function for one, two, and three pi sections. A mathematical justification for this is presented in the Appendix.

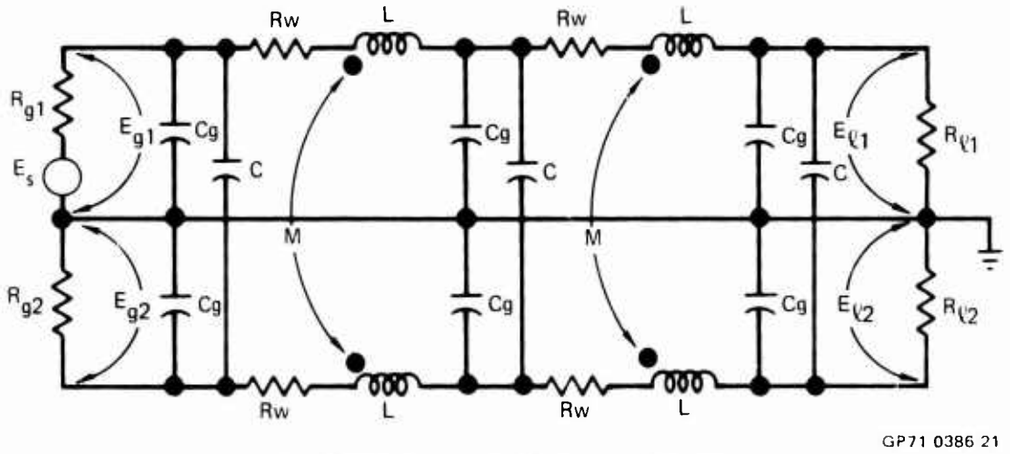

FIGURE 18 TWO PI CIRCUIT MODEL

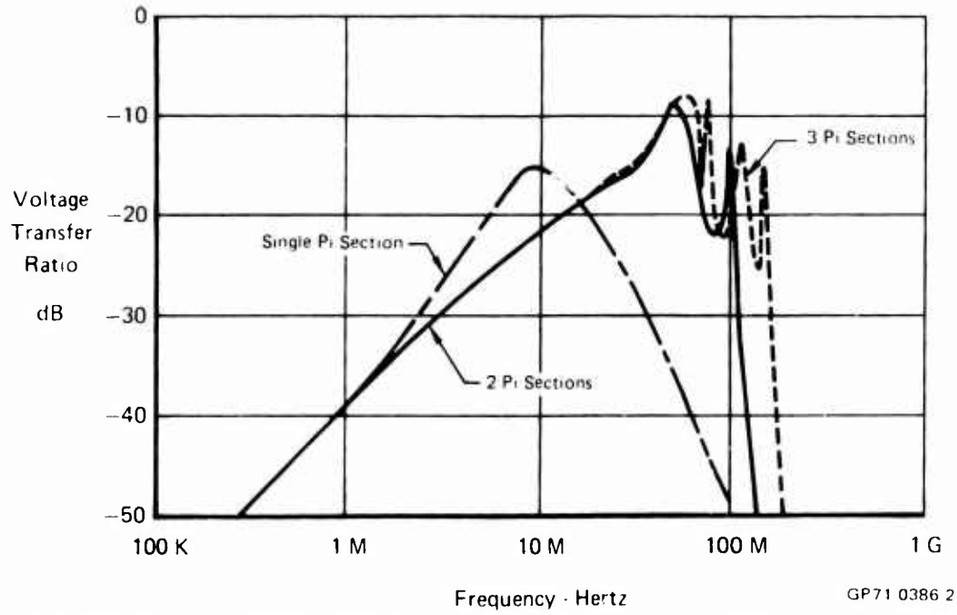

FIGURE 19 TRANSFER FUNCTION FOR 1, 2, and 3 PI LUMPED PARAMETER CIRCUIT MODELS (10 FT WIRES)

Frequency domain is used for the analysis because it allows the use of a varying number of pi sections. A single pi circuit is used at low frequencies, a double pi circuit at higher frequencies, and so on. Thus, maximum computer efficiency is achieved since the least complicated circuit is used consistent with accuracy. Also, frequency-dependent wire parameters, such as skin effect on wire resistance, can be included. Furthermore, the complex matrix equations resulting from frequency domain analysis can be more readily implemented on the computer than the numerical methods required to solve simultaneous differential equations in the time domain. Finally, frequency domain is directly relatable to EMC tests and specifications so that they can be applied directly to the analysis. If time domain parameters of the interference are required, they can be obtained from the complex numbers by the inverse Fourier transform.

For the wire-to-wire problem, simultaneous analysis is used since it is more efficient on the computer and can account for second and higher order effects. (Higher order effects result from signals coupling onto one wire, these signals then coupling onto other wires, these signals coupling onto still more wires, and so on. In other words, every wire effects every other wire.) By solving the entire circuit simultaneously, these effects are automatically included. Our investigation showed it is practical to analyze a two pi circuit of 60 conductors on the CDC 6600 computer ($250K_8$ memory). Larger bundles can be divided and run in segments, or only the worst-case sources and receptors can be analyzed.

4.2.2 Circuit Parameters

The parameters involved (Figure 17) are the inter-wire capacitances and mutual inductances, wire self-inductance, wire resistance, and wire capacitance to ground. These are divided into frequency-independent and frequency-dependent categories. In the following, all units are in the rationalized MKS system.

4.2.2.1 Constant Parameters

The frequency-independent parameters include the external self-inductances, mutual inductances, capacitance to ground, and inter-wire capacitances.

Self-inductance of wires and shields are best determined by considering the effects of internal and external magnetic fields. Skin effect involves only the internal fields, so that the external fields are frequency independent. The external self-inductance of a wire of radius r_1, length l, height h, carrying a current I_1, as shown in Figure 20, is defined by (Ref. 12)

$$L_e = \frac{1}{I_1} \int_{A_1} \vec{B}_1 \cdot d\vec{A}_1. \qquad (4.1)$$

$\vec{B}_1$ is the magnetic flux density resulting from I_1, and A_1 is the surface between the wire and its image in the ground plane. Evaluating Equation (4.1) for Figure 20 leads to

$$L_e = \frac{\mu}{2\pi} \log_e \left(\frac{2h}{r_1} - 1 \right) \tag{4.2}$$

henries/meter where μ is the permeability of the medium. Since Equation (4.2) only involves the external fields, it also applies if the wire is hollow. Thus, this applies both to solid wires and to shields.

The situation for the mutual inductance between two wires is shown in Figure 21. Mutual inductance is defined by (Ref. 12)

$$M_{12} = \frac{1}{I_1} \int_{A_2} \vec{B}_1 \cdot d\vec{A}_2 \tag{4.3}$$

where B_1 is the magnetic flux density from wire 1 and A_2 is formed by wire 2 and its ground plane image. Note that reciprocity applies so that $M_{12} = M_{21}$. For the mutual inductance to a wire or shield to another wire or shield, Equation (4.3) results in

$$M_{12} = \frac{\mu}{4\pi} \log_e \left[\left(\frac{2h}{s} \right)^2 + 1 \right] \tag{4.4}$$

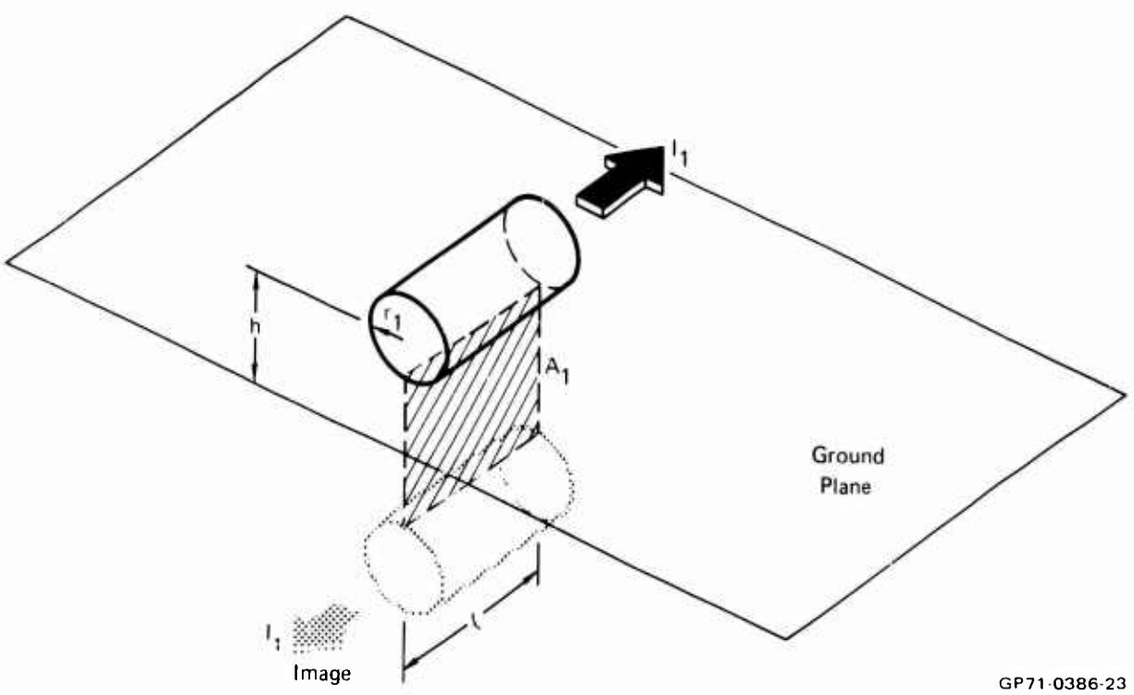

FIGURE 20 EXTERNAL SELF-INDUCTANCE OF WIRE OR SHIELD

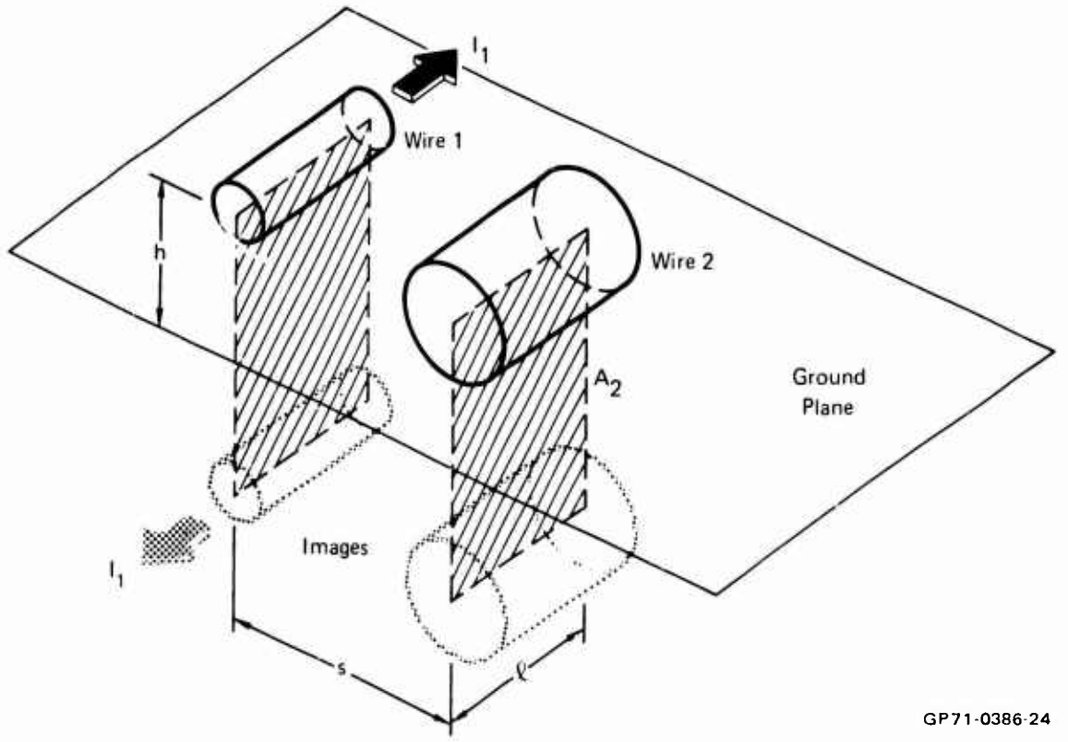

FIGURE 21 MUTUAL INDUCTANCE BETWEEN WIRES OR SHIELDS

henries/meter where s is the separation between centers. For the case of a wire to its own shield, as shown in Figure 22, Equation (4.3) becomes

$$M_{ws} = \frac{\mu}{4\pi} \log_e \left[\frac{2h}{r_o} - 1 \right] \tag{4.5}$$

where r_o is the outer radius of the shield.

Capacitance parameters are determined from the basic electrostatic charge and potential relations. For the case of two wires above ground, as shown in Figure 23, the relations between charge and potential are (Ref. 12)

$$\begin{aligned} \phi_1 &= p_{11} Q_1 + p_{12} Q_2 \\ \phi_2 &= p_{21} Q_1 + p_{22} Q_2. \end{aligned} \tag{4.6}$$

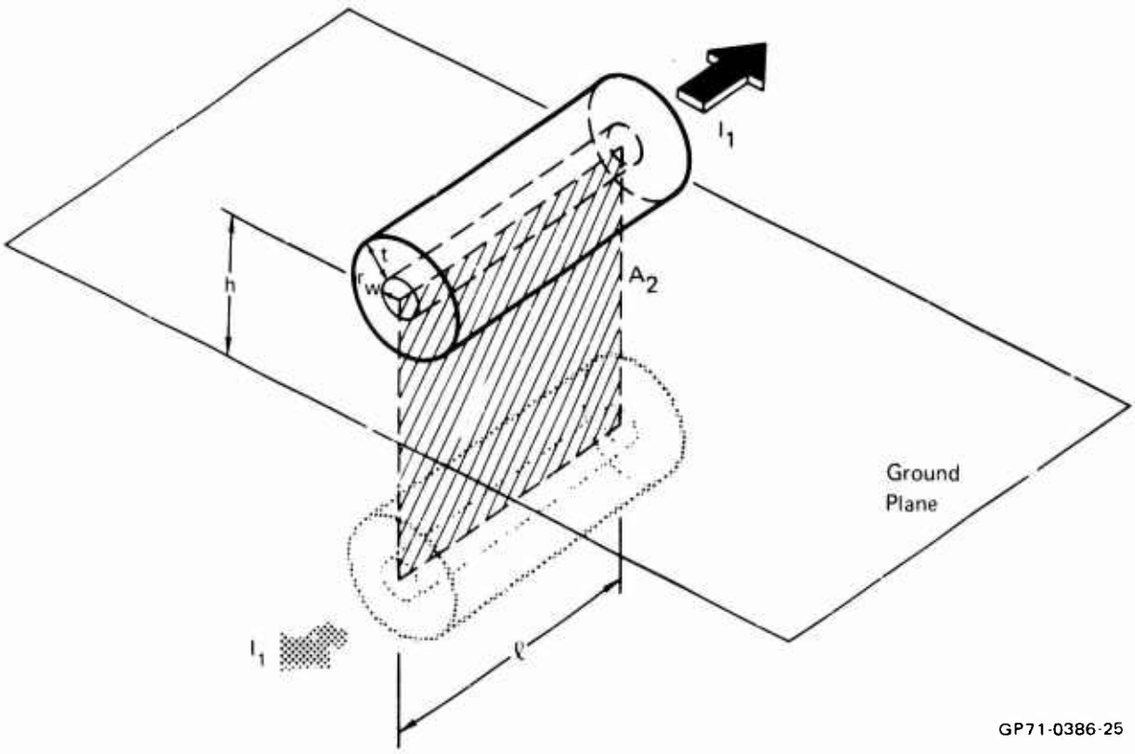

FIGURE 22 MUTUAL INDUCTANCE FROM INTERNAL WIRE TO SHIELD

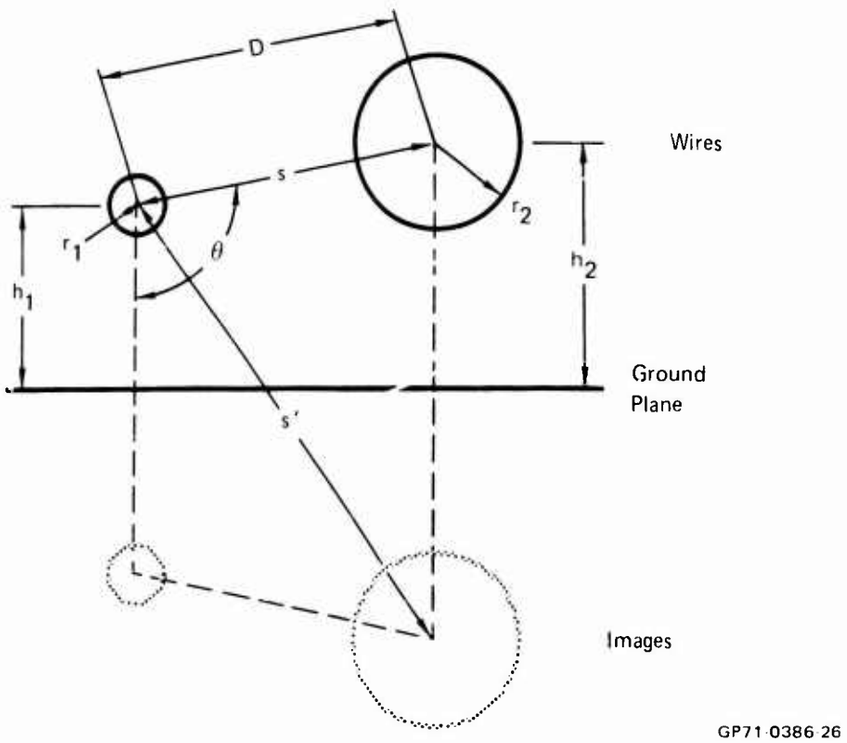

FIGURE 23 SITUATION FOR OPEN WIRE CAPACITANCE CALCULATION

Here, ϕ_1 and ϕ_2 are the potentials, and Q_1 and Q_2 are the charges on wires 1 and 2, respectively. For given charges, the potentials can be determined using the method of equipotential surfaces (Refs. 12, 13, 14). Referring to Figure 23, the coefficients of Equation (4.6) are as follows:

$$p_{11} = \cosh^{-1}(h_1/r_1) \tag{4.7}$$

$$p_{22} = \cosh^{-1}(h_2/r_2) \tag{4.8}$$

$$p_{12} = p_{21} = \frac{1}{2}\left\{\cosh^{-1}\left[\frac{s^2 + (r_1^2 - r_2^2)}{2sr_1}\right] + \cosh^{-1}\left[\frac{s^2 - (r_1^2 - r_2^2)}{2sr_2}\right]\right.$$
$$\left. - \cosh^{-1}\left[\frac{s'^2 + (r_1^2 - r_2^2)}{2s'r_1}\right] - \cosh^{-1}\left[\frac{s'^2 - (r_1^2 - r_2^2)}{2s'r_2}\right]\right\} \tag{4.9}$$

where s' is the diagonal separation to the image and is given by

$$s' = \sqrt{s^2 + (2h_1)^2 - 4sh\cos\theta}. \tag{4.10}$$

Then, the capacitance relations are

$$C_{1G} = \frac{2\pi\epsilon\, p_{11}}{\det} \tag{4.11}$$

$$C_{2G} = \frac{2\pi\epsilon\, p_{22}}{\det} \tag{4.12}$$

$$C_{12} = \frac{-2\pi\epsilon_{eff}\, p_{12}}{\det} \tag{4.13}$$

where $\det = p_{11}\, p_{22} - p_{12}^2$ is the determinate of the p matrix.

The effective permittivity, ϵ_{eff}, is given by (Ref. 7)

$$\epsilon_{eff} = \epsilon_0 + \frac{\left[\frac{R_1 + R_2}{r_1 + r_2}\right]^2 - 1}{\frac{1}{2}\left[\frac{2s + R_1 + R_2}{r_1 + r_2}\right]^2 - 1}(\epsilon - \epsilon_0) \tag{4.14}$$

where R_1 and R_2 are the wire radii including the insulation.

In the above, C_{1G} and C_{2G} are the capacitances to ground, and C_{12} is the inter-wire capacitance in farads/meter. These equations apply to hollow as well as solid wires and therefore can be used for shield-to-shield, shield-to-wire, and shield-to-ground capacitances.

A similar approach can be used for wires within a shield. The shield is used for reference in place of the ground plane, and capacitance from

wires within the shield to external wires and to the ground plane are assumed zero. The model can handle up to 4 shielded wires. For a single shielded wire, the wire to shield capacitance is (Ref. 12)

$$C_{ws} = \frac{2\pi\epsilon}{\log_e\left(\frac{r_{si}}{r_w}\right)} \tag{4.15}$$

farads/meter where r_{si} is the internal shield radius and r_w is the inner conductor radius.

For shielded groups of from two to four wires, the following procedure is used: The potential coefficient matrix terms can be calculated using

$$p_{ij} = \begin{cases} \cosh^{-1}(h_2/r_w) & \text{for } i-j=0 \\ \log_e(D_1/D_2) & \text{for } |i-j| \text{ odd} \\ \log_e \dfrac{2a+2b+c}{2b+c} & \text{for } |i-j| \text{ even} \end{cases} \tag{4.16}$$

where

$$b = x(r_w + t_w) \tag{4.17}$$

In Equation (4.17), x is given in Table II - r_w is the wire radius, t_w is the wire insulation thickness. Next,

$$h_1 = (r_{si}^2 + r_w^2 - b^2)/(2b) \tag{4.18}$$

where R_{si} is the shield internal radius. Then,

$$a = \sqrt{h_1^2 - r_w^2} \tag{4.19}$$

$$c = h_1 - b - a \tag{4.20}$$

$$h_2 = a + c \tag{4.21}$$

The expressions for D_1 and D_2 are given in Table II.

TABLE II SHIELDED WIRE CAPACITANCE PARAMETERS

No. of Wires in Shield	X (Eq 4.17)	D_1	D_2
2	1.0000	$b + h_1 + a$	$2b + c$
3	1.1547	$\sqrt{(h_1+a)^2 + b^2 + (h_1+a)\,b}$	$\sqrt{b^2 + (b+c)^2 + b\,(b+c)}$
4	1.4142	$\sqrt{(h_1+a)^2 + b^2}$	$\sqrt{b^2 + (b+c)^2}$

GP71-0386-19

The inverse p matrix is calculated such that

$$[c] = [p]^{-1} \tag{4.22}$$

Then, the capacitances are found using

$$C_{is} = 2\pi\epsilon \sum_{\ell=1}^{n} c_{i\ell} \tag{4.23}$$

$$C_{ij} = -2\pi\epsilon\, c_{ij} \quad \text{for } i \neq j \tag{4.24}$$

C_{is} is the capacitance between the i^{th} wire and the shield, and C_{ij} is the capacitance between the i^{th} and j^{th} wires in farads/meter.

4.2.2.2 Frequency-Dependent Parameters

These parameters involve the internal impedance of the wires and shields.

The Helmholtz equation can be applied to this problem, to obtain complex internal impedance of a solid wire (Ref. 12)

$$Z_{int} = \frac{j}{\pi r_o}\sqrt{\frac{\pi f \mu}{2\sigma}}\left[\frac{\mathrm{Ber}\left(\frac{\sqrt{2}}{\delta} r_o\right) + j\,\mathrm{Bei}\left(\frac{\sqrt{2}}{\delta} r_o\right)}{\mathrm{Ber}'\left(\frac{\sqrt{2}}{\delta} r_o\right) + j\,\mathrm{Bei}'\left(\frac{\sqrt{2}}{\delta} r_o\right)}\right] \tag{4.25}$$

where the primes denote differentiation of the Bessel functions with respect to their arguments. Breaking this into real and imaginary parts leads to expressions for the resistance and internal self-inductance per meter of wire. In practice, computations of these involved expressions can be simplified by fitting them with approximation curves. In the computer program, these fitted curves are much faster and give results within 2 percent of the above expression.

Frequency-dependent shield parameters can be analyzed in the same fashion. For large radius of curvature and large shield thickness compared to skin depth, the following simplified results can be applied for the resistance and inductance of a shield (Ref. 12)

where

$\delta = 1/\sqrt{\pi i \mu \sigma}$

$R_s = \dfrac{1}{\sigma\delta}$

t_s = shield thickness

D_s = shield inside diameter

$$R_{SH} = \frac{R_s}{\pi D_s}\left[\frac{\sinh\left(\frac{2t_s}{\delta}\right) + \sin\left(\frac{2t_s}{\delta}\right)}{\cosh\left(\frac{2t_s}{\delta}\right) - \cos\left(\frac{2t_s}{\delta}\right)}\right] \tag{4.26}$$

and

$$\omega L_{iSH} = \frac{R_s}{\pi D_s}\left[\frac{\sinh\left(\frac{2t_s}{\delta}\right) - \sin\left(\frac{2t_s}{\delta}\right)}{\cosh\left(\frac{2t_s}{\delta}\right) - \cos\left(\frac{2t_s}{\delta}\right)}\right] \tag{4.27}$$

4.2.3 Application of Model to Twisting and Shielding

Twisting and shielding are important methods for controlling wire-to-wire EMI. Consequently, the program must have an accurate method for accounting for them.

Since most shields used in aerospace vehicles are low permeability, their primary effect is to reduce capacitive coupling. In the model, therefore, capacitance from shielded wires to external wires is set to zero. The low permeability, however, does not prevent magnetic coupling, and the mutual inductance is retained. Shield pigtails are modeled as inductances of 0.02 μhy if the exact impedance is not known. An application of this to the WTWCAP model is illustrated in Figure 24.

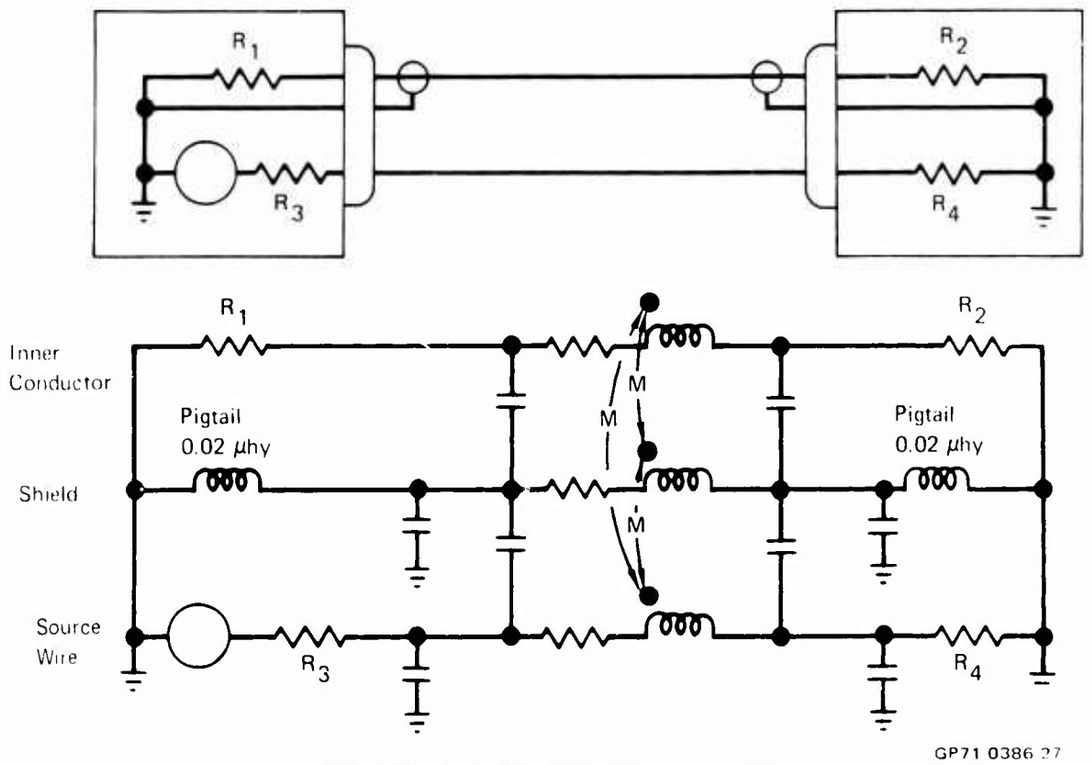

FIGURE 24 SHIELDED WIRE MODEL

To reduce magnetically coupled EMI, twisted wires are used. This situation is illustrated in Figure 25 in which currents in the source wire (I_s) induce equal noise currents (I_n) in the two receptor wires. In practice, however, the receptor wires are not perfectly balanced with respect to the source wire. For this reason, the mutual inductance in the model from the source wire to the return wire is reduced slightly.

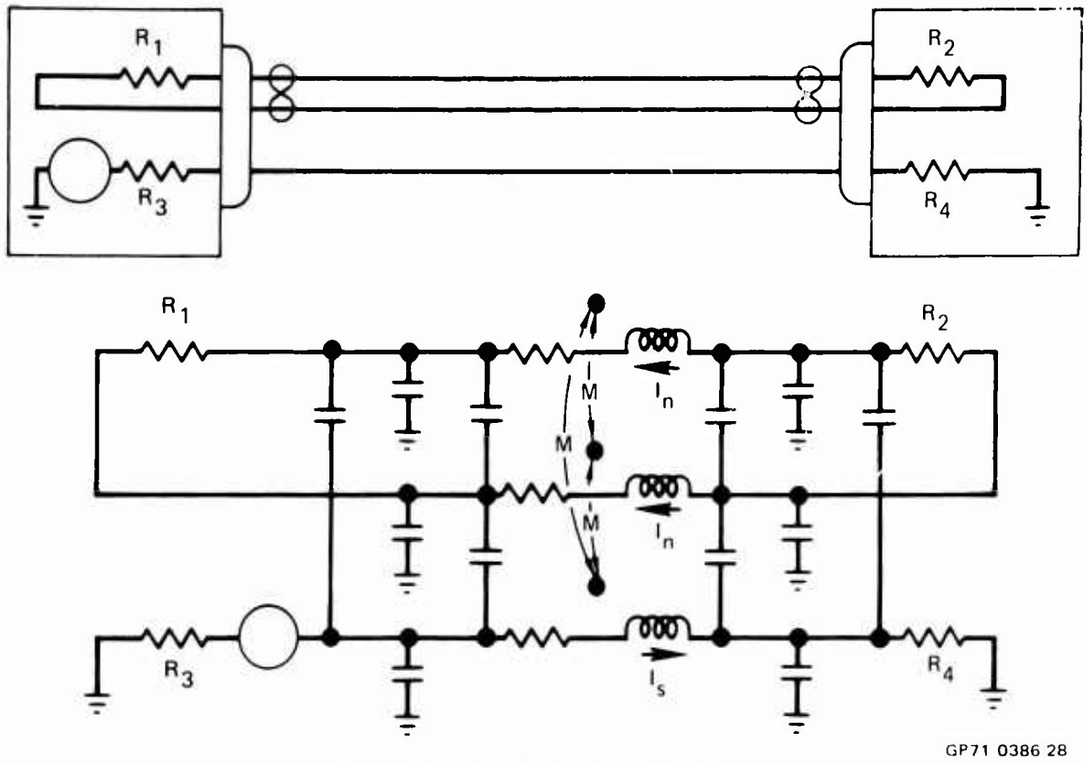

FIGURE 25 TWISTED PAIR MODEL

4.2.4 Wire Separation Considerations

An extensive investigation of wire positioning within a bundle showed that the exact location of a given wire cannot be determined exactly but can only be estimated on a probability basis. For this reason and since worst-case EMI is desired, the wire parameters are calculated assuming minimum separation. The only exception is for twisted groups, as previously discussed.

4.3 COMPUTER PROGRAM DESCRIPTION

4.3.1 Input Data Required

The input data is easily obtained from information usually available to the user. In some cases, options are available to allow the user to specify data in the form in which it is available.

Wire Characteristics Table - To free the user from having to specify and remember nominal wire characteristics for each type of wire, a table of these parameters is first specified. Each type of wire is identified by a user supplied, alphanumeric name (e.g., 22TFE to identify 22 gage, teflon

insulated wires). Wire diameter, conductivity, insulation thickness and dielectric constant, and shield data, where applicable, are specified. In specifying the bundle data, only the wire name is used to identify the type, and the computer obtains the nominal characteristics from the table.

General Bundle Data - This data aids in identifying the bundle in a run and gives general parameters. The following are included:

- Bundle designation or nomenclature
- Subsystem and unit nomenclature
- Connector nomenclature
- Bundle length
- Height above ground

Individual Wire Data - This data specifies parameters associated with each wire, twisted wire groupings, and grounding. The following are included:

- Wire type designation
- Twisted group information
- Pin designations
- Signal reference or return
- Function of loads (voltage source, voltage sensitive load, current source, current sensitive load, grounded wire, etc.)
- Termination impedances
- Shield termination data
- Source and/or susceptibility spectra

Spectra data - Source and/or susceptibility spectra data can be specified three ways:

- Read-in from measured data
- Built-in EMC specifications
- Built-in spectrum calculation routines.

If the spectrum is known, such as from measured data, it can be specified by giving points on the curve. The program interpolates (log-linearly) between these points. If EMC military specification spectra for power lines is desired, the program has built-in MIL-STD-704A ripple data and MIL-STD-461

data for conducted susceptibility. Finally, if commonly encountered time-domain wave forms are known, the program will calculate the spectrum from the wave form parameters. These waveforms include:

- Step function (switch)
- Rectangular pulse
- Trapezoidal pulse
- Spike

Additional Inputs - Additional inputs provide control of the analysis and output. A title is read and printed in the output for run identification. A printout limit is specified, and cases with EMI margins below that level are not printed. Details of a given frequency range and a plot of the calculated EMI can be ordered.

4.3.2 Default Assumptions and Options

As with ATACAP, many parameters that are required are unknown or unavailable. The default assumptions and options contained in WTWCAP are summarized below.

Unless otherwise specified, the following bundle parameters are assumed:

- 4 inch height above ground
- 10K load impedance
- 0.02 μhy impedance from the shield termination to ground

If the bundle length is unknown and the box locations in the vehicle are known, the length is approximated by calculating twice the distance between the boxes.

4.3.3 Analysis Procedure (Algorithm)

An algorithm flowchart is presented in Figure 26. The input data is first read and processed. The alphanumeric codes are then decoded and tested for errors, the default values are inserted, and the appropriate spectra data are calculated, where required. The input data summary is printed.

The constant circuit model wire parameters are then calculated. Where shields are encountered, they are set up as additional wires with the appropriate parameters. For shielded wire groups, the capacitance to ground and capacitance to external wires are set to zero. Mutual and external self-inductances are then computed for all wires.

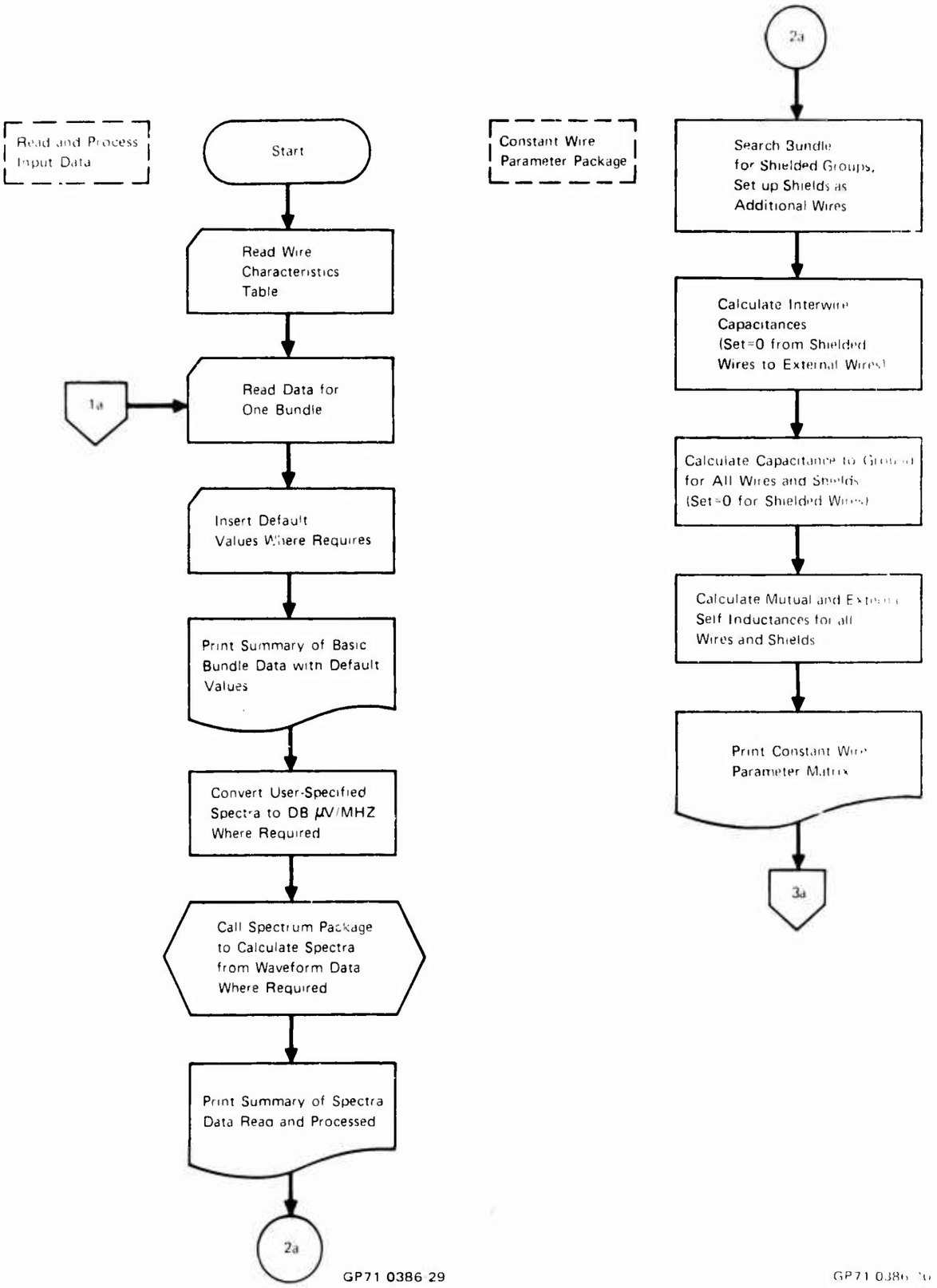

FIGURE 26 WTWCAP ALGORITHM FLOWCHART

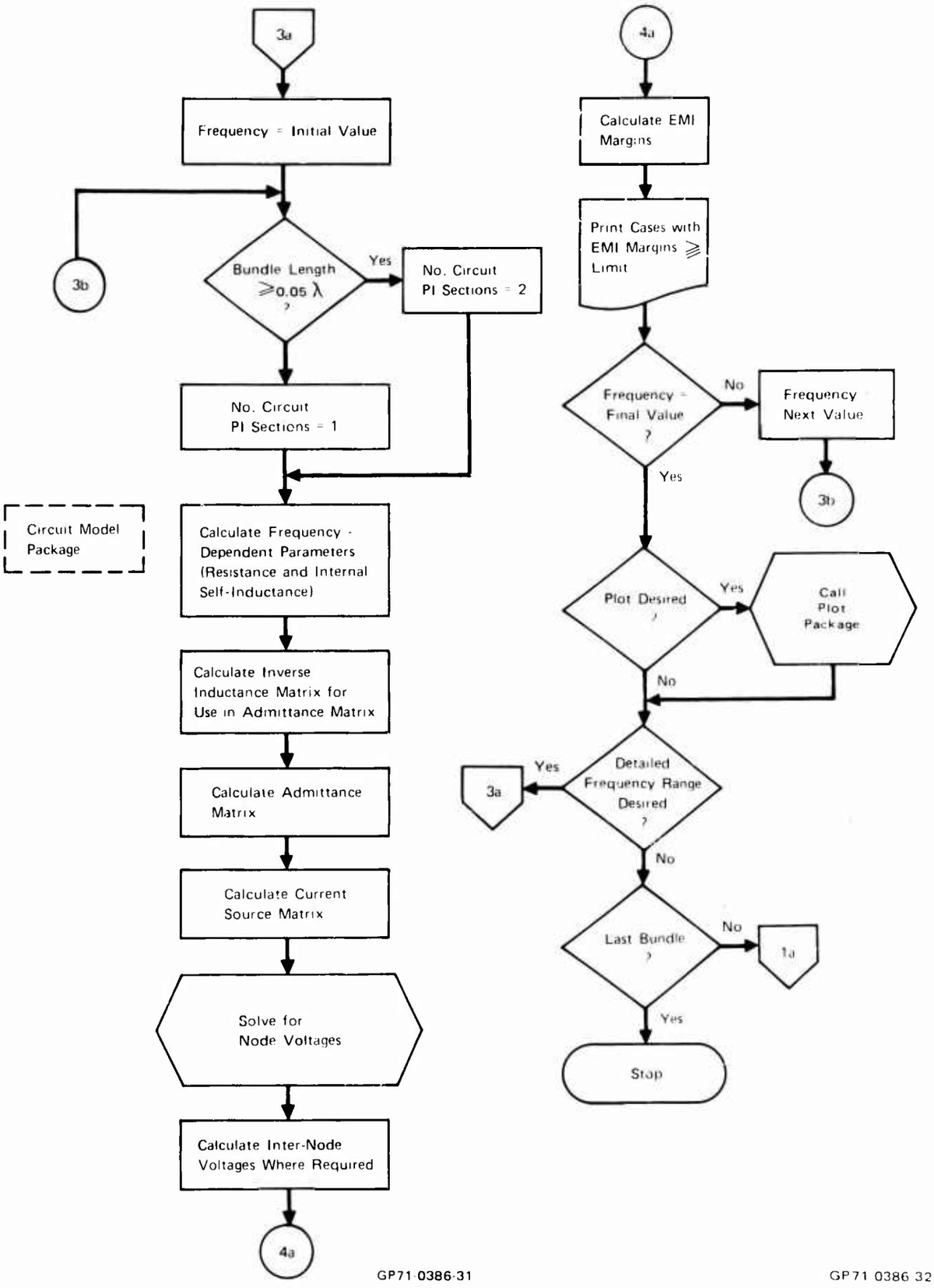

GP71-0386-31

GP71-0386-32

FIGURE 26 (CONCLUDED) WTWCAP ALGORITHM FLOWCHART

The EMI analysis is initiated by setting the frequency to the initial value (usually 100 Hz). Based on the ratio of wavelength to bundle length, the number of circuit pi sections is selected. The circuit model package is then called into use.

The heart of the program is the circuit model package. It contains a completely general scheme for setting up and solving by nodel analysis the circuit model with a specified number of pi sections. (The number of pi sections is limited to two only because of core memory. If desired, more pi sections could be run with fewer wires using this routine.)

First, the frequency-dependent parameters, internal self-inductance and wire resistance, are calculated. The inductance matrix is calculated and inverted for use in the nodal admittance matrix. Next, the admittance matrix is calculated. Included are the wire parameters lumped to the specified number of pi sections. The termination admittances are included, connected to ground or between nodes as required.

The current source matrix is then computed. The output of each source at the present frequency is determined from its spectrum, and voltage sources are converted to current sources. The appropriate inter-node and ground connections are included.

The circuit equations are solved by using a Gaussian elimination routine for symmetrical complex matrices to obtain the complex node voltages. Then, where necessary, inter-node voltages and load currents for current-sensitive loads are calculated. The susceptibility at the present frequency is determined for each load, and the EMI margins are calculated and printed.

The circuit analysis is repeated for all desired frequencies. Plots, if desired, are then generated. This process is repeated for all bundles.

4.3.4 Program Outputs

As with the other programs, a complete summary of the input data including any default values is first printed. The constant wire parameter matrix is also printed, if desired. This shows how the shields, shielded wire groups, etc., were handled by the program.

Next, the frequency by frequency analysis is printed. For each susceptible receptor, the EMI margin, received signal level (both magnitude and phase), and susceptibility levels are printed for each interference source. The complex sum of EMI from all sources is also printed in each case.

If plots of the interference are desired, the computer sorts the calculated data, figures the scale factors, and generates semi-log plots on the printer.

If they were requested, detailed frequency range analysis outputs are then printed, using the same format as the general analysis. As of this report, no plots are available for the detailed analyses.

4.4 PRELIMINARY VERIFICATION

A few, limited tests were performed to verify the basic assumptions used in the analysis. The tested bundle is shown in Figure 27, and the measured and calculated results are shown in Figure 28 for the twisted pair from the 28 volt switch.

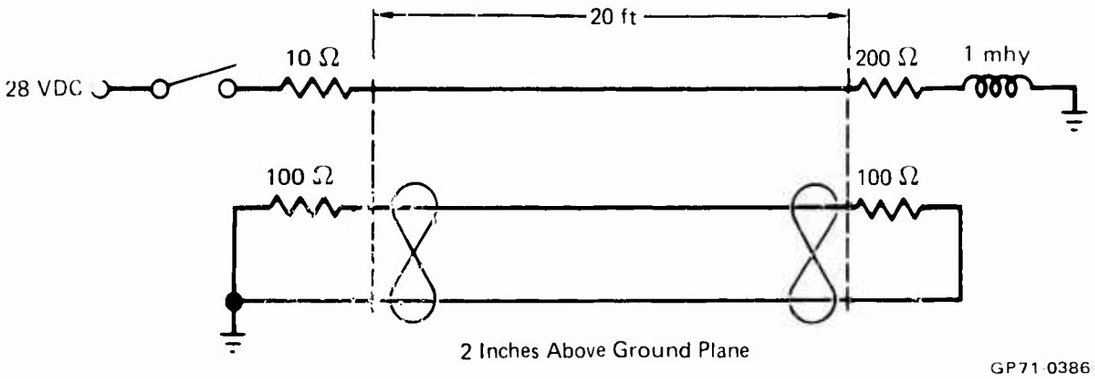

FIGURE 27 PRELIMINARY VERIFICATION TEST BUNDLE

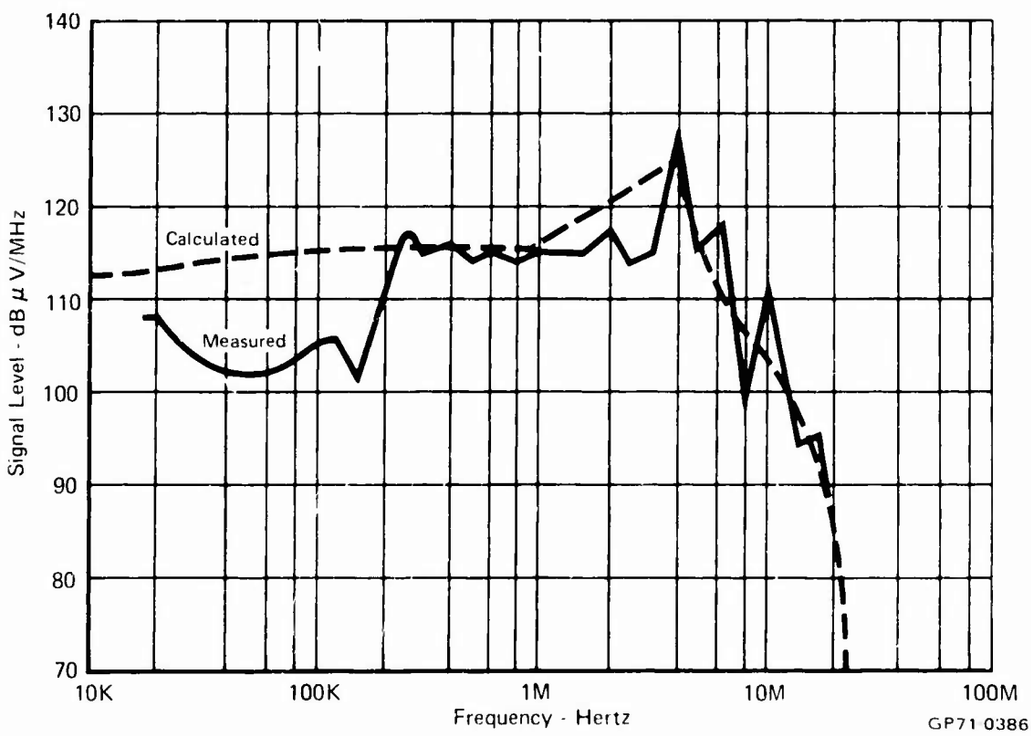

FIGURE 28 MEASURED vs CALCULATED EMI INTO TWISTED PAIR
(LOAD END OF BUNDLE)

4.5 APPLICATION EXAMPLE AND SAMPLE OUTPUT

A typical use of WTWCAP can be demonstrated by the case shown in Figure 29. In this example, a digital receiver output is connected to an on-board computer input. The minimum spike rejected by the computer input logic circuitry is also shown. To achieve EMC, the following information is required:

- Is it feasible to use this bundle in the aircraft EM environment?
- Is the given spike rejection level adequate?
- What type of wiring will give adequate EMI protection with minimum weight?

To answer these questions, a bundle was devised containing the worst-case sources and three receptor wire configurations. This bundle is shown in Figure 30. In this way, the various receptor wires could be tested.

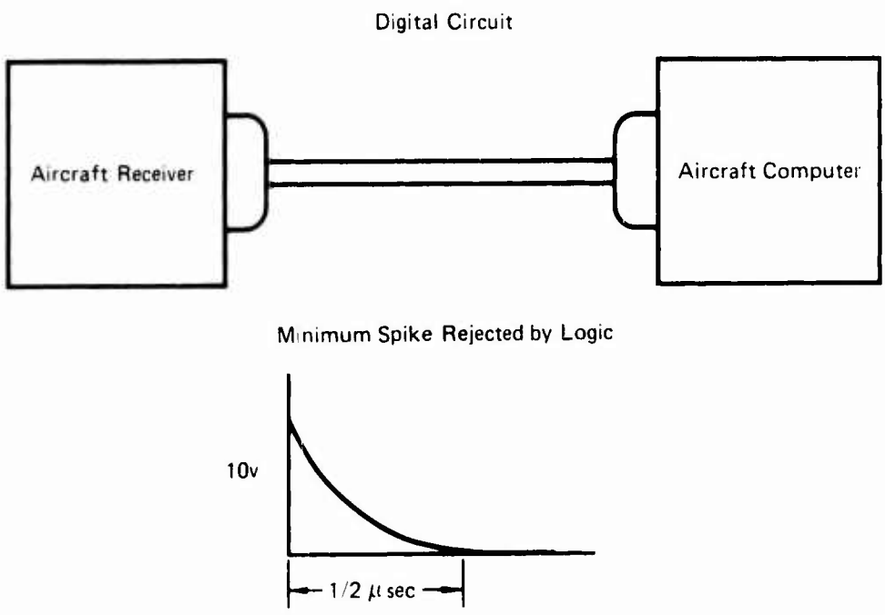

FIGURE 29 WIRE-TO-WIRE APPLICATION EXAMPLE

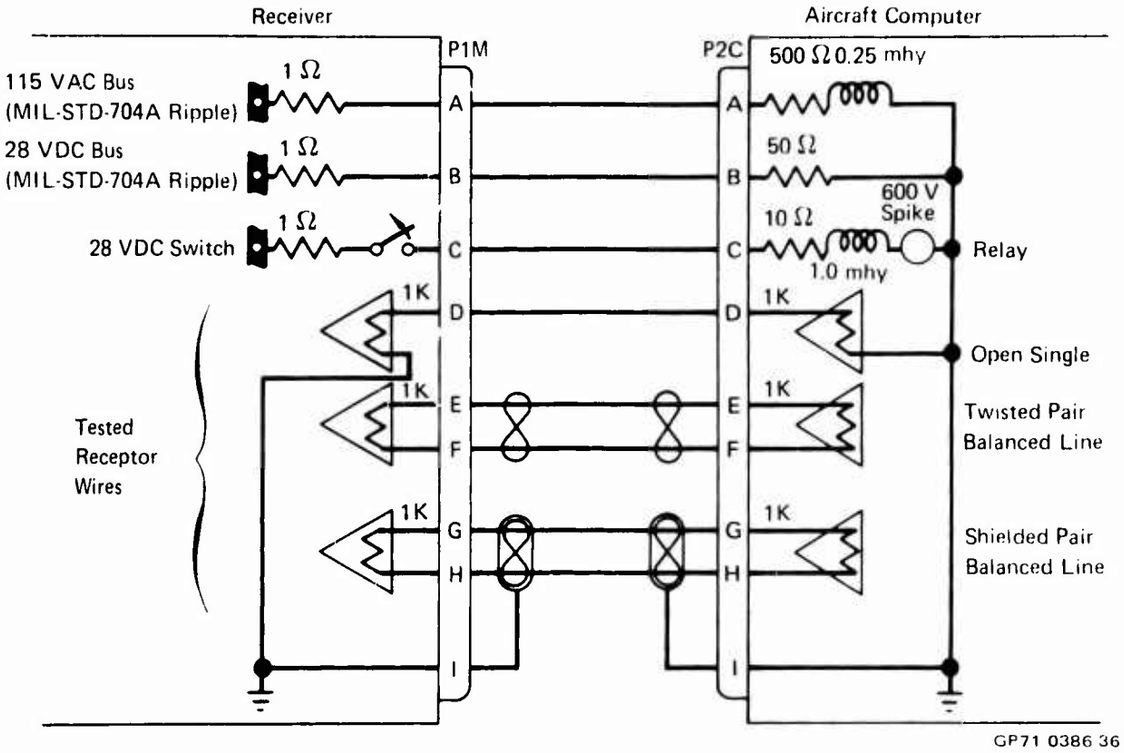

FIGURE 30 DIGITAL CIRCUIT TEST BUNDLE FOR APPLICATION EXAMPLE

The results of the WTWCAP analysis are summarized in Figures 31 through 35. Figure 31 shows the induced EMI from the MIL-STD-704A, 115 volt, 400 Hz power line. As shown, the shielded pair had no EMI, the twisted pair was marginal, and the open wire has definite EMI. Similarly, the EMI from the 28 VDC line and the 600 volt relay spike are shown in Figures 32 and 33, respectively. A portion of the printed computer output is shown in Figure 34, and a sample computer plot is shown in Figure 35.

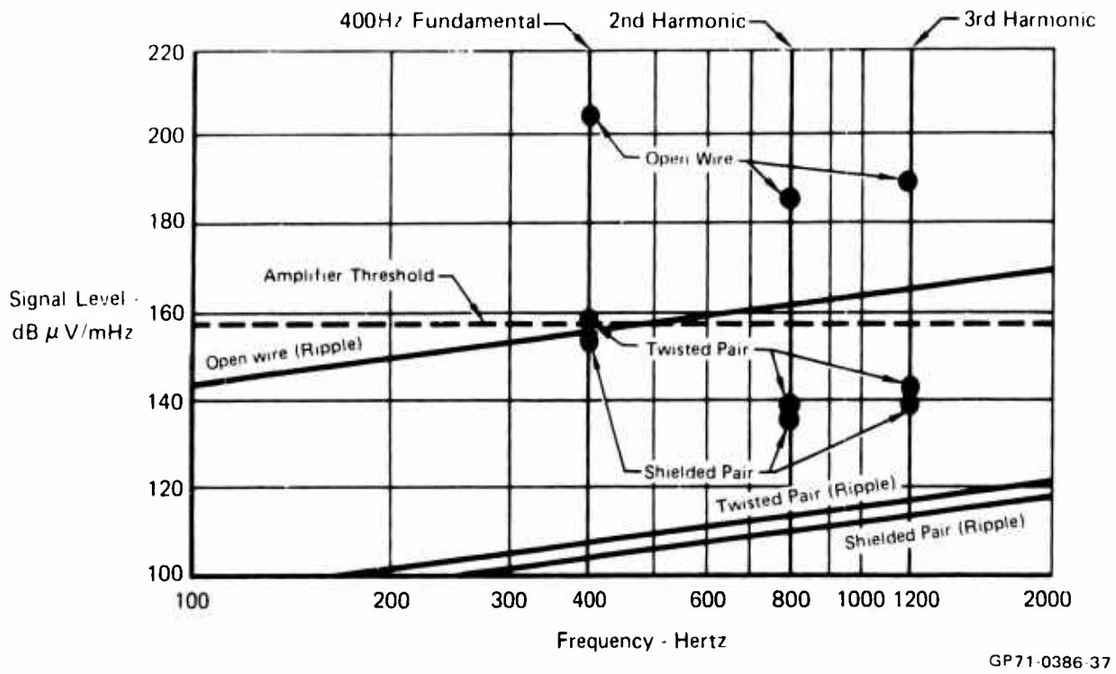

FIGURE 31 CALCULATED INTERFERENCE LEVELS FROM MIL-STD-704A 115VAC 400 Hz POWER LINE

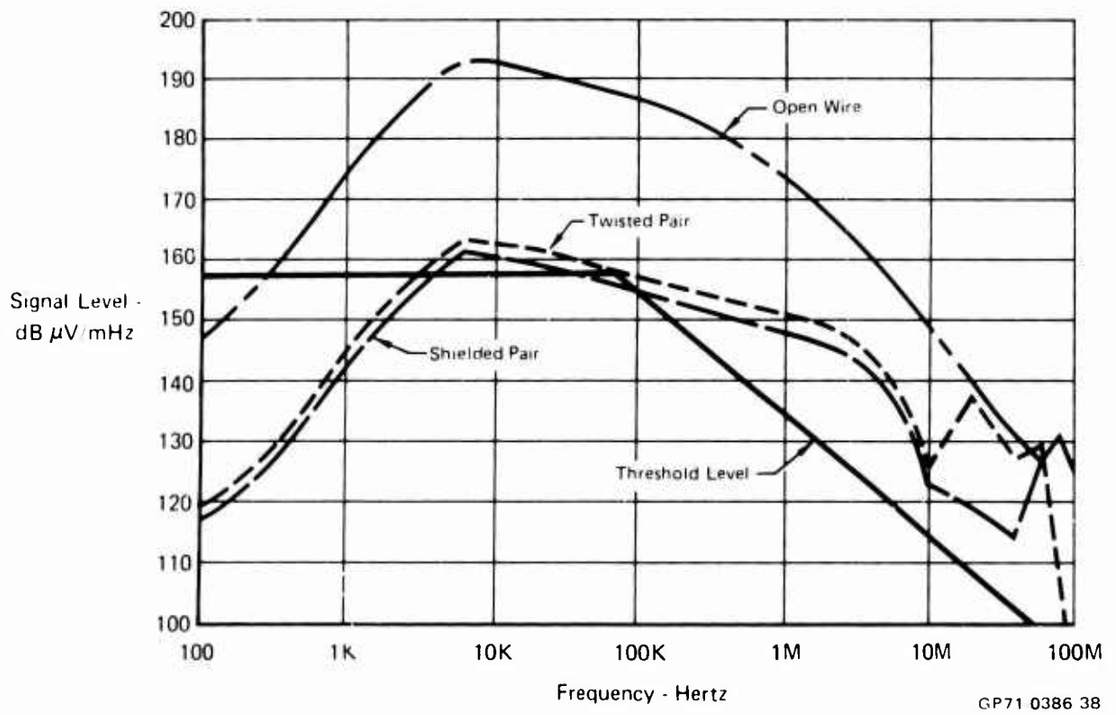

FIGURE 32 CALCULATED INTERFERENCE LEVELS FROM MIL-STD-704A RIPPLE ON 28VDC POWER LINE

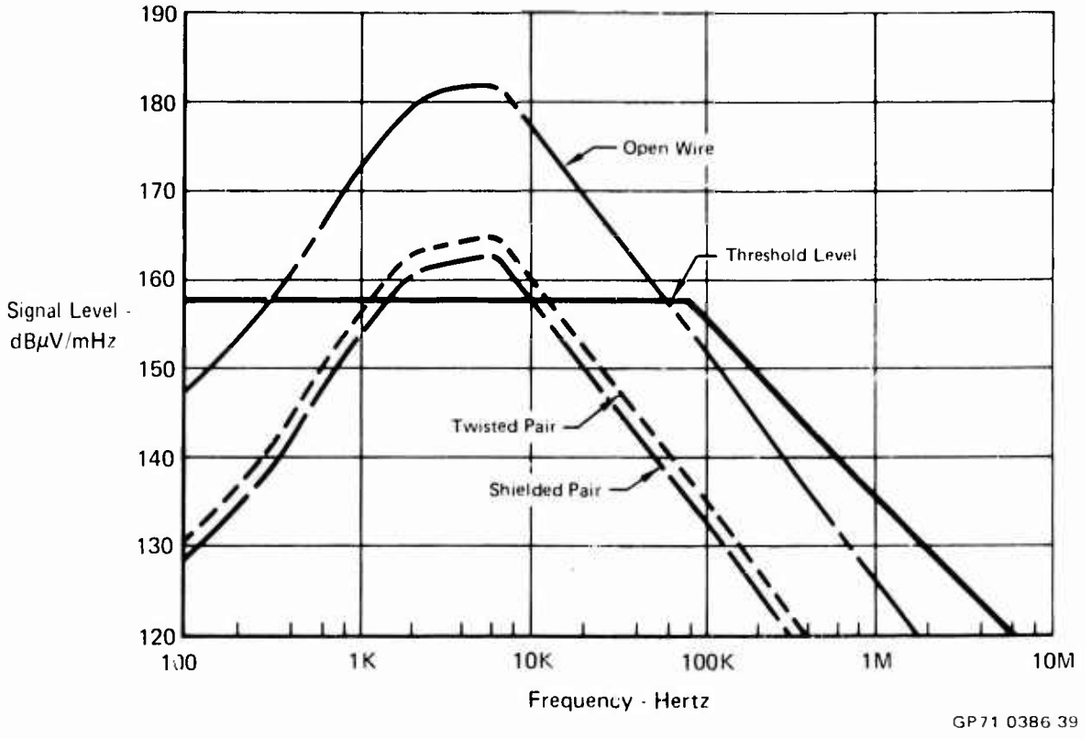

FIGURE 33 CALCULATED INTERFERENCE LEVEL FROM RELAY SPIKE

SWITCHING LOGIC TEST BUNDLE
ANALYSIS RESULTS FOR BUNDLE = TEST CONFG 2

FREQUENCY	RECEPTOR CONN.	RECEPTOR PIN	SOURCE CONN.	SOURCE PIN	EMI MARG (DB)	RCVD SIGNAL DBUV/MHZ	RCVD SIGNAL PHSE	SUSCP LEV DBUV/MHZ
20.0 KHZ								
	P1 M	G	P1 M	C	-39.4	117.2	87.8	156.7
	P1 M	G	P2 C	C	15.0	171.7	-92.2	156.7
	P1 M	G	ALL SOURCES		12.9	169.6	-92.2	156.7
	P2 C	G	P1 M	B	1.8	158.5	-92.2	156.7
	P2 C	G	P1 M	C	-39.4	117.2	-92.2	156.7
	P2 C	G	P2 C	C	15.0	171.7	87.8	156.7
	P2 C	G	ALL SOURCES		12.9	169.6	87.8	156.7
40.0 KHZ								
	P2 C	A	P2 C	C	-46.1	195.6	85.5	241.7
	P2 C	A	ALL SOURCES		-48.3	193.4	85.5	241.7
	P2 C	B	P2 C	C	-45.1	195.4	85.5	240.5
	P2 C	B	ALL SOURCES		-45.1	195.4	85.5	240.5
	P1 M	D	P1 M	B	32.3	188.9	84.1	156.7
	P1 M	D	P1 M	C	-15.4	141.3	83.1	156.7
	P1 M	D	P2 C	C	32.5	189.2	-98.1	156.7
	P1 M	D	ALL SOURCES		6.1	162.8	-151.6	156.7
	P2 C	D	P1 M	B	26.5	183.2	82.7	156.7
	P2 C	D	P1 M	C	-28.0	128.7	-84.1	156.7
	P2 C	D	P2 C	C	33.8	190.5	88.6	156.7
	P2 C	D	ALL SOURCES		36.9	193.6	86.9	156.7
	P1 M	E	P1 M	B	2.3	159.0	85.7	156.7
	P1 M	E	P1 M	C	-37.2	119.5	85.5	156.7
	P1 M	E	P2 C	C	15.6	172.2	-94.5	156.7
	P1 M	E	ALL SOURCES		13.4	170.1	-94.5	156.7
	P2 C	E	P1 M	B	2.3	159.0	-94.3	156.7
	P2 C	E	P1 M	C	-37.2	119.5	-94.5	156.7
	P2 C	E	P2 C	C	15.6	172.2	85.5	156.7
	P2 C	E	ALL SOURCES		13.4	170.1	85.5	156.7
	P1 M	G	P1 M	B	0.1	156.7	85.7	156.7
	P1 M	G	P1 M	C	-39.5	117.2	85.6	156.7
	P1 M	G	P2 C	C	13.3	170.0	-94.4	156.7
	P1 M	G	ALL SOURCES		11.2	167.8	-94.5	156.7
	P2 C	G	P1 M	B	0.1	156.7	-94.3	156.7
	P2 C	G	P1 M	C	-39.5	117.2	-94.4	156.7
	P2 C	G	P2 C	C	13.3	170.0	85.6	156.7
	P2 C	G	ALL SOURCES		11.2	167.8	85.5	156.7
60.0 KHZ								
	P2 C	A	P2 C	C	-46.7	194.6	83.3	241.2
	P2 C	A	ALL SOURCES		-48.8	192.4	83.3	241.2
	P2 C	B	P2 C	C	-45.6	194.4	83.3	240.0
	P2 C	B	ALL SOURCES		-45.6	194.4	83.3	240.0

GP71 0386 54

FIGURE 34 WTWCAP SAMPLE NUMERICAL OUTPUT FOR BUNDLE OF FIGURE 30

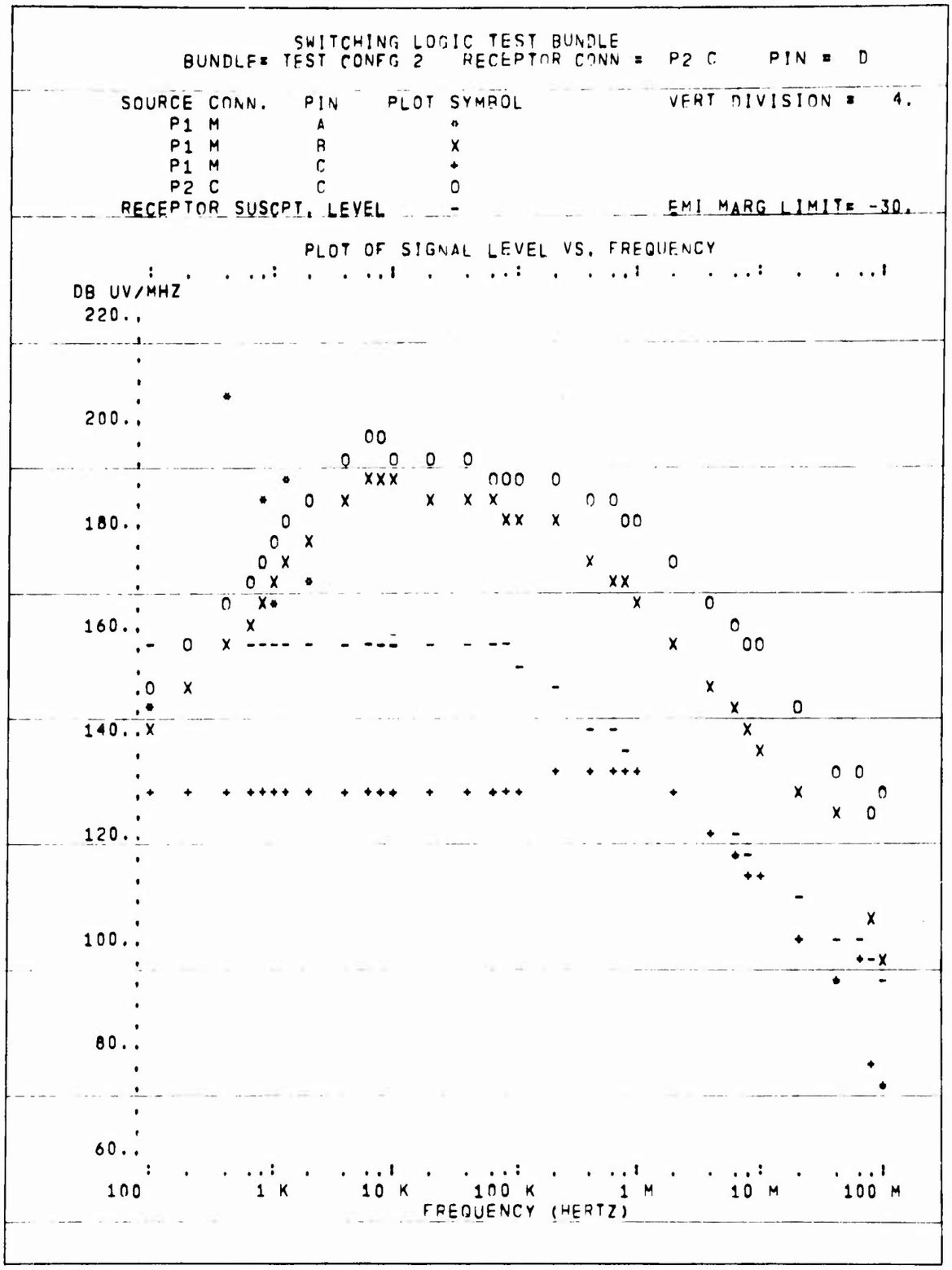

GP71-0386-55

FIGURE 35 WTWCAP SAMPLE PLOT OUTPUT FOR BUNDLE OF FIGURE 30

SECTION 5

ELECTROMAGNETIC FIELD-TO-WIRE COMPATIBILITY ANALYSIS PROGRAM (FTWCAP)

5.1 BACKGROUND

The coupling from external electromagnetic fields onto internal wiring is important in the design of aerospace vehicles. Usually, the fields enter the vehicle through dielectric apertures in the vehicle skin and couple onto wires immediately adjacent. These apertures include radomes, canopies, landing gear doors, camera windows and air intakes. FTWCAP presently analyzes only coupling onto wires from on-board transmitting antennas, but the computation method is completely general. It can be readily adapted to analyze EMI from other RF energy sources, such as ground-based transmitters, lightning, and EMP.

5.2 DETAILED DESCRIPTION OF MODEL

To obtain the equivalent plane-wave RF power density at each aperture from the on-board radiating antennas, the propagation model from ATACAP is used. The exposed wires are assumed to be adjacent to the aperture, and the amount of RF energy coupled depends on the aperture size and location. A transmission line model is then used to compute the currents induced in the wire loads (Refs 15, 16). Worst-case electromagnetic field vector orientation is determined and used for the calculation.

5.2.1 Field-to-Transmission Line Equations

Figure 36 shows a transmission line exposed to an electromagnetic field.

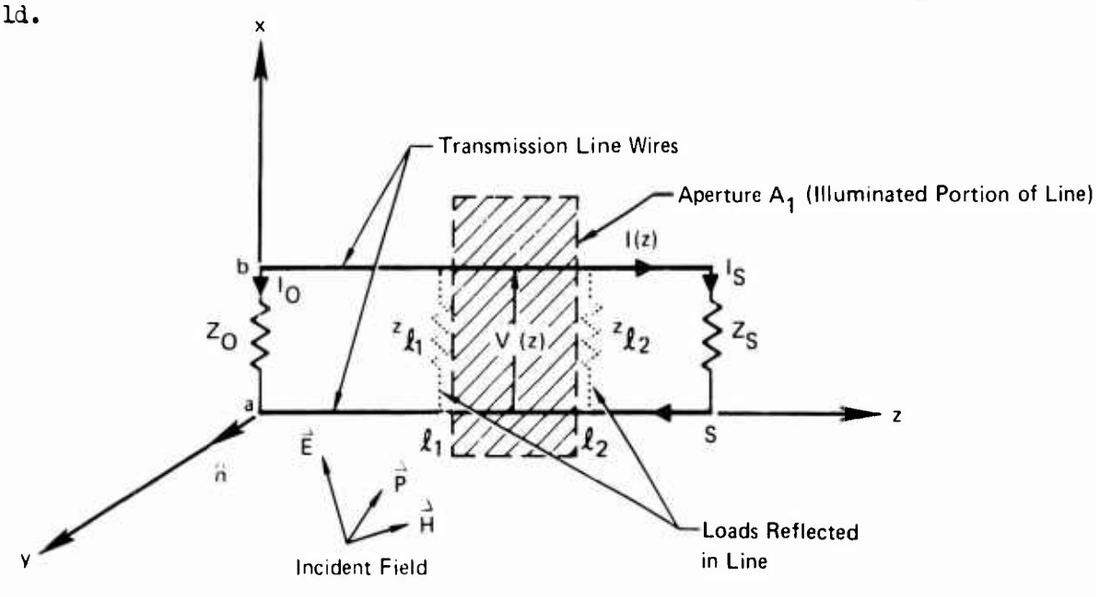

GP71-0386-40

FIGURE 36 TRANSMISSION LINE ILLUMINATED BY ELECTROMAGNETIC FIELD

Integration of Faraday's law over the surface of the transmission line results in (Ref 13)

$$\int_{A_1} (\nabla \times \dot{E}) \cdot \hat{n}\, dS = -\frac{\partial}{\partial t} \int \dot{B} \cdot \hat{n}\, dS \tag{5.1}$$

Defining the voltage across the wires at a given z as

$$V(z) = -\int_0^b E_x(x, z)\, dx \tag{5.2}$$

leads to the following transmission line partial differential equations with voltage and current sources included (Ref 16):

$$\frac{\partial V(z)}{\partial z} + Z I(z) = j\omega \int_0^b B_y^i(x, z)\, dx \tag{5.3}$$

and

$$\frac{\partial I(z)}{\partial z} + Y V(z) = j\omega Y \int_0^b E_x^i(x, z)\, dx \tag{5.4}$$

where a sinusoidal time dependence is assumed, E^i and B^i are the incident fields, and Y and Z are the transmission line admittance and impedance, respectively (Ref 16).

Equations (5.3) and (5.4) can then be used to derive two inhomogeneous second order differential equations for the transmission line currents and voltages (Ref 15). These equations are solved using the method of variation of parameters (Ref 17).

When the entire transmission line is not exposed to the incident field, expressions for the equivalent impedance of the unexposed transmission line and the physical loads replace Z_o and Z_s in Figure 36 and the equations. The resulting current in Z_o is then

$$I_o = \frac{Z_c}{D\,[Z_c \cosh(\gamma \ell_1) - Z_{\ell_1} \sinh(\gamma \ell_1)]} \cdot$$

$$\Bigg[\int_{\ell_1}^{\ell_2} [E_z^i(b, z) - E_z^i(o, z)]\, [Z_c \cosh \gamma(\ell_2 - z) + Z_{\ell_2} \sinh \gamma(\ell_2 - z)]\, dz \tag{5.5}$$

$$+ [Z_c \cosh \gamma(\ell_2 - \ell_1) + Z_{\ell_2} \sinh \gamma(\ell_2 - \ell_1)] \int_0^b E_x^i(x, \ell_1)\, dx$$

$$- Z_c \int_0^b E_x^i(x, \ell_2)\, dx. \Bigg]$$

Likewise, the current in Z_s is given by

$$I_s = \frac{Z_c}{D\,[Z_c \cosh\gamma\,(s-\ell_2) + Z_{\ell_2} \sinh\gamma\,(s-\ell_2)]} \cdot$$

$$\left[\int_{\ell_1}^{\ell_2} [E^i_z(b,z) - E^i_z(0,z)]\,[Z_c \cosh\gamma\,(z-\ell_1) + Z_{\ell 1} \sinh\gamma\,(z-\ell_1)]\,dz \right. \tag{5.6}$$

$$\left. -[Z_c \cosh(\gamma\ell_2) + Z_{\ell_1} \sinh(\gamma\ell_2)] \int_o^b E^i_x(x,\ell_2)\,dx + Z_c \int_o^b E^i_x(x,\ell_1)\,dx \right]$$

where

Z_c = transmission line characteristic impedance

γ = complex propagation constant

b = separation between wires

s = total length of transmission line (5.7)

ℓ_1 and ℓ_2 = define exposed portion of line

and

$$D = (Z_c Z_{\ell 1} + Z_{\ell 2} Z_c) \cosh\gamma\,(\ell_2 - \ell_1) + (Z_c^2 + Z_{\ell 2} Z_{\ell 1}) \sinh\gamma\,(\ell_2 - \ell_1)$$

$Z_{\ell 1}$ and $Z_{\ell 2}$ are the termination impedances as seen at the aperture edges. They are given by

$$Z_{\ell 1} = Z_c \frac{Z_o - Z_c \tanh\gamma\ell_1}{Z_c - Z_o \tanh\gamma\ell_1} \tag{5.8}$$

and

$$Z_{\ell 2} = Z_c \frac{Z_s + Z_c \tanh\gamma\,(s-\ell_2)}{Z_c + Z_s \tanh\gamma\,(s-\ell_2)} \tag{5.9}$$

These equations are dependent only on the incident electric fields, since the scattered fields have been accounted for in the induced transmission line currents.

5.2.2 Multiple Exposures

The above analysis can be easily extended to wires routed close to more than one aperture. Using superposition, the analysis is used to calculate the currents from each exposure, and the resulting complex currents are summed.

5.2.3 Ground Plane Effects

This analysis can also be applied to circuits with a ground plane return. In this case, the transmission line is formed by using the ground plane image of the primary wire. The above equations are applied using twice the height above ground for the wire separation.

5.2.4 Shielding Factors

Allowance must be made in the model for the overall bundle and individual wire shields. Since solid shields are seldom used in aerospace vehicles because of weight and flexibility considerations, determining the exact degree of electromagnetic field attenuation is an involved task. This determination involves the size and shape of the shield weave, the number of picks or openings per unit length, and many unknown factors. Therefore, the shielding factor for the FTWCAP model was based on empirical data. From many measurements on all types of braided shields, the curve shown in Figure 37 was selected as representative. Two typical measured curves for a single overall shield are also shown. The shielding effectiveness package in FTWCAP is separate from the rest of the program and can easily be updated or changed if other shielding effectiveness is desired.

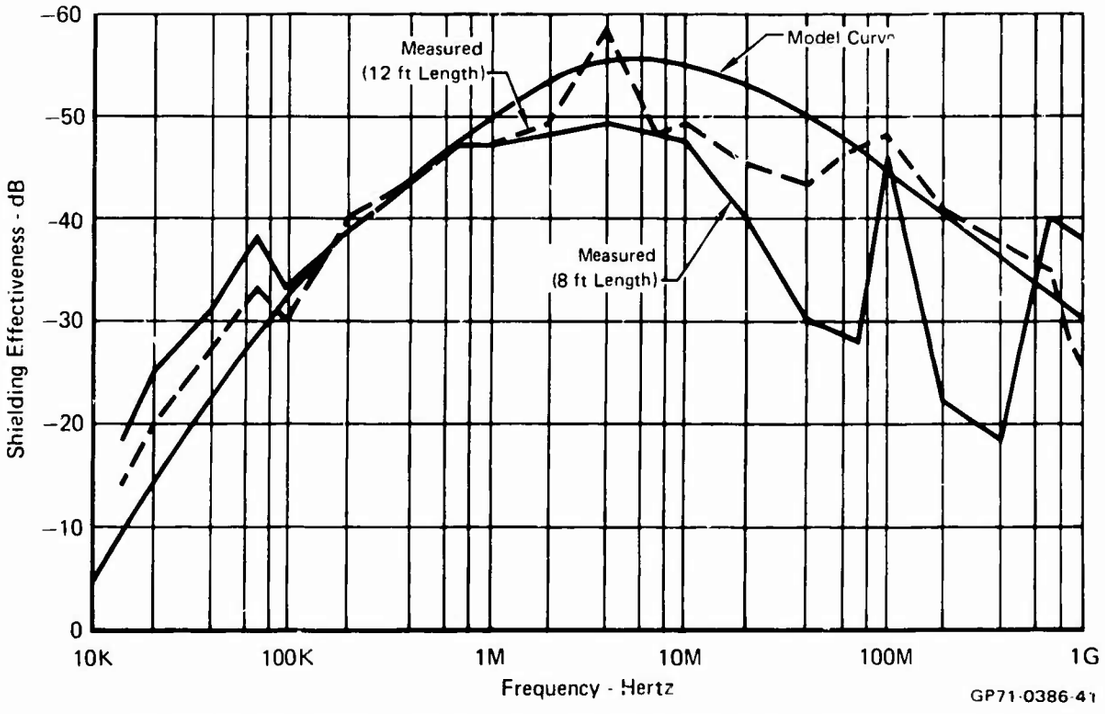

FIGURE 37 MODEL AND TYPICAL MEASURED SHIELDING EFFECTIVENESS CURVES FOR SINGLE OVERALL SHIELD

5.2.5 Bandwidth Considerations

Since most wire load susceptibilities are broad band, the received signal must be in terms of spectral density (μV/MHz) before they can be compared and an EMI margin calculated. Thus, a factor is used to convert the relatively narrow band transmitter emission to the equivalent broad band terms of the susceptibilities. Thus, the received signal can be expressed in dB above 1 μV/MHz.

5.3 COMPUTER PROGRAM DESCRIPTION

5.3.1 Input Data Required

The data format for FTWCAP is designed to be compatible with the other programs. The radiating subsystem data and aircraft data are identical to that used by ATACAP, as described in Section 3.4.1. The security classification feature of ATACAP is also contained in this program. Further, the wire bundle data is identical to that used by WTWCAP, as described in Section 4.3.1. The only additional data required is for the apertures in the aircraft skin exposing the wire bundle.

Aperture Data. The following data are required for each aperture exposing the given wire bundle:

- o Identification nomenclature
- o Location on aircraft (BL, WL, FS)
- o Connector locations (BL, WL, FS)
- o Bundle lengths to each aperture (for default values see below)
- o Aperture length and width

5.3.2 Default Assumptions

The default assumptions in ATACAP and WTWCAP also apply here. This is true for the aircraft, radiating subsystem, and wire bundle data. An additional default assumption applies to the bundle lengths to the apertures. If unknown, the conical spiral (Equation 3.11) is used to estimate them. (Note that this results in a different estimate of the total bundle length for each aperture.)

5.3.3 Analysis Procedure

The algorithm used in FTWCAP is summarized in the flowchart of Figure 38. After the data is read, the default values calculated, and the data summaries are printed, the analysis is begun.

A transmitter-antenna source is selected from the data. Using the same propagation model as ATACAP, the RF power density is computed at each aperture exposing the bundle. The transmission line equations are then used to calculate the complex currents induced in each susceptible load

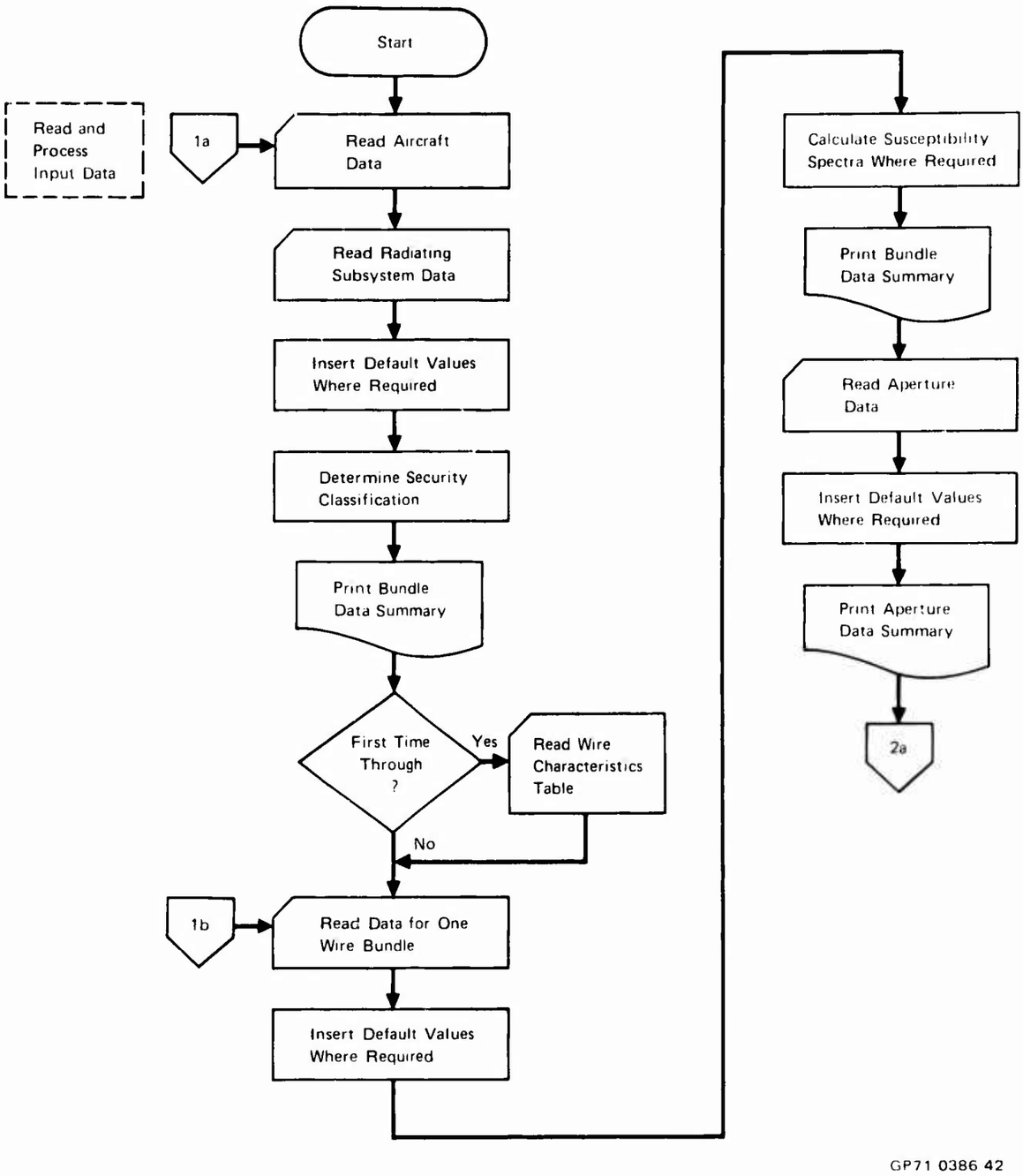

FIGURE 38 FTWCAP ALGORITHM FLOWCHART

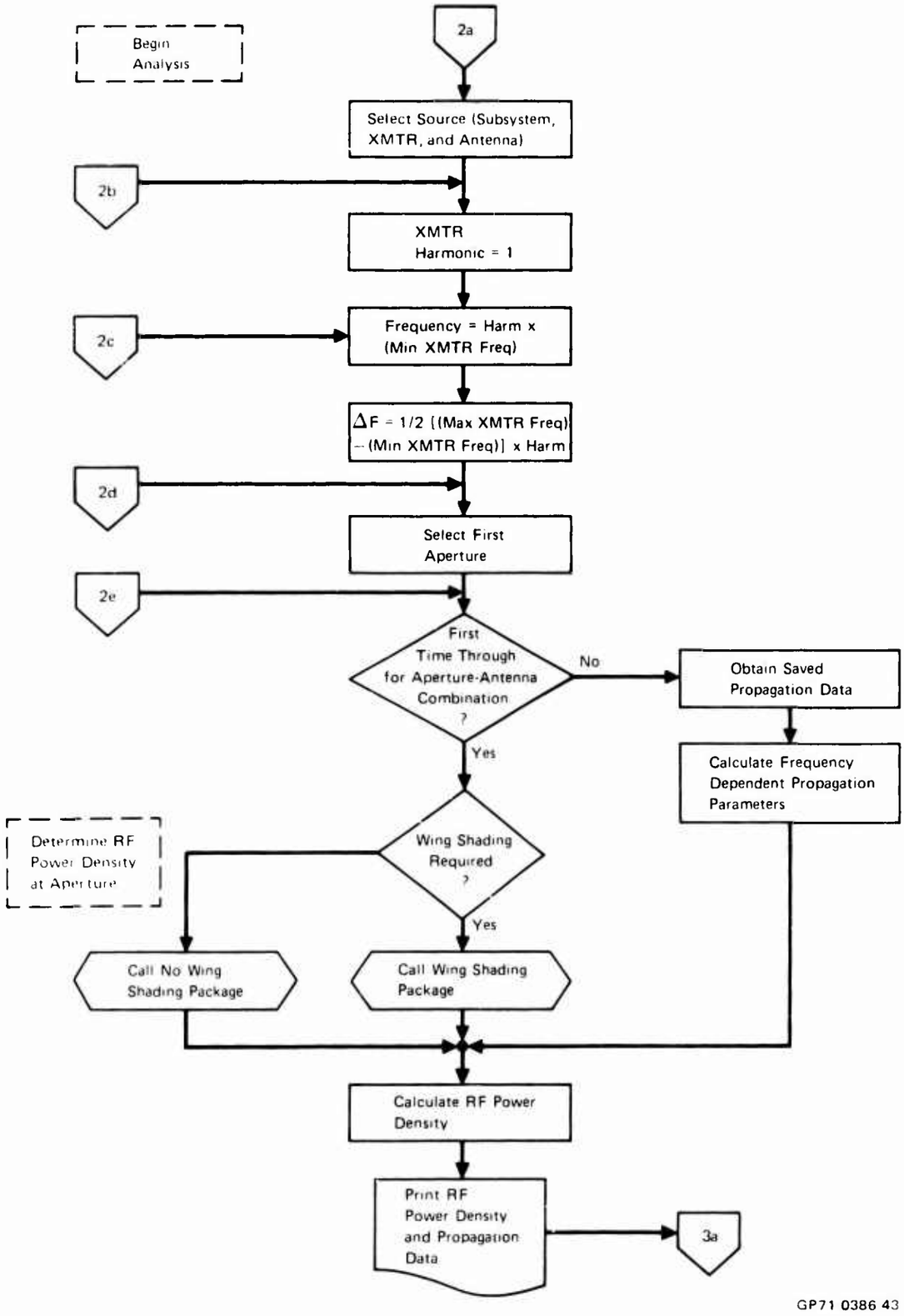

FIGURE 38 (CONTINUED) FTWCAP ALGORITHM FLOWCHART

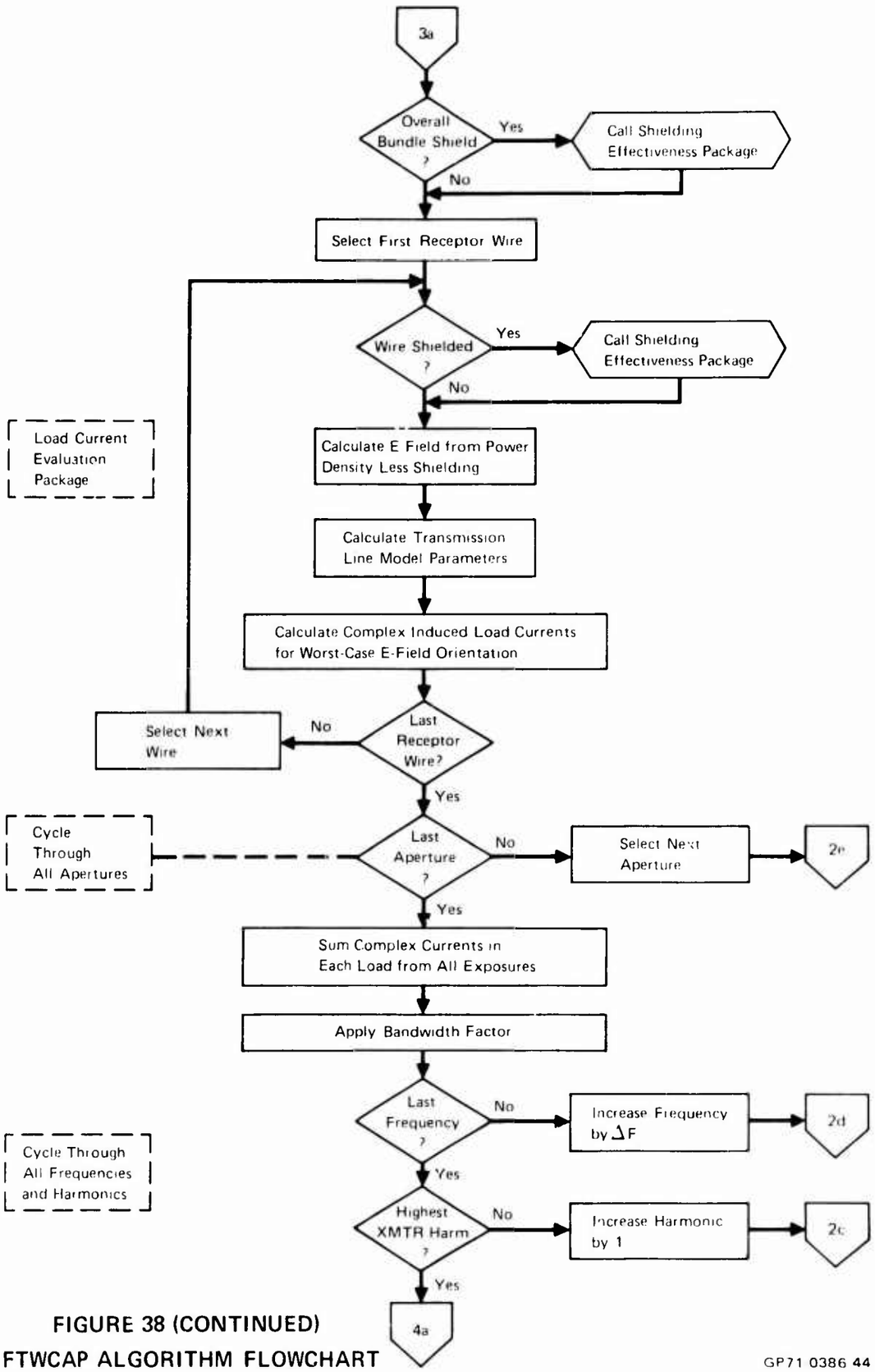

FIGURE 38 (CONTINUED)
FTWCAP ALGORITHM FLOWCHART

GP71 0386 44

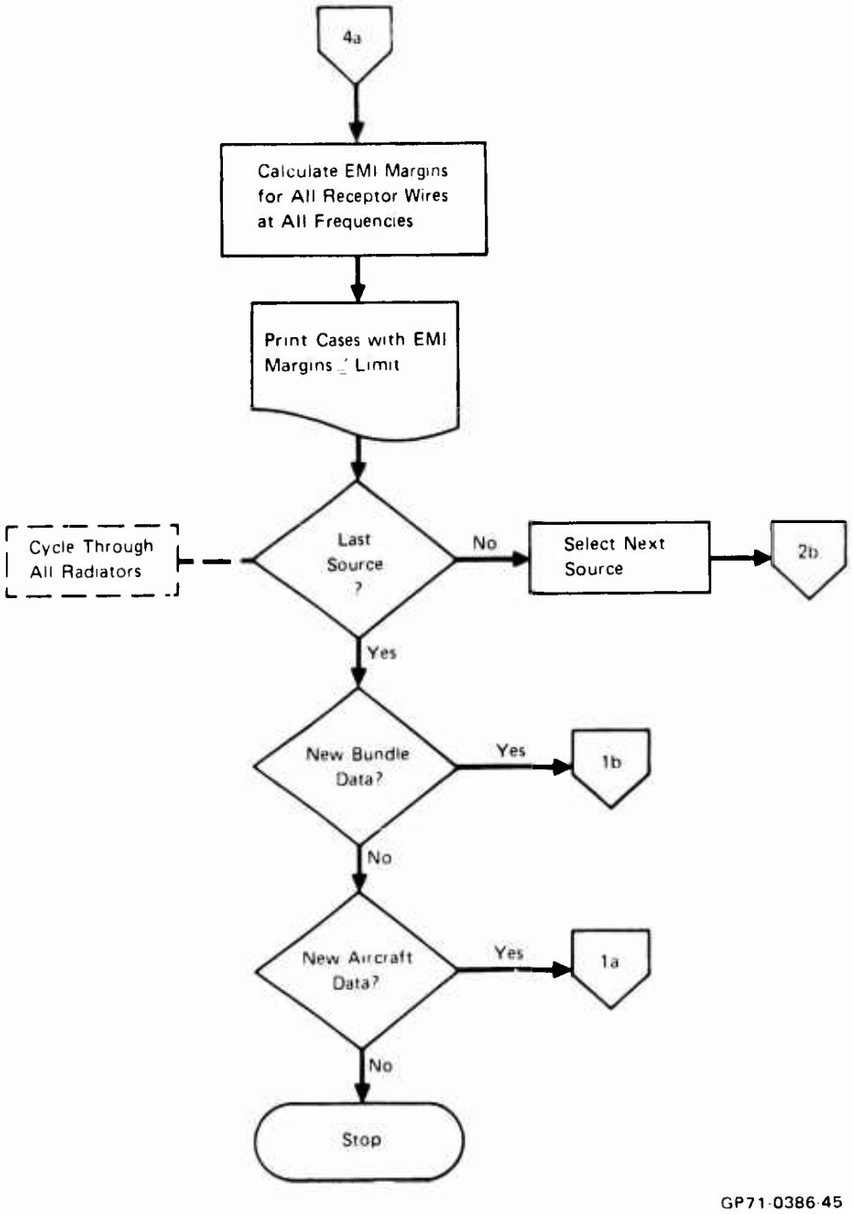

FIGURE 38 (CONCLUDED) FTWCAP ALGORITHM FLOWCHART

in the bundle. This is calculated for both horizontal and vertical polarization, and the worst-case value is selected. Included is any attenuation to the RF fields caused by overall bundle and individual wire shields. The complex signals induced in the loads from each exposing aperture are summed to obtain the total received signal level. EMI margins for each load are then calculated and printed when greater than the printout limit.

Calculations are made at the lowest, center, and highest frequency for each transmitter at the fundamental and at each significant harmonic. This procedure is repeated for each transmitter-antenna source on the vehicle.

5.3.4 Program Outputs

In addition to the input data summary, FTWCAP provides complete information regarding the analysis. The information is divided into RF power density and EMI margin sections. The propagation data for each aperture and frequency is given in the RF power density section. These outputs include the RF power densities in watts per square meter, propagation path code, and shading from wings and fuselage. The EMI margin section provides the information pertinent to the transmission line calculation. For each receptor pin, the EMI margin, total received signal (magnitude and phase), shielding attenuation used, and the susceptibility level are given. In addition, the security classification, if required, is printed on the top and bottom of each page.

5.4 APPLICATION EXAMPLE AND SAMPLE OUTPUT

An actual case of interference on an F-4D aircraft provides a good example of an application of FTWCAP. In this case, radiation from the upper UHF communications antenna was entering two apertures and coupling onto a video coaxial line of a receiving system. The situation is shown in Figures 39 and 40. This information was fed into FTWCAP to generate the outputs shown in Figures 41 and 42. From this, it could be seen that interference would occur. (The fix was to install an overall shield on the bundle.)

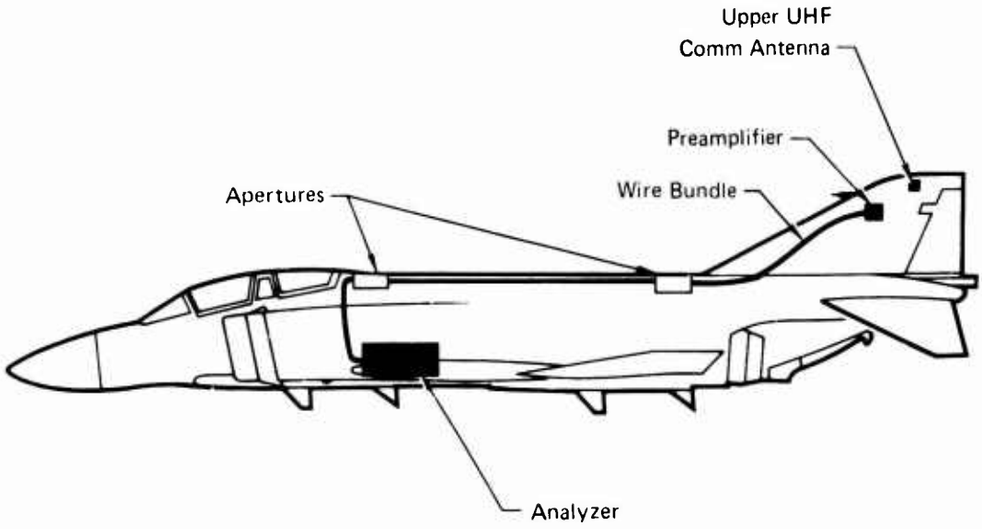

GP71-0386-46

FIGURE 39 F-4D APPLICATION EXAMPLE
ELECTROMAGNETIC FIELD-TO-WIRE ANALYSIS

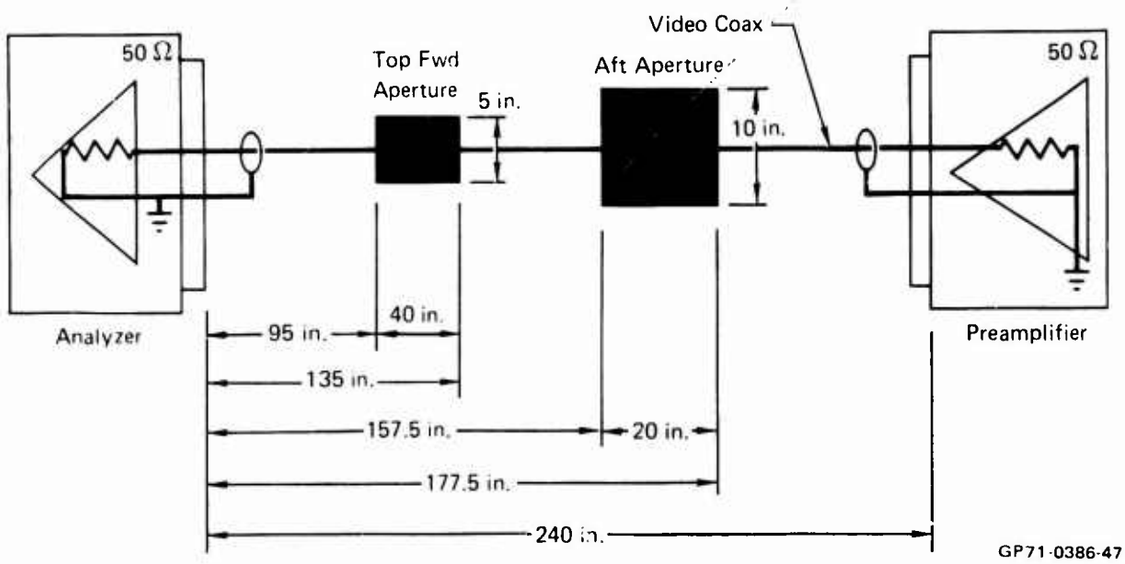

GP71-0386-47

FIGURE 40 SCHEMATIC REPRESENTATION OF SITUATION IN FIGURE 39

FTWCAP APPLICATION EXAMPLE, VIDEO COAX PICKUP,

SOURCE -- SUBSYS = UHF COMM, XMTR = 1, ANTENNA = FINCAP
RF POWER DENSITIES

FREQUENCY (MHZ)	HARM	APERTURE	RF PWR DENS (W/SQ M)	PROP CODE	FUSL SHDG	WING SHDG	ANTENNA LOBE
225,000	1						
		TOPFWD	1.457E-01	900	0.0	0.0	MAIN
		AFT	1.733E+01	900	0.0	0.0	MAIN
312,450	1						
		TOPFWD	1.457E-01	900	0.0	0.0	MAIN
		AFT	1.733E+01	900	0.0	0.0	MAIN
399,900	1						
		TOPFWD	1.457E-01	900	0.0	0.0	MAIN
		AFT	1.733E+01	900	0.0	0.0	MAIN
450,000	2						
		TOPFWD	1.457E-06	900	0.0	0.0	MAIN
		AFT	1.733E-04	900	0.0	0.0	MAIN
624,900	2						
		TOPFWD	1.457E-06	900	0.0	0.0	MAIN
		AFT	1.733E-04	900	0.0	0.0	MAIN
799,800	2						
		TOPFWD	1.457E-06	900	0.0	0.0	MAIN
		AFT	1.733E-04	900	0.0	0.0	MAIN
675,000	3						
		TOPFWD	1.457E-11	900	0.0	0.0	MAIN
		AFT	1.733E-09	900	0.0	0.0	MAIN
937,350	3						
		TOPFWD	1.457E-11	900	0.0	0.0	MAIN
		AFT	1.733E-09	900	0.0	0.0	MAIN
1199,700	3						
		TOPFWD	1.457E-11	900	0.0	0.0	MAIN
		AFT	1.733E-09	900	0.0	0.0	MAIN

GP71-0386-57

FIGURE 41 SAMPLE RF POWER DENSITY FIELD-TO-WIRE COMPUTER OUTPUT

FINCAP APPLICATION EXAMPLE, VIDEO COAX PICKUP.

SOURCE -- SUBSYS = UHF COMM, XMTR = 1, ANTENNA = FINCAP

FREQUENCY (MHZ)	RECEPTOR CONN	PIN	EMI MARGINS EMI MARG (DB)	TOTAL RCVD SIG DBUV/MHZ	PHASE	SUS LEV	SHIELDING OVALL	WIRE
225.000								
	J1	1	21.4	121.8	-132.8	100.0	0.0	-48.1
	J2	A	26.9	126.9	-101.4	100.0	0.0	-48.1
312.450								
	J1	1	27.0	127.0	-81.4	100.0	0.0	-48.1
	J2	A	25.3	125.3	-79.8	100.0	0.0	-48.1
399.900								
	J1	1	23.2	123.2	48.5	100.0	0.0	-48.1
	J2	A	10.5	110.5	139.2	100.0	0.0	-48.1
450.000								
	J1	1	-52.3	67.7	-50.8	100.0	0.0	-48.1
	J2	A	-36.8	83.2	-31.7	100.0	0.0	-48.1
624.900								
	J1	1	-41.1	58.9	70.3	100.0	0.0	-48.1
	J2	A	-33.9	66.1	-91.3	100.0	0.0	-48.1
799.800								
	J1	1	-36.2	63.8	-35.1	100.0	0.0	-48.1
	J2	A	-33.1	66.9	131.4	100.0	0.0	-48.1
675.000								
	J1	1	-97.6	2.2	17.7	100.0	0.0	-48.1
	J2	A	-89.3	10.7	86.8	100.0	0.0	-48.1
937.350								
	J1	1	-90.8	9.2	83.0	100.0	0.0	-48.1
	J2	A	-91.6	8.4	92.4	100.0	0.0	-48.1
1199.700								
	J1	1	-97.9	2.1	47.0	100.0	0.0	-48.1
	J2	A	-97.2	2.8	59.1	100.0	0.0	-48.1

GP71-0386-58

FIGURE 42 SAMPLE EMI MARGIN FIELD-TO-WIRE COMPUTER OUTPUT

SECTION 6

BOX-TO-BOX COMPATIBILITY ANALYSIS PROGRAM (BTBCAP)

6.1 BACKGROUND

The increased density of avionics in present day and future aerospace vehicles has dramatically increased the problem of box-to-box magnetic coupling. This applies to direct, radiated coupling. Conducted box-to-box interference usually involves wire-to-wire coupling, which is covered by WTWCAP.

An extensive literature search was conducted, but very little previous work has been done in this area. (Ref 8 and 18). A survey of MDC and USAF experience indicated that most direct box-to-box interference problems were magnetically coupled at power frequencies. Enclosures of most avionics equipment are good attenuators of RF energy, but for cost and weight considerations, these enclosures are of low permeability materials and are therefore poor magnetic shields.

This program, therefore, considers only power frequency, magnetic box-to-box coupling. This includes the 400 Hz fundamental as well as the predominant 1200 Hz third harmonic of the three-phase power systems. The program accepts transformer and equipment parameters for theoretical calculation or experimental data for empirical calculation. This applies both to source and susceptibility data. The theoretical and/or empirical data are then fitted to a magnetic dipole mathematical model.

6.2 DETAILED DESCRIPTION OF MODEL

6.2.1 Source Models

From physical principles, AC magnetic fields from the equipment can be represented as magnetic dipoles. That is, the field source can be represented as a series of circulating current elements, each producing a magnetic field. As the observation distance increases, these fields merge, and they appear to originate from a single dipole source. Hence, the spatial variation of these fields can be modeled using the magnetic dipole relations.

In most instances, power transformers in the equipment are responsible for the magnetic fields. The magnetic flux from the primary which does not reach the secondary and leaks from the core laminations form such fields, as illustrated in Figure 43. Leakage flux accounts for a large portion of the efficiency loss. Although many other factors such as eddy currents and core saturation also result in efficiency losses, for worst-case, all efficiency loss is assumed due to the leakage flux (Ref 8). The presence of the core material results in involved expressions for the leakage flux near the transformer. However, these effects diminish quickly with distance, and a dipole model may be used.

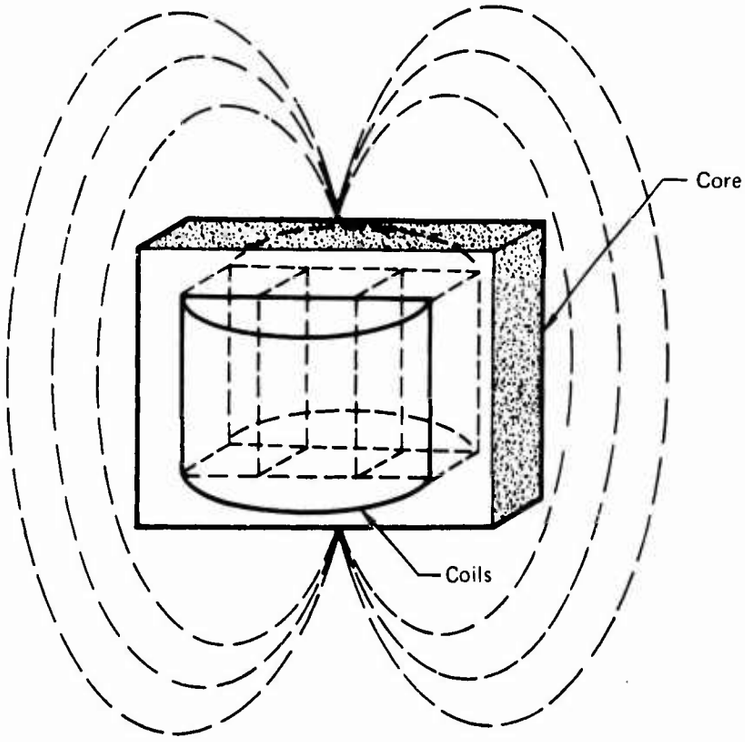

FIGURE 43 LEAKAGE FLUX FROM TRANSFORMER

GP71-0386-48

Magnetic Dipole Model for Calculated Data. The expression for the flux density from wire loop carrying current I along the loop is (Ref 1[9])

$$B = \frac{\mu_o I a^2 N}{2 (a^2+z^2)^{3/2}} \qquad (6.1)$$

where B = magnetic flux density (webers/m^2)

μ_o = permeability of free space

I = current in the loop (amperes)

a = radius of the loop (meters)

z = distance from center of loop to observation point (meters)

N = number of turns in loop

As applied to HTBCAP, an equivalent current is obtained based on the transformer efficiency such that B represents the worst-case leakage flux.

It is given in terms of the input current to the transformer, I_p, by

$$I_e = I_p \sqrt{1-\eta} \tag{6.2}$$

where η is the transformer efficiency. From Equation (6.2) combined with Equation (6.1), the flux density versus distance from the transformer can be determined.

Measured Data. If measured data is available, it can be fitted to the dipole model, and the model can be used to extrapolate the field at other points. Measurements of the magnetic flux density at two points are required. The magnetic flux is then given by

$$B(z_2) = B(z_1) \left[\frac{a_e^2 + z_1^2}{a_e^2 + z_2^2} \right]^{3/2} \tag{6.3}$$

where a_e is the equivalent loop radius,

$$a_e = \sqrt{\frac{z_1^2 \left[\frac{B(z_1)}{B(z_2)} \right]^{3/2} - z_2^2}{1 - \left[\frac{B(z_1)}{B(z_2)} \right]^{2/3}}} \tag{6.4}$$

In the above z_1 and z_2 are the two measurement distances from the transformer center, and $B(z_1)$ and $B(z_2)$ are the measured flux densities in webers/m^2.

6.2.2 Receptor Models

Receptors of low frequency, magnetic interference in boxes are usually transformers. Such transformers are used for inputs to high gain audio-frequency amplifiers, such as intercom and servo amplifiers. In the calculated data case, a dipole model similar to the above can be used to calculate the interference. If measured data is available such that the box is susceptible to a known magnetic field, the source and susceptibility fields only need be compared to obtain the EMI margin.

Calculated Data. The calculated susceptibility is based on the frequency-domain (Fourier transformed) version of Maxwell's induction law

$$\nabla \times \vec{E} = -j\omega \vec{B} \tag{6.5}$$

The induced EMF in the secondary of the transformer can be obtained by integrating Equation (6.5) over the loop area. It is

$$\mathcal{E} = \omega BA \tag{6.6}$$

where

$\mathcal{E}$ = induced EMF in loop (volts)

ω = angular frequency

B = total flux density in the loop

A = area of the loop.

The susceptibility is determined by assuming the transformer to be an M turn loop with a high permeability core. For worst-case, the medium permeability is assumed to be that of the core. The open-circuit potential induced in the secondary can be calculated using Faraday's induction law, and this is compared to the amplifier input susceptibility level to obtain the EMI margin. (Note: This is worst-case; the maximum error by using open-circuit potential is 6 dB.) This induced potential is

$$V_i = \omega M B(z) \mu A \tag{6.7}$$

where $B(z)$ is the flux density from Equation (6.1) or (6.3), as applicable, z is the distance between source and receptor, μ is the receptor core permeability, and A is the receptor core area.

Measured Data. If data is available from MIL-STD-461 RS01 tests, it can be used. In this test, a loop of wire is placed near the equipment at a known distance, and the loop current is increased until the specification limit is obtained. The dipole relation, Equation (6.1), can be used to calculate the equivalent free space magnetic flux density at the box center location. Thus, the box is known to be susceptible to a certain equivalent flux density at its center. To obtain the EMI margin from a given source, Equation (6.1) or (6.3), as applicable, is used to obtain the flux density at the box center, and this level and the susceptibility level are compared.

6.3 COMPUTER PROGRAM DESCRIPTION

6.3.1 Input Data Required

The input data is easily obtained from information normally supplied to the user. In some cases, a number of options are available to aid the user in specifying data in the form in which it is available.

General Box Data. This data aids in identifying the equipment boxes being considered in the run. The following are included:

- Subsystem designation or nomenclature
- Number of boxes in each subsystem with respective nomenclature
- Box location in vehicle (geometric center BL, WL, FS)
- Number of transformers in each equipment box

Individual Transformer Data. This data specifies parameters associated with each transformer. The following are included:

- o Transformer location with respect to geometric center of respective boxes
- o Input and output voltages and currents
- o Core material magnetic permeability
- o Number of turns in primary and secondary windings
- o Susceptibility level of devices being fed by receptor transformer secondary
- o Loop area of coil winding

6.3.2 Default Options

The default options usable in the BTBCAP are summarized below:

- o Transformer locations are assumed to be at the geometric center of the respective boxes.
- o When experimental emission or susceptibility data is available, the box is treated as a single transformer.

6.3.3 Analysis Procedure

An algorithm flowchart is presented in Figure 44. The input data pertaining to each subsystem boxes and respective transformers are read and processed. The default options are inserted, and an input data summary is printed.

The experimental data is then read and processed for emission and susceptibility. If experimental emission data is available then, only for emission purposes, the box is treated as a transformer. The same holds true for susceptibility data.

The analysis is begun by selecting the first specified receptor and computing the EMI coupled to it from all source transformers. The first source is selected, and the methods used for emission and receptor data are denoted. The EMI margin is then calculated and contained in the output if it exceeds the printout limit.

This process is continued until all the emitters have been considered. Upon the completion of the emitter cycle, the routine indexes to the next receptor, and the process is continued for all receptors.

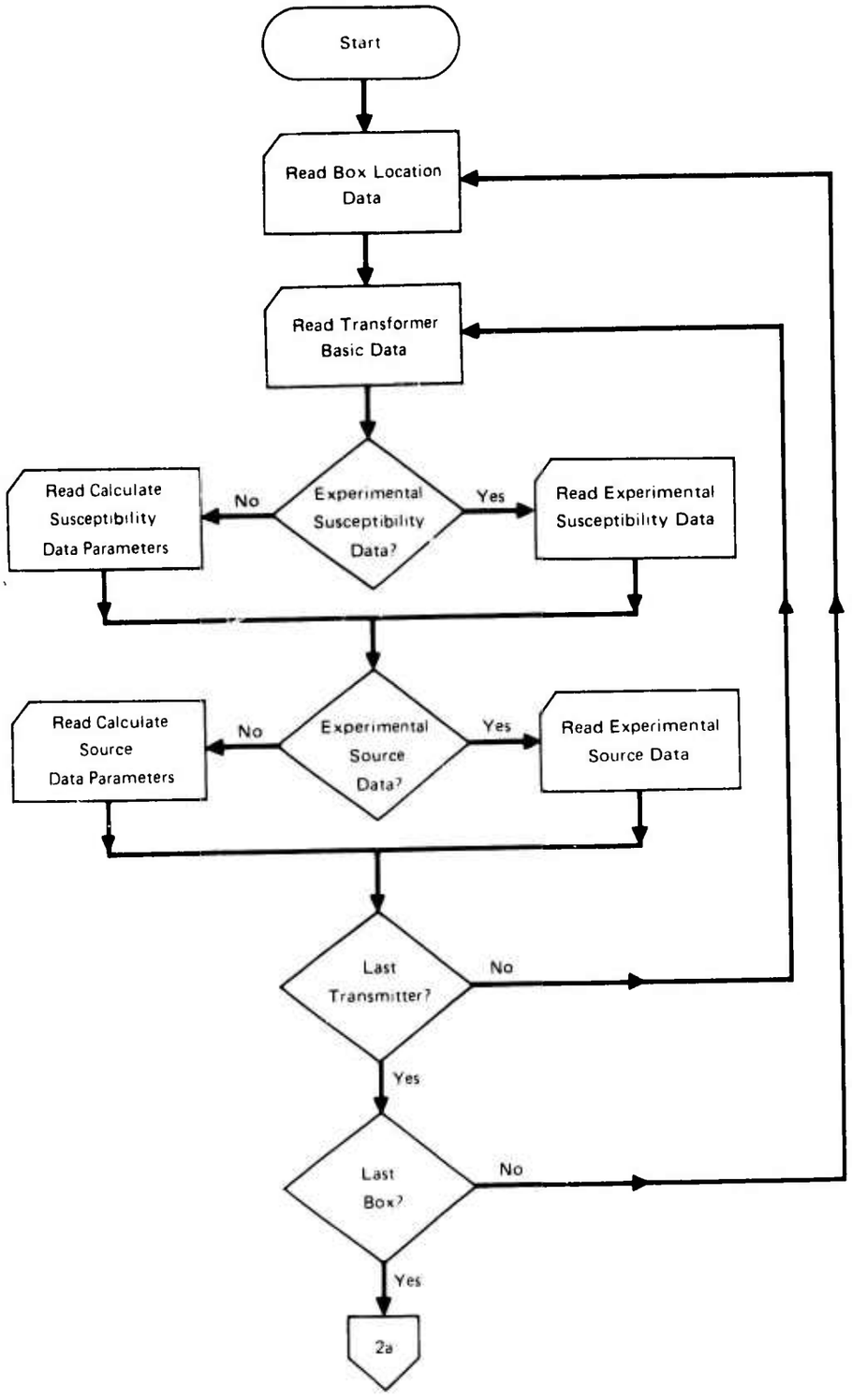

GP71 0386 49

FIGURE 44 BTBCAP ALGORITHM FLOWCHART

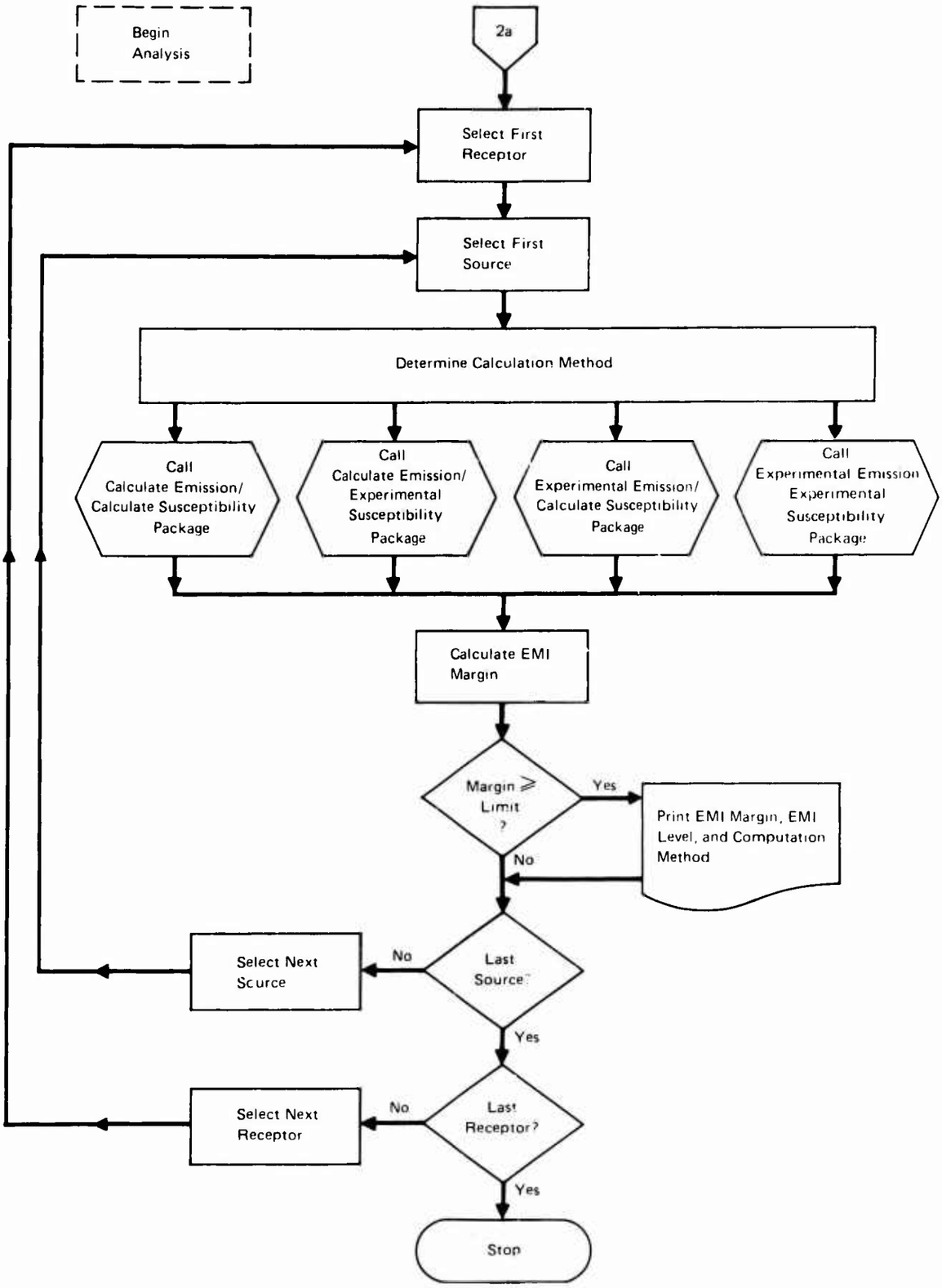

FIGURE 44 (CONCLUDED) BTBCAP ALGORITHM FLOWCHART

GP71 0386 50

6.3.4 Program Outputs

As with the other programs, a complete summary of the input data including any default values is first printed. Next, the complete analysis of each receptor is printed, specifying the source, EMI margin, and the method of calculation.

SECTION 7

CONCLUSIONS AND RECOMMENDATIONS

The mathematical models and the computer programs described in this report are accurate, practical, and useful tools for establishing intra-vehicle electromagnetic compatibility. They aid the user in determining and fixing potential EMI problems on a vehicle for the four primary coupling paths. They also aid in establishing the EMC implications of modifications to the vehicle and specification alterations.

The purpose of these programs is to rapidly survey the data and quickly indicate potential EMI. As a result, the models contain some approximations and worst-case assumptions. In a few instances, the predicted EMI situations require further investigation. The auxiliary outputs of the programs can be used to aid in these additional efforts. For example, the constant wire inductance/capacitance matrix in WTWCAP can be used in devising input data for a time-domain circuit analysis program such as CIRCUS, SEPTRE, or ECAP. Also, the ATACAP outputs can be used to determine which antenna pairs need near-field calculations (Ref 19).

This part presents the work done in the research and development phases of the contract but not the verification phase. Consequently, the models presented here have not been thoroughly tested yet (with the exception of ATACAP). Where preliminary verification data was available, it has been presented to validate the assumptions and approximations. During the next phase, extensive verification tests will be performed and the results contained in part II.

The mathematical models encompass more than four specific EMI paths. Because they are basic models of the physical mechanisms of EMI coupling, they are readily adapted for other specific coupling paths. For example, the magnetic dipole transformer model from BTBCAP and the wire circuit model from WTWCAP could be combined and adapted for transformer-to-wire EMI calculations. Thus, the models can be used as basic building blocks for all combinations of EMI sources and receptors including antenna-to-box, wire-to-box, wire-to-antenna, etc. These models also have wide application to other areas related to intra-vehicle EMC. This includes interference from sources off of the vehicle such as ground-based emitters, other vehicles, EMP, and lightning.

APPENDIX

VALIDATION OF LUMPED PARAMETER MODEL

Consider the circuit in Figure 45.

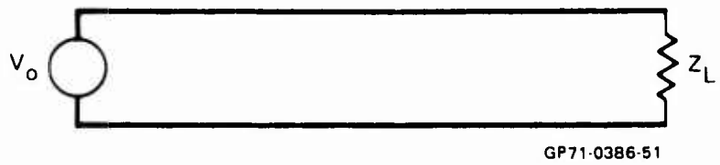

FIGURE 45 TRANSMISSION LINE

The differential equations required for the solution of this transmission line problem are

$$\frac{dV}{dx} = -Z\,I \tag{A.1}$$

$$\frac{dI}{dx} = -YV \tag{A.2}$$

where Z is the complex line impedance per unit length and Y is the complex shunt admittance per unit length of the line. These equations can be solved for the voltage across the load impedance Z_L by differentiating (A.1) and using (A.2)

$$\frac{d^2V}{dx^2} = (ZY)\,V \tag{A.3}$$

The solution of the previous differential equation is

$$V(x) = Ae^{x\sqrt{ZY}} + Be^{-x\sqrt{ZY}} \tag{A.4}$$

Applying the appropriate boundary conditions leads to an expression for the equivalent impedance as seen from the generator

$$Z_i = Z_o\left[\frac{Z_L \cosh(\gamma\ell) + Z_o \sinh(\gamma\ell)}{Z_o \cosh(\gamma\ell) + Z_L \sinh(\gamma\ell)}\right] \tag{A.5}$$

Z_o and γ in the above are respectively the characteristic impedance and the propagation constant of the transmission line.

$$Z_o = \sqrt{\frac{Z}{Y}} \tag{A.6}$$

$$\gamma = \sqrt{ZY} \tag{A.7}$$

Compare this to the lumped parameter circuit in Figure 46.

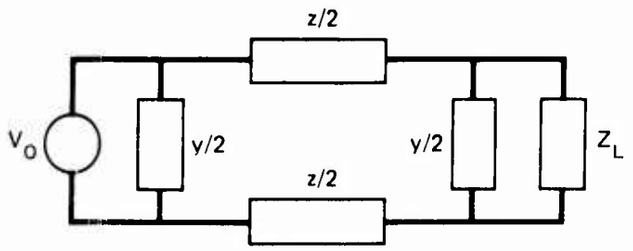

FIGURE 46 EQUIVALENT LUMPED PARAMETER CIRCUIT

The impedance as seen from the generator is

$$Z_i = \frac{\left(\frac{Z}{Y}\right) + \left(\frac{Z_L}{Y}\right) + \left(\frac{ZZ_L}{2}\right)}{\left(\frac{1}{Y}\right) + Z_L + \left(\frac{Z}{2}\right) + \left(\frac{ZYZ_L}{4}\right)} \qquad \text{(A.8)}$$

Considering $(ZYZ_L)/4$ to be negligible in comparison with the other terms in the denominator of (A.8), this expression is identical to (A.5) where the hyperbolic functions are expanded to second order. This shows that when the previous approximations are valid, the two formulations are equivalent. For cases where the approximation in (A.8) and the expansion to second order of (A.5) are not valid, additional parameters (pi sections) are added.

REFERENCES

Cited References

1. M. D. Siegel, "Aircraft Antenna - Coupled Interference Analysis," IEEE Electromagnetic Compatibility Symposium Record, June 17-19, 1969, pp 85-90.

2. John D. Kraus, Antennas, New York: McGraw-Hill, 1950, pp 25, 54-55.

3. "Antenna Models Based on Statistical Tendencies of Spectrum Signature Data," Electromagnetic Compatibility Analysis Center Report ECAC-TN003263, Sept 1966.

4. G. Hasserjian and A. Ishmirau, "Exitation of a Conducting Cylindrical Surface of Large Radius of Curvature," Transactions of the IRE, Vol. AP-10, No. 3, May 1962, pp 264-273.

5. J. B. Keller, "Geometrical Theory of Diffraction," Journal of the Optical Society of America, Vol 52, No. 2, pp 116-130, February 1962.

6. M. Born and E. Wolf, Principles of Optics, New York: MacMillan Company, 1959, pp 553-590.

7. R. Goldman, A. Kalviste, and H. L. Rehkopf, "Application of Computer Techniques to System Interference Analysis, Electro-Interference, Class II Research," Boeing Company Document No. D2-23036, 1963.

8. T. K. Foley and A. Rudzitis, "Feasibility Study of Computer Prediction of Broadband Near-Field Electromagnetic Interference in a Space Vehicle - Final Report," Contract NAS 8-5608, Boeing Document No. D2-90642-1, Dec 31, 1964, AD 463972.

9. B. L. Carlson, W. R. Marcelja, D. A. King, "Computer Analysis of Cable Coupling for Intra-System Electromagnetic Compatibility," U.S. Air Force Report No. AFAL-TR-65-142, May 1965, AD 465040.

10. W. R. Johnson, B. D. Cooperstein, and A. K. Thomas, "Development of a Space Vehicle Electromagnetic Interference/Compatibility Specification," Final Report, NASA Contract No. 9-7305, Vols 1 & 2, TRW Document No. 08900-6001-1000, June 28, 1968.

11. R. D. Parlo, E. R. Freeman, H. M. Sachs, and A. M. Singer, "An Intra-System Compatibility Analysis Program (ISCAP)," USAF Air Force Report No. ESD-TR-70-261, June 1970.

12. S. Ramo, J. R. Whinnery, T. VanDuzer, Fields and Waves in Communication Electronics, New York: John Wiley and Sons, Inc., 1967, pp 291-321.

13. W. R. Smythe, Static and Dynamic Electricity, Third Edition, New York: McGraw-Hill, 1968.

14. P. M. Morse and H. Feshbach, Methods of Theoretical Physics, Vol II, New York: McGraw-Hill, 1953, p. 1181.

REFERENCES (Continued)

15. W. L. Weeks, Electromagnetic Theory for Engineering Applications, New York: John Wiley and Sons, Inc., 1964, Ch. 2.

16. C. D. Taylor, S. Satterwhite, C. W. Harrison, Jr., "The Response of a Terminated Two-Wire Transmission Line Excited by a Nonuniform Electromagnetic Field," IEEE Transactions Antennas and Propagation, Vol AP-13, Nov. 1965, pp 987-989.

17. E. Kreyszig, Advanced Engineering Mathematics, New York: John Wiley and Sons, Inc., 1963, p. 157.

18. C. W. Stuckey, J. C. Toler, and O. B. Francis, "Statistical Description of Near Zone Spurious Emissions," U.S. Air Force Report AFAL-TR-67-37, AD 815146.

19. M. D. Siegel, "Near Field Antenna Coupling on Aerospace Vehicles," IEEE Electromagnetic Compatibility Symposium Record, July 14-16, 1970, pp 211-216.

General References

"An Analysis Technique for Investigating Aerospace Data Link Susceptibility to Electromagnetic Compatibility," U.S. Air Force Report No. AL-TDR-64-184, Sept 14, 1964, AD 447508.

William G. Duff, J. E. Balwin, Jr., F. F. Ferrante, et al, "Electromagnetic Compatibility Prediction Studies," U.S. Air Force Report No. RADC-TR-66-560, Nov 1966.

J. A. M. Lyon, C. J. Dignis, et al, "Electromagnetic Coupling Reduction Techniques," U.S. Air Force Report No. TR-68-132, June 1968, AD 834900.

J. A. M. Lyon, C. J. Dignis, et al, "Derivation of Aerospace Coupling - Factor Interference Prediction Techniques," U.S. Air Force Report No. AFAL-TR-66-57, AD 483051.

O. M. Salati, "Compatibility Studies," U.S. Air Force Report No. RADC-TR-67-636, Vol I, Feb 1968.

14. KEY WORDS	LINK A		LINK B		LINK C	
	ROLE	WT	ROLE	WT	ROLE	WT
Electromagnetic Interference						
Electromagnetic Compatibility						
Computerized Interference Analysis						
Interference Prediction Models						
Mathematical Models						
Intra-Vehicle Compatibility						
Antenna Coupling Analysis						
Wire Bundle Coupling Analysis						
Electromagnetic Field Coupling Analysis						
Magnetic Field Coupling Analysis						